Flexural Strengthening of Timber Beams with GFRP Bars

By

Jeremy S. Walker

A Thesis
Submitted to the Faculty of Graduate Studies
In Partial Fulfillment of the Requirements
For the Degree of

MASTER OF SCIENCE

Structural Engineering Division
Department of Civil Engineering
University of Manitoba
Winnipeg, Manitoba
Canada

THE UNIVERSITY OF MANITOBA

FACULTY OF GRADUATE STUDIES

*****

COPYRIGHT PERMISSION

Flexural Strengthening of Timber Beams with GFRP Bars

by

Jeremy S. Walker

A Thesis/Practicum submitted to the Faculty of Graduate Studies of The University of Manitoba in partial fulfillment of the requirement of the degree

of

Master of Science

Abstract

The large and aging stock of timber bridges in North America coupled with the increased loads imposed by the transportation industry have forced the structural engineering community to determine cost effective alternatives to total bridge replacement. Recent research on the strengthening of timber bridges is focused on the use of glass fibre reinforced polymer (GFRP). This innovative strengthening material is light weight and has very high tensile strength. The research has shown encouraging results in terms of increased strength and reduction in variability. There have also been a number of field projects that demonstrated that this is an economically viable option. This thesis addresses two areas; namely the bond durability, and the minimum reinforcement ratio of the GFRP to be used in flexural strengthening projects.

Since the majority of timber bridges in Manitoba are treated with creosote, bond durability is an important consideration. The durability tests involved subjecting specimens to a 24-week accelerated aging process to simulate extreme environmental conditions. The creosote-treated, Douglas-fir samples were tested in direct shear and it was found that the creosote treatment decreased the bond strength by 27.5% for GFRP sheets at 45°.

With the increase in GFRP research in the last decade, the CAN/CSA-S6-06 Canadian Highway Bridge Design Code (CHBDC) established a minimum reinforcement ratio for strengthening timber bridges with near surface mounted GFRP rods of $\rho = 0.2\%$. Douglas-fir beams

were used in this project. Their rating was decreased to Number 3 grade by introducing artificial defects by a statistically random process. The beams were reinforced using two reinforcement ratios, 0.1% and 0.2%. The beams were tested in three point bending and there was no significant difference in strength between beams with reinforcement ratio of 0.1% and 0.2%. The strengthened beams carried 24.5% more load than the control beams and increased the minimum failure load by 42.8% by decreasing the variability of the results.

An analysis of variance shows that there was no significant difference in the results between the different reinforcement ratios, however there was a significant difference between control beams and the strengthened beams. A linear FEM model was successfully used to accurately model a timber beam.

Acknowledgments

The author would like to express his sincere gratitude and appreciation to Dr. Dagmar Svecova for her advice, guidance, and vision that made this project possible. He would also like to thank Dr. Baidar Bakht for sharing his knowledge and expertise.

The financial support for this research was provided by ISIS Canada Network of Centres of Excellence on Intelligent Sensing for Innovative Structures and the University of Manitoba and is gratefully acknowledged. The technical expertise of Speciality Construction Products Ltd. and Vector Construction Group for the strengthening of the timber specimens was very much appreciated.

The author would also like for express his appreciation to the technical staff of the W.R. McQuade Structures Laboratory, including Mr. Moray McVey, Mr. Grant Whiteside, Mr. Chad Klowak, Ms. Liting Han, Ms. Evangeline Rivera.

Finally, the author wishes to thank his family for their support and encouragement. Special thanks to Ms. Sara Gomez for sharing her knowledge and experience. The support of fellow graduate students Mr. Hugues Vogel, Mr. Shahryar Davoudi, and Ms. Ccee Chan is also gratefully acknowledged.

Contents

3 Experimental Program 32

List of Figures

List of Tables

Chapter 1

Introduction

1.1 General

North America has a large inventory of timber bridges that have been essential to the transportation network in the last 100 years. In the United States, an estimated 10% of the bridge inventory is composed of timber bridges [23]. In the Province of Manitoba, over 30% of the bridges are made of timber [50]. The transportation industry has made large advances in recent years to increase the efficiency of their business, resulting in larger trucks, and therefore heavier loads on Roads and Transportation Association of Canada (RTAC) routes. Existing bridges are thereby subjected to loads that exceed the bridges' original design loads. Timber is still considered a viable option for short span bridges today, however with a less abundant supply of high grade timber than in the past, the construction of new timber bridges is not very common. The majority of existing timber bridges are approaching or have already exceeded their service life, bringing the timber bridge infrastructure to the forefront of current engineering issues.

1.2 Problem Definition

The Province of Manitoba has approximately 750 timber bridges, with 225 to 250 of these bridges located on RTAC routes [50]. Many of the bridges are approaching or have exceeded their service life. Total replacement of the bridge inventory on RTAC routes is an estimated $42.75 million [8], making replacement a non-viable economic solution. It is therefore imperative to develop repair and rehabilitation techniques that can extend the service life of timber bridges.

Glass fibre reinforced polymer (GFRP) sheets and dowels have been previously investigated as feasible reinforcement for timber ([8] [28] [30] [32] [33] [37] [50] [57]). However, there has been limited research done on the durability of bond between creosote-treated timber and FRP ([34] [51] [52]). Since the majority of timber bridges are treated with creosote, bond durability is an important consideration that needs to be addressed before wide-spread application of this strengthening method.

With the increase in GFRP research in the last decade and the favorable results reported, the

CAN/CSA-S6-06 Canadian Highway Bridge Design Code (CHBDC) [18] established minimum reinforcement ratios for strengthening timber bridges with GFRP materials. Research work reported to date did not however use a smaller amount of reinforcement than the minimum suggested by CAN/CSA-S6-06. To make FRP strengthening more economical, it is necessary to determine if the minimum reinforcement ratio of 0.2% specified for near surface mounted GFRP rods is over conservative.

1.3 Objectives

The objectives of this research are to:

1. Compare the shear strength of timber beams strengthened with GFRP sheets and GFRP dowels
2. Determine the bond durability of creosote-treated timber strengthened with GFRP sheets and dowels
3. Evaluate the minimum flexural reinforcement ratio required for strengthening timber beams with near surface mounted GFRP rods
4. Quantify the position of the neutral axis using finite element model
5. Use statistical analysis to justify the experimental results

1.4 Scope

The scope of this experimental program was limited to only Douglas-fir timber. Bending tests were conducted on 75 x 250 x 2400 mm beams loaded statically in three point bending and beam strengthening was limited to GFRP rods. Durability tests included a 24 week accelerated aging program and did not include long-term natural aging. Shear tests were preformed on beams strengthened with GFRP rods and sheets using monotonic loading. Dynamic loading and fatigue were not considered in any part of this experimental program.

Chapter 2

Literature Review

2.1 General

This chapter presents a literature review to provide background into the experimental program. Information on the structural behaviour of timber and the properties of FRP materials has been investigated. Recent research on the strengthening of timber with FRP, the durability of strengthened timber, and artificial defects are discussed.

2.2 Composition of Wood

Timber is a naturally occurring anisotropic, heterogeneous, and visco-elastic material and is composed of small tube-like wood cells that are light-weight, but still quite strong in the direction of the cells. These cells act as a composite material when they are closely packed, giving wood a very high strength to weight ratio.

Wood is composed of sapwood and heartwood. Sapwood is found very close to the outside of the tree and consists of both active and inactive cells, occupying a relatively small percentage of a tree's area and has a radial thickness commonly between 38–50 mm. Heartwood, which occupies the cental area of the tree, was once sapwood, but is now composed of inactive cells. The moisture content of sapwood is approximately three times that of heartwood.

The rings of a tree are formed from the different growth rates that occur at different times of the year. Earlywood cells are formed in the first two months of the growing season while latewood cells are formed later in the growing season. Earlywood cells are lighter in color and less dense while latewood cells are darker and more dense. Due to the variability in growth within a piece of wood, it is important to grade wood products such a beams.

Wood species are classified as either softwoods or hardwoods. Softwoods bear designations such as "Hem-Fir", "S-P-F", etc. The type of wood is important when considering pressure preservative treatment since some species are not treatable. Due to the unavailability of grade-marked hardwood, an inadequate database for material properties, and that hard-

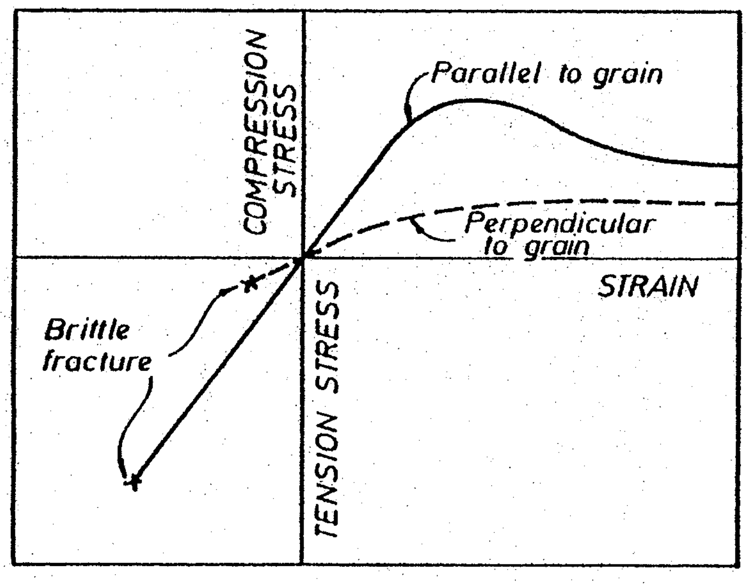

Figure 2.1: Stress Strain Relationship for Wood [15]

woods are not suitable for preservative treatment, the CHBDC does not permit the use of hardwoods for use on permanent structures [18]. Hardwoods can be used for temporary structures.

Figure 2.1 [15] depicts the stress-strain relationship of wood and shows its anisotropic nature. In tension, wood exhibits a linear stress-strain relationship to maximum load and fails with a sudden brittle fracture. In compression, the stress-strain behaviour is linear only up to the yield point, after which ductile yielding occurs. It is also observed that wood can undergo much larger stresses parallel to the grain opposed to perpendicular to the grain.

The stress-strain distribution can be simplified using a bilinear model, which is illustrated in Figure 2.2.

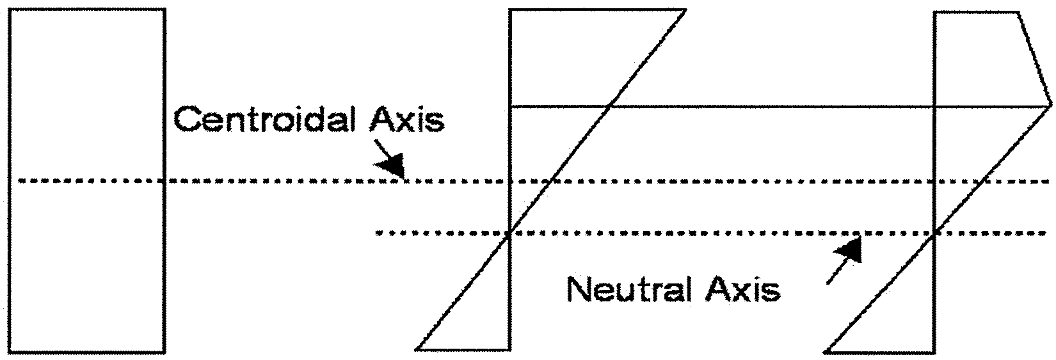

(a) (b) (c)

Figure 2.2: Distribution of Stress and Strain for Bilinear Stress- Strain Relationship [16] (a) cross-section (b) strain profile (c) stress distribution

2.3 Structural Behaviour of Timber

It is important to differentiate between wood and timber since these terms are often used interchangeably. Madsen [40] defines wood as *defect-free wood* while timber is defined as *a useful construction material produced from logs of trees.* When subjected to bending, wood and timber have different failure modes. Wood fails by wrinkles in the compression zone while timber fails in tension perpendicular to the grain where fibres have been disturbed in the vicinity of a knot and a localized slope of grain has been created. Wood has a relatively constant strength along its length, while timber has much variation in strength along its length due to knots and other defects. Therefore, Madsen proposed that timber strength should be a probabilistic entity opposed to a deterministic value. The structural properties for timber are based on the 5th percentile value, meaning that only 5% of the samples will have strength below the 5th percentile value.

Timber beams used for structural applications, such as Douglas–fir are cut from large trees. The location of the timber beams within the rings of the tree will vary from piece to piece, which can effect the mechanical properties of the timber.

The high-strength, light-weight, and energy-absorbing properties of timber make it a desirable and economically competitive construction material for short-span bridges. By using wood preservatives to protect from moisture, timber bridges can have a service life of more than 50 years [47]. Natural occurring defects and discontinuities such as knots, splits, checks, and the slope of grain negatively affect the strength of timber and increase the variability in its mechanical properties, making timber grading a necessity for engineering applications.

2.3.1 Environmental Factors affecting Strength

Moisture Content

Compression strength parallel to the grain is highly sensitive to moisture content while tensile strength is not. Compression and tension perpendicular to the grain are sensitive to moisture content. Bending strength is sensitive to moisture content in the strong portion of the strength distribution. Table 2.1 shows the approximate effect of moisture content on wood properties.

The only practical method of measuring moisture content in timber is by electrical resistance

Table 2.1: Relative Change in Property from 12% Moisture Content [47]

Property	**6% MC**	**20% MC**
Tensile Strength Parallel to Grain	8	-15
Compression Strength Parallel to Grain	35	-35
Shear Strength Parallel to Grain	18	-18
Bending Strength	30	-25

measurements [40]. This method uses insulated needles to measure the electrical resistance in the timber. Moisture meter readings must be adjusted for different wood species and adjustment factors. Since these factors differ between the manufacturers and wood scientists, this method is easy to use but somewhat unreliable.

Temperature

The mechanical properties of wood decrease at high temperatures and increase at low temperatures. As long as the wood is exposed to short durations of heat and temperatures less than 65 °C, the mechanical properties are recoverable [47]. In the field, temperature rarely impacts the mechanical properties of wood under service conditions.

2.3.2 Timber Grading

Timber is a heterogenous, anisotropic material. Therefore, no two pieces will have exactly the same properties as discussed above. The strength and stiffness will vary due to the natural defects present and each piece of timber must be graded for use as a structural engineering material. Timber is commonly graded in one of two ways:

1. Visual stress grading

2. Mechanical stress grading

Visual stress grading is the most widely used grading method. It involves visually inspecting pieces of timber for strength–reducing defects such as knots, checks and splits, slope of grain, and rate of growth. These defects will decrease the strength and stiffness of a piece of timber relative to a clear wood sample. Knots represent a discontinuity and change in direction of the wood fibres. The factors affecting the magnitude of the knots influence are size, location, shape, and soundness of the knots [25]. Checking and splitting are caused by changing moisture content. Checking in particular is the result of rapid lowering of surface moisture content combined with differential moisture contents of the inner and outer portions of the piece. The outer cells tend to lose moisture more rapidly than the inner cells, causing different rates of shrinkage and in turn leading to stresses in the timber which causes checking [1]. The slope of grain will also impact the strength of timber. As the slope increases, the strength will decrease.

In Canada, the National Lumber Grades Authority (NLGA) is used to grade timber. Timber beams that are 50–100 mm (2" to 4") thick and 125 mm (5"+) wide are classified as structural joists and planks and are graded using the following categories:

1. Select Structural

2. Number 1
3. Number 2
4. Number 3

Mechanical stress grading or machine stress rating (MSR) is a non-destructive procedure for determining the modulus of elasticity of a piece of timber using a mechanical device. The modulus of elasticity is then correlated to the bending strength of the timber. The machine measured modulus of elasticity is the primary grading technique of MSR, however if large defects are present, visual grading will supersede MSR.

2.3.3 Behaviour of Timber in Bending

Buchanan [15] investigated the bending strength of timber and classified four separate failure modes, which are dependent on the relative tensile and compressive strengths of the timber. The four failure modes are as follows.

1. A beam with a tensile strength lower than the limit stress in compression will fail by brittle fracture with no compression yielding. This failure mode occurs in weak members.
2. A beam with a tensile strength between the compression limit stress and the ultimate compression strength will still fail in tension. However, some compression yielding will

take place and the neutral axis will shift towards the tension side of the beam as the compression yielding occurs. This failure mode is characteristic of stronger beams than those which fail in mode one.

3. In a beam with a considerably higher tensile strength than compressive strength, compressive yielding is reached well before ultimate tensile strength. The compressive stress will decrease after yielding has occurred while tensile stresses will continue to increase until rupture in the tension zone occurs.

4. In an extreme case, a beam that is much stronger in tension than compression, no tension failure occurs. This failure mode is affected by moisture content, which reduces compressive strength much more than the tensile strength.

Most timber beams fail by modes 1–3, depending on the grade of the timber. Clear wood specimens or high grade timber will likely fail by modes 2 or 3 because there are no, or very few, tensile strength–reducing defects to cause mode 1 failure. Bending also produces horizontal shear stress parallel to the grain and compression perpendicular to the grain at the supports. Figure 2.3 [47] illustrates the stresses acting on a beam in bending.

2.4 Creosote

Timber used for outdoor applications is often treated with preservatives to protect its structural properties and extend its service life. Creosote is one of the oldest wood preservatives

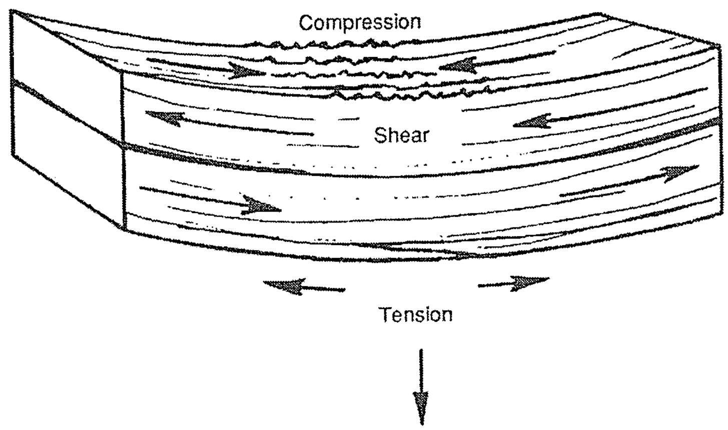

Figure 2.3: Behaviour of Timber in Bending [47]

and is derived from the distillation of coal to produce coke. Its high viscosity provides excellent protection against moisture changes in wood, preventing splitting and checking; making timber an economically feasible construction material for bridges. Many highway and rail structures treated with creosote have provided more than 60 years of satisfactory service. Creosote is a complex mixture of over 300 compounds, and contain toxic mechanisms that are still poorly understood [47]. Brooks [14] conducted a study on the environmental effects of creosote treated timber bridges. It was concluded that there was little environmental risk associated and that proper construction and maintenance practices could further reduce the risks. Therefore, it is reasonable to move forward and study the effect of creosote on bond strength of the timber – FRP interface.

2.5 FRP Materials

Fibre Reinforced Polymers (FRPs) are becoming increasingly popular for civil engineering applications due to their many advantages over materials such as steel. There are many engineering, economic and environmental advantages to using FRP materials in conjuction with timber [19], including:

1. High strength
2. High stiffness
3. Enhanced ductility, providing safer failure mechanism
4. Improved creep characteristics, which improves serviceability
5. Less variability in mechanical properties, allowing higher design values
6. Allows for use of lower grade timber
7. Improves structural efficiency, reducing member size and weight requirements
8. Reduction in cost
9. Reduced demand on timber supply
10. Ease of installation

FRPs are advanced composite materials consisting of a matrix (resin) and reinforcing fibres. The fibres are carbon (CFRP), glass (GFRP), or aramid (AFRP) and all vary in mechanical properties and cost. The mechanical properties of the final FRP product depend on the fibre quality, orientation, shape, volumetric ratio, adhesion to the matrix, and the process of manufacturing. In order to utilize the full fibre strength, the resin must be able to develop a higher ultimate strain than the fibres [48]. The matrix is used to protect the fibres from aggressive environments and mechanical abrasion, to transfer stresses between the fibres, allowing them to act as one system, and to prevent fibre dislocation [29]. The two commonly used types of polymers as matrices are thermosetting and thermoplastic. Thermosetting polymers are the most common and include polyesters, vinyl esters, and epoxies. They are joined together by chemical cross-links and therefore cannot be reshaped by applying heat or pressure. They have good thermal stability and chemical resistance and undergo low creep and stress relaxation [48]. Thermoplastic polymers, held in place by weak secondary bonds, can be destroyed by heat or pressure and can be reshaped multiple times by heating. Most commonly available FRP bars are made using thermosetting polymers.

2.6 Strengthening Timber Beams with FRP

2.6.1 Flexure

Sheets

Plevris and Triantifillou [45] and Triantafillou and Deskovic [53] studied the effect of reinforcing sawn wood beams with non-prestressed and prestressed CFRP sheets externally bonded to the tension face of the beam, respectively. It was found that the CFRP sheets increased the strength, stiffness, and ductility characteristics of the wood when tested in three-point bending. Their experimental results were verified with accurate analytical models.

Nine small–scale Hemlock beams were testied in three-point loading by Abdel-Magid et al. [7]. Three beams were reinforced with steel, three with CFRP sheets, two with AFRP sheets, and one with unidirectional AFRP sheets, all bonded to the tension face of the beams. The CFRP reinforcement exhibited a 9% increase in modulus of elasticity and a 32% increase in ultimate load while the AFRP sheets were less economical, showing no significant strength increase.

Johns and Lacroix [36] and Johns and Racine [37] tested 150–39 x 89 mm and 70–39 x 140 mm commercial SPF (spruce-pine-fir) sawn timbers in four point bending. Half of the samples were non-strengthened while the other half were strengthened. Johns and Lacroix used three different strengthening schemes, including two using CFRP sheets and one using

GFRP sheets. A 40 to 100% increase in the strength of the weakest beams was observed by adding the FRP reinforcement due to local bridging and confining action of the FRP on the wood. Johns and Racine [37] strengthened the beams using only GFRP sheets. The beams tested were larger and weaker than the 39 x 89 mm beams previously tested. They had strength increases of up to 240% for the weakest beams. The weakest beams are of the greatest interest for the designer, making the results very encouraging.

There has also been research performed on FRP strengthening of glulam beams. Hirasawa et al. [35] strengthened glulam with CFRP sheets, CFRP plates and a combination of the sheets and plate. The sheets were determined to be the most effective relative to their reinforcement ratio and a strength increase of approximately 50% was established.

Bars

An experimental program was undertaken by Gentile et al. [28] in which 22–100 x 300 x 4300 mm small scale timber beams and 4–200 x 600 x 10000 mm full-scale beams were tested in four-point bending. The beams were reinforced with GFRP bars using three different reinforcing ratios and were installed in grooves cut into the tension faces of the beams. The addition of FRP bars shifted the mode of failure from brittle tension to a more ductile compression-initiated failure mode and increased the flexural strength by 18 to 46%. Gentile also tested the bond strength between the creosote-treated timber, epoxy resin, and GFRP bars for six small timber beams. He determined that the bond strength was adequate for short-term behaviour, however long-term behaviour was not studied.

Micelli et al. [42] strengthened timber beams with CFRP rods for flexural reinforcement. A significant increase in ultimate capacity and stiffness was observed.

Twenty–200 x 200 x 4000 mm timber beams were tested in four-point bending by Borri et al. [13]. The following reinforcing schemes were used: eight beams with CFRP sheets ($\rho =$ 0.082% or 0.123%), four beams with pre-stressed CFRP sheets ($\rho = 0.082\%$ or 0.123%), five beams with CFRP bars ($\rho = 0.11\%$ or 0.22%), and three control beams. Reinforcement with CFRP sheets was the most effective technique, providing up to a 60% increase in strength for $\rho = 0.123\%$ and 55% for $\rho = 0.082\%$. The prestressed CFRP sheets and the CFRP bars both provided a maximum strength increase of 52%. The CFRP sheets utilized a smaller reinforcement ratio while providing the highest strength increase. The maximum stiffness increase was 28%.

Strips

Gilfillan et al. [30] preformed bending tests on Sitka spruce beams and laminated veneer lumber (LVL) reinforced with CFRP or GFRP pultruded strips in the tension and/or compression zones. The addition of reinforcement led to a desirable ductile compression failure and a significant increase in ultimate load. The most efficient reinforcing scheme was using only tensile reinforcement, rather than balancing the reinforcement between the two zones.

The benefits of strengthening the LVL beams were less evident due to their stronger, stiffer, and more uniform properties.

2.6.2 Shear

Sheets

Triantafillou [54] tested 21 wood beams designed to fail in shear and reinforced them with externally bonded carbon fibre reinforced polymer sheets in the shear span. The FRP sheets are most effective for increasing the shear capacity of the beams when the fibres are placed in the longitudinal direction. An analytical model was also developed that accurately predicted the experimental shear capacity within 10%.

Hay [33] tested 37 small-scale timbers in three-point bending with the applied load acting at the quarter span to allow two tests to be preformed on each beam. Ten beams were control beams, five were reinforced with vertical GFRP sheets, and 21 were reinforced with diagonal GFRP sheets. The GFRP sheets were externally bonded to the timber in the critical shear region using an epoxy resin and the edges were rounded at a minimum radius of 12.5 mm to ensure good bonding. Hay concluded that GFRP sheets increased the strength of the timber stringers by 19% and 39% for the vertical and diagonal reinforcing schemes, respectively. The vertical sheets tore up easily in the vicinity of horizontal splits while the diagonal sheets were subjected primarily to tension and therefore preformed much better. Specimens with vertical sheets failed in flexure while the diagonal sheet specimens experienced primarily bearing failure.

Dowels

Direct shear tests were preformed on 9–100 x 150 x 290 mm Douglas-fir specimens by Boon [12]. Three specimens were control specimens, three were reinforced with steel dowels, and three with GFRP dowels. The dowels did not provide a significant increase in shear capacity of the timber, however it did decrease the variability and increased the ductility of the timber. An adequate bond did not develop between the steel dowels, timber and epoxy, making GFRP reinforcement the most desirable reinforcing material.

Gomez [32] tested 20–75 x 190 x 774 mm Douglas-fir sawn timber specimens in shear using five different reinforcing schemes. The specimens were cut longitudinally in half to predefine the shear plane to isolate the strength of the reinforcement in pure shear. Reinforcing schemes included GFRP dowels at 30°, 45°, and 90° and GFRP sheets at 30° and 45°. The 30° configurations for both the dowels and sheets preformed better than the 45° configurations, however a larger reinforcement ratio was used. The GFRP sheets preformed better than the dowels, however if the timber had been creosote treated, the strength of the sheets would likely have decreased.

2.6.3 Flexure and Shear

Sheets

Wegner and Gasmo [57] investigated the flexural strength and rigidity of three groups of wood beam; unreinforced, reinforced and undamaged, and damaged and repaired with GFRP laminates. GFRP was applied on the tensile face of the beam, the side faces of the beam, and both the tensile and side faces. The damaged beams recovered a minimum of 90% of their original strength and stiffness. The bond strength was identified as the limiting factor for the strength of the reinforced beams.

Gomez [32] tested nine–100 x 400 x 3650 mm beams that were strengthened with 2 layers of GFRP sheets along the bottom of the beam and GFRP sheets on each end of the beam in the critical shear zone. The sheets were bonded to each side of the beam at 45° and tested in three-point bending. The average strength increase was 10.8% and the stiffness increase ranged from 9 to 60%. The failure modes of the nine beams tested were: four in shear, four in bearing at the location of the point load, and one in flexure.

Bars

Svecova and Eden [50] tested 50 small-scale beams and 2 full-scale timber stringers in four-point bending. The small scale beams were reinforced with GFRP bars using nine different reinforcing schemes. The four schemes with shear and flexural reinforcement showed a strength increase of 47 to 52% while the shear reinforcing schemes showed an increase of 17 to 35%. Similar to Gentile [28], Svecova and Eden also observed a shift in failure mode from brittle tension to a more ductile compression-initiated failure. It was concluded that the optimal reinforcing scheme included shear and flexural reinforcement along the entire length of the beam. This reinforcement acted as a truss member within the beam to bridge local defects and discontinuities in the timber, hence reducing variability in the mechanical properties of the beams.

Twenty-six full scale dapped timber stringers were tested in three point bending by Amy [8]. The dapped ends were found to decrease the strength of the beams significantly. Amy concluded that by adding GFRP bars in flexure has very little impact on strength since this reinforcement cannot prevent dap failures. Dap failures are failures parallel to the grain close to the bottom of the cross-section, where the dap is introduced.Adding shear and flexural GFRP reinforcement increased the beam strength approximately 20% over both the control and flexurally reinforced specimens and shift the failure mode to ductile-compression. The bond between the creosote timber and the GFRP bars remained intact for all tests.

2.6.4 Durability

Durability of the timber–FRP interface is a critical issue to ensure that FRPs are able to reach their full strength potential. Accelerated aging is often used prior to static loading to test the durability of materials. An accelerated aging test is defined in ASTM E 632–82 [4] as *an aging test in which the degradation of building components or materials is intentionally accelerated over that expected in service.*

Accelerated Aging

A number of durability studies have been undertaken using accelerated aging to test the performance of FRPs. Using temperatures higher than those normally found in service accelerates temperature effects while moisture effects are accelerated by water soaking to maximum moisture content [31].

Deppe [22] developed an accelerated aging test, XENOTEST to simulate exterior exposure using historical data. The "normal climate", which make up approximately 50% of the time was excluded, leaving more "critical" events such as high or low temperatures, precipitation, global irradiation, frost, and fog. The XENOTEST was determined to accelerate aging effects by approximately 10 times when compared to results from standard exterior exposure.

Raknes [46] studied the durability of wood adhesives after 30 years of aging and compared the results to three different accelerated aging processes:

1. Standard atmosphere (20 °C, 65% r.h.) for 5 years
2. Cycling between 20 – 25 °C/ 85 – 90% r.h. and 50 °C/ 60% r.h. for 1 month periods ("humid/hot") for 3 years.

Table 2.2: Environmental Chamber Cycles used by Gomez

Cycle	Temperature	Relative Humidity
1	20 °C	85%
2	40 °C	60%
3	20 °C	85%
4	25 °C	25%

3. Cycling between 20 – 25 °C/ 85 – 90% r.h. and 25 – 30 °C/ 25 – 30% r.h. for 1 month periods ("humid/dry") for 5 years.

It was determined that the humid/hot cycles lead to the highest strength loss in the bonds and accelerated aging results can be correlated quite well to natural aging.

Gomez [32] adapted a four-cycle accelerated aging process from Raknes [46] to test the bond durability of GFRP sheets and creosote-treated timber of nine 100 x 400 x 3650 mm beams previously tested in flexure. The timbers were aged for four months, with the temperature and relative humidity changing every week, as shown in Table 2.2. The initial assessment of the bond durability based on visual inspection was not conclusive on the long-term performance of the bond. The observations showed that changing temperature and relative humidity could have a negative effect on the bond between the FRP and timber, especially if the sheets were initially debonded due to stress damage.

The degradation of GFRP is a complex function of the resin and glass fiber, residual stresses in the fibres, matrix shrinkage, production methods, void content, FRP surface treatment, external stresses, and environmental conditions [11]. Therefore, it is extremely difficult to isolate individual factors and determine their exact contribution to the overall FRP degradation. ASTM E 632–82 [4] states that it is difficult to develop accelerated aging tests to predict long-term performance for the following reasons:

- degradation mechanisms are complex and seldom understood
- it is difficult to quantify external factors that affect performance
- testing configuration often vary from in-service conditions

The standard [4] states that although there are shortcomings, accelerated aging tests are still useful and necessary to provide durability data. Accelerated aging should be regarded as a qualitative tool necessary for studying bond durability without waiting years for natural aging to take place.

FRP–Wood Bonds

Davis [21] studied the performance of adhesive systems for structural timbers. A number of factors were found to impact bond strength including:

1. surface condition of the timber;
2. moisture content of the timber;
3. adhesive compatibility;

4. magnitude and direction of applied force;

5. stability in the operating environment; and

6. design life

There will be considerable variation in these qualities depending on the cutting, drying, and storage methods. A well prepared timber surface will provide a good substrate for adhesive bonding.

The interface bond strength between wood and FRP composite materials must be high and durable. Research has been performed on the use of various wood primers to enhance the durability of the wood–epoxy bond in severe conditions. The strength of this bond is often the major factor in limiting the strength and stiffness of wood members provided by FRPs.

Gardner et al. [27] and Sonti [49] determined that priming the wood surface with resorcinol formaldehyde (RF) can significantly increase the bond strength under wet conditions. Gardner et al. [27] concluded that while many adhesives provided adequate bond under dry conditions, the RF adhesive was also suitable for exterior exposure. Sonti [49] used accelerated aging to test the durability of a number of different adhesives including epoxy, polyurethane, isopolyester, RF, and phenolic based RF. It was found that the RF/epoxy resins combination preformed the best. The epoxy had a very high dry shear strength while the RF is able to maintain at least 50% of its dry shear strength after aging.

Vick [55] [56], Lopez-Anido et al. [38], Lyons and Ahmed [39], and Davalos et al. [20] determined that hydroxymethylated resorcinol (HMR) can be effectively used to prime the surface of many hardwoods and softwoods. Vick [55] found HMR to increase delamination resistance, shear strength, and deformation resistance for Douglas-fir so that epoxy bonds can meet the ASTM D 2559 requirements. Lopez-Anido et al. [38] tested adhesive bonding of eastern hemlock glulam panels with E-glass/vinyl ester reinforcement. Results showed that the vinyl ester resin with a HMR primer can form a strong and durable adhesive bond with wood for exterior exposure. Lyons and Ahmed [39] investigated the effects of a number of factors on the bond between polymer composites and wood. Resin type, wood moisture content and surface roughness were all found to impact bond strength. The application of HMR to the wood surface improved overall bond strength in wet exposure conditions.

Davalos et al. [20] studied the durability of FRP-wood bonded interfaces. While several adhesive systems had been successfully implemented in the past, little information has been provided as to the long-term service performance and delamination behaviour of FRP-wood bonded interfaces. Davalos et al. [20] subjected small, clear wood samples to an accelerated aging process consisting of:

1. vacuum/pressure soaking followed by oven-drying,
2. steam/pressure soaking followed by oven-drying, and
3. repeat first cycle making a total test period of 3 days.

It was found that bond strength decreases due to aging when certain bonding agents are used. Further priming the wood with a hydroxmethylated resorcinol (HMR) coupling agent and then applying epoxy as a saturant provided more favorable results compared to using phenolic (instead of epoxy) and resorcinol formaldehyde (instead of HMR). All this research has shown that FRPs can be successfully bonded to wood by selecting suitable primer/saturant combinations.

Impact of Creosote Treatment on Bond Performance

The durability of Rotafix CB10T Slowset Epoxy that had been used in the Tourand Creek Bridge strengthening [28] was studied by Svecova and Mota [51]. Accelerated aging was preformed on 170 Douglas-fir shear specimens, complying with ASTM D4502–92 [2]. It was concluded that (a) the strength of samples without creosote treatment was higher than that of samples with creosote; and (b) constant moisture and higher temperatures reduce the bond strength of the epoxy.

Tascioglu et al. [52] studied the effect of preservative treatment on the durability of E-glass/phenolic composite interfaces. Wood treated with oil-borne preservatives, such as creosote, drastically increased the likeliness of delamination in the wood/FRP composite bond lines. The oily nature of the creosote severely interferes with the wettability of the resin and reduces the adhesion of the interface bond.

Herzog et al. [34] studied the effect of creosote treatment on FRP composite materials used for wood materials and focused on three mechanical properties. FRP consisting of E-glass fibre was bonded to the creosote-treated timber surface using an epoxy resin. The results showed that the interlaminar shear strength was adversely affected by the creosote treatment, suggesting that hydrocarbons impact epoxy resin. The longitudinal tensile strength of a pultruded FRP sheet bonded with urethane was also adversely affected by the creosote treatment. The longitudinal modulus of elasticity was not affected by the creosote treatment.

2.7 Artificial Defects

The introduction of artificial defects was previously studied by Falk [24] and Fridley [26]. Falk [24] studied the effect of drilled holes on the bending strength of large dimension Douglas-fir lumber. Holes were drilled at midspan in three different locations, with two different diameters. It was concluded that the hole location was as important as the hole size. A beam with a 25.4 mm diameter hole positioned at midspan was only slightly stronger (4 to 10%) than a 44 mm hole in the same position. Positioning the hole very close to the bottom of the beam or at the bottom led to 7 to 15% strength loss as compared to a beam with a hole 25 mm from the bottom. Therefore it is important to focus on both hole location and hole size in order to accurately introduce defects to the timber. In research by Fridley [26] it was assumed that holes affect timber strength similarly, but not identically to knots. In knots, the grain naturally "flows" around a knot, while a hole cuts through the grain. Results from both these studies were implemented in the current research.

Chapter 3

Experimental Program

3.1 General

The use of FRPs has been increasing in civil engineering applications due to their excellent mechanical properties and corrosion resistance. However, their widespread acceptance has been delayed by their susceptibility to the effects of stress and environmental weathering [11]. The lack of data on the testing of FRP–strengthened timber beams has also led to potentially over-reinforced beams. Therefore two experimental programs were undertaken to address these concerns.

The first experimental program was carried out to investigate the durability of the FRP–timber interface. Specimens were cycled in an environmental chamber to determine the impact of high temperature and humidity on FRP–timber bond. For quantitative assessment, the shear contribution of the FRP reinforcement was determined by isolating all other failure mechanisms.

The second experimental program involved strengthening timber beams with near surface mounted GFRP rods using 2 reinforcement ratios, and to determine whether the minimum reinforcement ratio required by the CHBDC [18] can be reduced. Artificial defects were added to the beams in order to reduce the grade of the beams, making them typical of beams in need of strengthening.

3.2 Durability Tests

Two different experimental programs were carried out at the University of Manitoba to investigate the shear strength and bond durability of GFRP strengthened timber. The first program was carried out by Gomez [32] on 19 non-treated timber specimens. The second experimental program, performed on treated timber specimens, is the subject of this thesis; however the work done by Gomez will be discussed for comparison purposes.

Table 3.1: Physical Properties of Wabo ®MBrace System Components

Wabo ®MBrace	**Ultimate Strength, F_{fu}** MPa	**Elastic Modulus, E_f** GPa	**Rupture Strain, ϵ_{fu}** %
EG900	1517	72.4	2.1
Saturant	55.2	3.034	3.5
Primer	17.2	0.717	40

3.2.1 Materials

Timber

Both creosote treated and untreated Douglas-fir specimens were used. The treated timber used was salvaged from stringers from dismantled timber bridges that had been in service for approximately 40 years.

GFRP

Two types of GFRP reinforcement were used for the tests, namely GFRP sheets and GFRP dowels. The reinforcing system used for the GFRP sheets was the commercially available Wabo ®MBrace system which consists of Wabo ®MBrace EG900 unidirectional E-glass fibre fabric, Wabo ®MBrace Saturant, and Wabo ®MBrace Primer. GFRP bars with a 9 mm diameter were used as dowels. Tables 3.1 and 3.2 list the material properties of the sheets and dowels, respectively.

Table 3.2: Physical Properties of Aslan 100 GFRP Bars

Diameter mm	**Nominal Diameter** mm	**Area** mm^2	**Tensile Modulus** GPa	**Ultimate Strength** MPa	**Shear Strength** MPa
9	9.53	84.32	40.8	760	152

3.2.2 Test Specimens

Small-scale, 100 x 200 x 780 mm timber specimens were obtained from 20–100 x 400 x 3650 mm treated timber stringers previously tested by Hay [33] and Gomez [32]. Two specimens were obtained from each of the 20 stringers and pre-existing cracks, FRP sheets, and epoxy were avoided when marking and cutting the specimens. Approximately 10 out of 40 specimens split in half when cutting, reducing the total number to 30.

The 30 specimens were taken to the Country Wood Enterprise's saw mill in Carmen, Manitoba where they were cut longitudinally in half in order to define the shear plane. Ten millimeter notches were cut at opposite ends of the two halves to facilitate loading in the testing frame. The saw mill's precision and the thin width of the saw's blade enabled the production of consistent size specimens and little material loss.

The sides of the specimens were already treated with creosote, however the ends and the top and bottom of the cut specimens were free of creosote. To prevent changes in moisture content and ultimately warping of the timber, spar urethane was painted onto all creosote free surfaces .

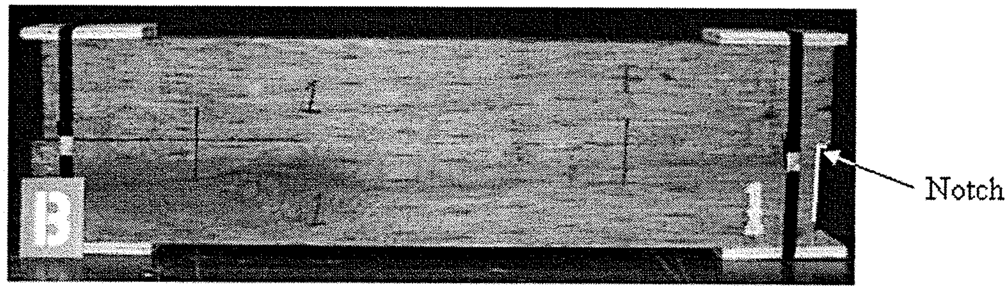

Figure 3.1: Strapped Timber Specimen

The timber specimens that had been cut in half were strapped back together using metal strapping at both ends and small pieces of plywood to prevent the crushing of the wood fibres. The two halves were lined up to ensure the same alignment as before cutting. See Figure 3.1 for a strapped specimen ready for strengthening.

Gomez [32] used 19–75 x 190 x 774 mm untreated samples for testing. The specimens were cut from large timbers and large splits and checks were avoided when cutting. These specimens were also cut in half longitudinally, notched, and strapped back together.

3.2.3 Strengthening of Specimens

The untreated specimens were strengthened with GFRP using five strengthening schemes, GFRP sheets at 30° and 45° and GFRP dowels at 30°, 45°, and 90°. The test results demonstrated that the GFRP sheets and dowels installed at 45° were very effective. They were able to provide a higher shear resistance than the 90° configuration and provided a very comparable resistance to 30° relative to the reinforcement ratio [32].

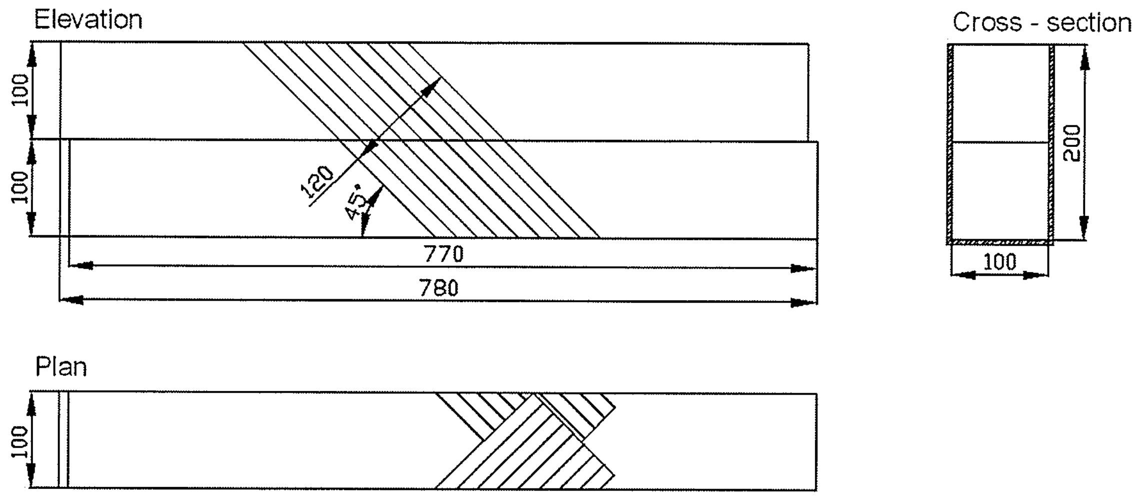

Figure 3.2: Layout of Sample with GFRP Sheet

Based on the results from the untreated samples, the remaining 30 samples were strengthened using the 45° configuration. Of the 30 samples, 15 samples were randomly selected and strengthened with exterior bonded GFRP sheets at 45°. The other 15 samples were strengthened with a GFRP dowel at 45° through the middle of the specimen. Refer to Figures 3.2 and 3.3 for the respective sheet and dowel reinforcement layouts.

The location of the sheets and dowels was marked appropriately on each specimen. The reinforcement surface of the timber beams was cleaned using a brush and vacuum to minimize the dust and debris that would interfere with the GFRP–timber bond. The specimens were strengthened at Vector Construction Group, in Winnipeg, Manitoba.

All samples were marked with a description. The first letter of the description refers to the type of reinforcement ('S' for sheet, 'D' for dowel). The second letter refers to the creosote treatment of the sample ('NT' for no creosote treatment, 'T' for creosote treatment). The

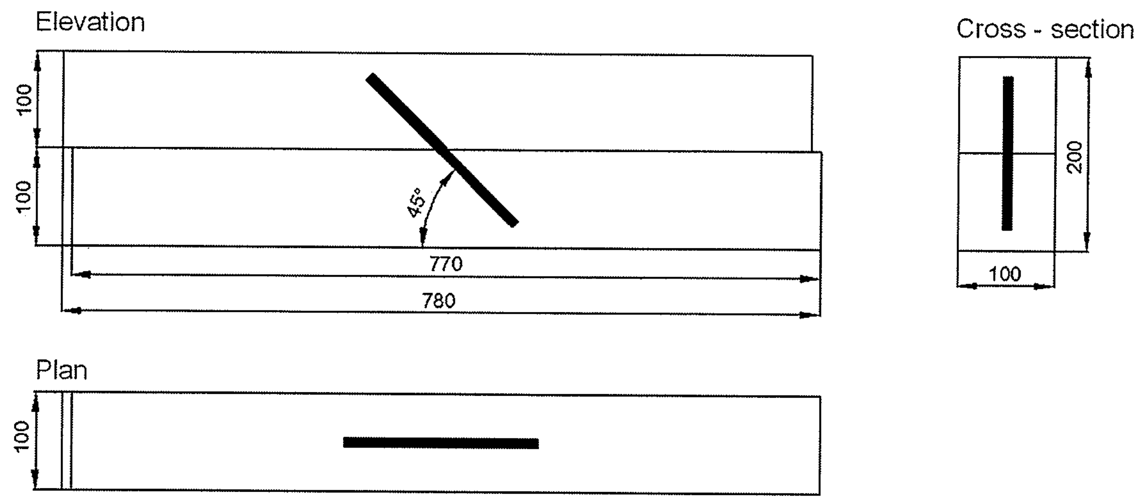

Figure 3.3: Layout of Sample with GFRP Dowel

third component of the description refers to the angle of reinforcement (30 °, 45 °, 90 °). The final description represents the testing environment ('C' for control, 'H' for high temperature [+40 °C], 'L' for low temperature [−20 °C]). It should be noted that the 'H' and 'L' samples were aged for 24 weeks in an environmental chamber and had a 45 ° inclination of GFRP. Specific letter designations were excluded if they are not needed to identify the samples. Refer to Table 3.3 for the designation of the 49 samples.

GFRP Sheets

The GFRP sheets were cut into 120 mm wide strips to achieve a reinforcement ratio of 0.158%. The reinforcement ratio was determined by calculating the area of cross-section of the GFRP sheet passing through the shear zone and dividing by the area of the timber in the shear zone as shown in Equation 3.1. The thickness of the sheets was assumed to be

Table 3.3: Specimen Description

Specimen Classification	**# of Samples**	**GFRP Type**	**Treatment**	**GFRP Angle**
$S-NT-30^{\circ}$	4	Sheets	No	30°
$S-NT-45^{\circ}$	4			45°
$D-NT-30^{\circ}$	3	Dowels		30°
$D-NT-45^{\circ}$	4			45°
$D-NT-90^{\circ}$	4			90°
$S-T-C$	5	Sheets	Yes	45°
$S-T-H$	5			
$S-T-L$	5			
$D-T-C$	5	Dowels		
$D-T-H$	5			
$D-T-L$	5			

0.353 mm [?]. Refer to Table 3.4 for reinforcement ratios for all specimens.

$$\rho_{sheets} = \frac{A_{GFRP}}{bd} = \frac{(120mm)(\sqrt{2})(0.353mm)}{(760mm)(100mm)} = 0.001569 = 0.157\% \tag{3.1}$$

According to Cl.16.12.3.1(h) of the CAN/CSA-S6-06, the corners of the specimens were rounded to a minimum radius of 12.5 mm to ensure that full contact of the sheet with the timber was maintained [18]. The first component that was applied to the timber surface was a viscous epoxy primer. It is designed to penetrate the pore structure of wood and provide a high bond base coat. After the surface was primed, the base coat of epoxy encapsulation resin was applied. The unidirectional E-glass fibre fabric was then installed on the sides of the specimens, running at 45° and crossed over on the bottom of the specimen. The top coat of the epoxy resin was applied to the GFRP sheets to fully encapsulate of the sheets. The GFRP sheets had a bonded surface area of 84 900 mm^2, which was very similar to the

Table 3.4: Reinforcement Details

Specimen Classification	**Reinforcement Ratio** $[\rho]$	**Bonded Surface Area** $[mm^2]$	**Development Length/Side [mm]**
$S-NT-30°$	0.30%	127 200	NA
$S-NT-45°$	0.21%	89 900	NA
$D-NT-30°$	0.30%		165
$D-NT-45°$	0.21%		120
$D-NT-90°$	0.30%		85
$S-T-C$			
$S-T-H$		84 900	
$S-T-L$	0.16%		
$D-T-C$			
$D-T-H$			100
$D-T-L$			

surface area of the 45° non-treated samples as shown in Table 3.4.

GFRP Dowels

The GFRP dowel specimens were un-strapped and a multi-purpose silicone sealant was applied between the two pieces of timber in a 100 mm diameter circle around the location of the dowel. The two halves were strapped together again. This procedure was to ensure that no epoxy would seep between the timbers when the dowels were being installed.

The GFRP dowel had a reinforcement ratio of 0.157%, which was very similar to the sheet specimens, thus evoking direct comparison. Equation 3.2 shows a detailed reinforcement ratio calculation while Table 3.4 contains reinforcement details for all of the samples.

$$\rho_{dowels} = \frac{A_{GFRP}}{bd} = \frac{(84.32mm^2)(\sqrt{2})}{(760mm)(100mm)} = 0.001576 = 0.158\% \quad (3.2)$$

The dowels were cut into 200 mm lengths and 3 strain gauges were installed on each dowel at the 20 mm, 100 mm, and 180 mm marks. Holes were drilled approximately 80% of the way through the middle of the specimen to make room for the dowels. A two-component, low viscosity, epoxy resin/hardener was injected into the hole, the dowel was inserted, and more epoxy was injected to fill the hole. The 200 mm dowels produced approximately 100 mm of development length on each side of the shear plane. Table 3.4 provides estimated development lengths for all specimens.

3.2.4 Accelerated Aging Cycles

Twenty of the treated specimens (10 dowel-reinforced and 10 sheet-reinforced) were placed in the environmental chamber. The walk-in environmental chamber was 2.5 m wide x 6.0 m long x 2.6 m high. It had temperature capabilities of +40 °C to −40 °C and humidity control up to 85% relative humidity limited by a +25 °C dew point. Air assisted spray nozzles were used to increase humidity and a chemical dryer was present to dehumidify the chamber. A touch-sensitive computer interface was located on the back of the chamber to control temperature/humidity settings. Refer to Table 3.5 for the weekly cycles which the

Table 3.5: Accelerated Aging Cycles

Cycle	Temperature	Relative Humidity
1	20 °C	85%
2	40 °C	60%
3	20 °C	25%

shear specimens were subjected to. The accelerated aging program lasted 24 weeks.

The cycles were adapted from Raknes [46], with the emphasis on subjecting the specimens to the most extreme conditions that the chamber would allow. Extremely warm temperatures were thought to have a greater impact on bond strength, so no negative temperatures were incorporated into the aging program. Therefore cycles 1 and 2 use the highest relative humidity and temperature respectively that the chamber can produce, which has been demonstrated by Gillespie [31] and Raknes [46] to accelerate aging. Cycle 3 is used to dry out and bring them back to normal temperature and humidity conditions before further testing. The environmental chamber is capable of shifting from one cycle to the next in just over one hour. The control specimens were tested at room temperature and were not subjected to accelerated aging. The samples subjected to accelerated aging were load tested at high and low temperatures. A total of 10 specimens were tested in shear at +40 °C and an additional 10 were tested at −20 °C. The samples were exposed to either the warm or cold exposure for a minimum of 48 hours prior to testing.

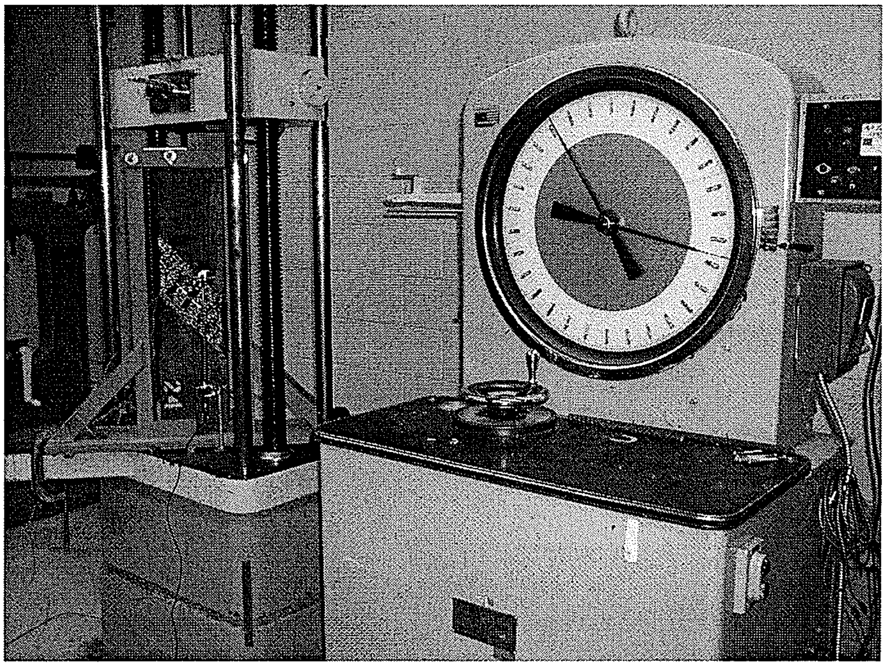

Figure 3.4: Universal Testing Machine

3.2.5 Test Setup

Two different testing machines were used in the experimental program. The 19 untreated specimens ($S-NT$ and $D-NT$) and the 10 treated, control specimens ($S-T-C$ and $D-T-C$) were tested using a 250 kN universal testing machine. The testing machine was manually controlled, with the objective to load the samples at a constant rate of loading. The test setup is shown in Figure 3.4.

The 20 aged samples were tested using a 350 kN testing machine in the environmental chamber in which 10 samples were tested at +40 °C and the other 10 at −20 °C. The rate of loading was 1 mm/min. Refer to Figure 3.5 for the load frame setup in the environmental

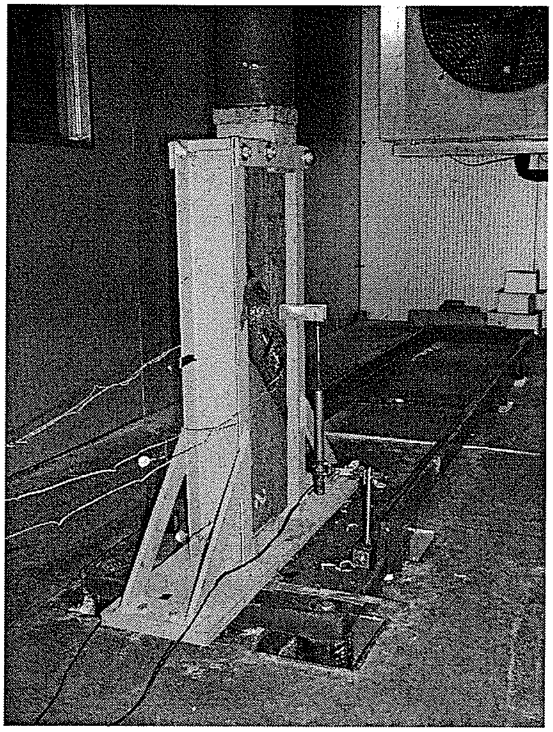

Figure 3.5: Test setup in Environmental Chamber

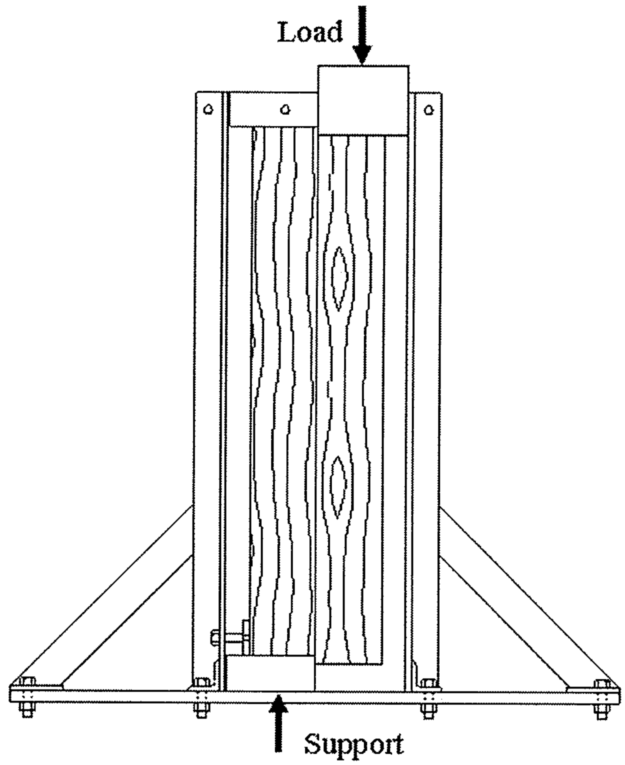

Figure 3.6: Load Frame [32]

chamber. The remaining samples were tested at ambient temperatures.

The specimens were loaded using a specially designed load frame to ensure proper alignment of the specimens with minimal horizontal movement. The frame was originally designed and first used by Gomez [32]. The frame utilizes two steel blocks, one underneath the fixed side of the specimen and the other attached to the loading head of the testing machine in order to apply a load to the non-fixed side of the specimen. Static loads were applied after the testing equipment was calibrated with a data acquisition system (DAQ). The load frame is shown in Figure 3.6.

ASTM D 198–99 [6] states that for static tests of lumber in structural sizes, maximum load should be achieved in about 10 minutes. ASTM D 143–94 [3] requires that for small clear specimens of timber in shear, the rate of loading should be 0.6 mm/min so that the small specimens fail very quickly. Therefore the rate of loading used ensured failure in approximately 5 to 10 minutes in accordance with ASTM Standards.

3.2.6 Instrumentation

The untreated specimens were instrumented with a pi-gauge to measure strain in the direction of the reinforcement. For the treated specimens, strain gauges were used to increase the accuracy of the results and measure strain in the actual reinforcement. The $S-T$ specimens were instrumented with 4–6 mm strain gauges, 2 on each sheet. The gauges were located approximately 50 mm apart and were centered with respect to the centerline of the specimen and were aligned parallel to the direction of the fibres. The dowel specimens had been previously instrumented with 3 strain gauges located at 20 mm, 100 mm, and 180 mm along the 200 mm bar before the bars were inserted into the specimens, as shown in Figure 3.7.

All 49 specimens were instrumented with 2 linear variable displacement transducers (LVDT's). One LVDT was placed on each side of the specimen and was centered in the middle of the non-fixed half of the specimen to measure vertical displacement relative to the fixed half of the specimen. See Figure 3.8 for the typical LVDT placement.

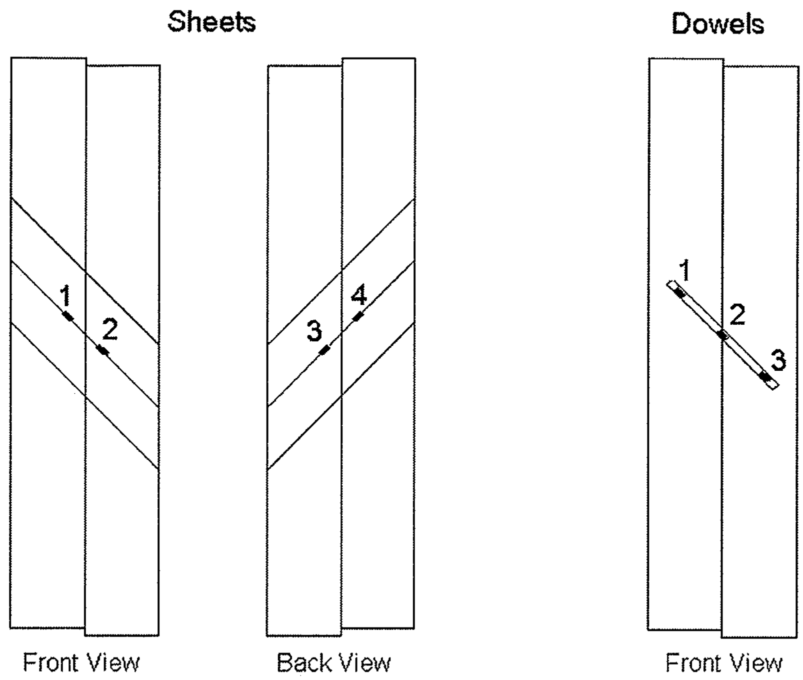

Figure 3.7: Strain Gauge Locations on $S-T$ and $D-T$ Specimens

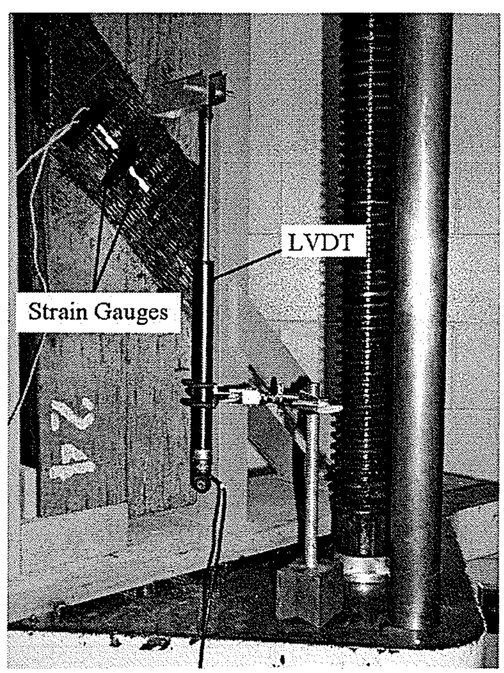

Figure 3.8: LVDT Set-up

3.3 Bending Tests

3.3.1 Material

Timber

The timber for the tests was purchased from Brown & Rutherford in Winnipeg. It was rough sawn coastal Douglas-fir and was graded No.2 & better. It was freshly cut and therefore had a high moisture content compared to timber that had been stored outdoors for a number of years and was allowed to dry out. The average moisture content of coastal Douglas-fir green wood is 37% in the heartwood and 115% in the sapwood [47]. The timber was not treated with creosote and therefore was much more susceptible to drying out than timber pressure treated with creosote.

GFRP

GFRP bars were used for flexural strengthening. The bars used were 5 mm Rotafix Rods composed of glass fibre and epoxy resin and are designed specifically for strengthening timber. The composition is 80% by weight of glass and 20% of epoxy resin. The rods provide high strength and rigidity, good flexural stress behaviour, and excellent corrosion resistance. The physical properties are shown in Table 3.6.

Table 3.6: Physical Properties of Rotafix GFRP Rods

Diameter mm	**Area** mm^2	**Tensile Modulus** GPa	**Ultimate Strength** MPa
5	25.0	40.0	1000

3.3.2 Test Specimens

Fifty-eight timber beams with dimensions of 2400 x 250 x 75 mm (8′ x 10″ x 3″) were used in this program. All beams were graded using the National Lumber Grades Authority (NLGA) Standard Grading Rules for Canadian Lumber [44]. Refer to Table A.7 for the grades for all the timber beams at the time of purchase. Of the 58 beams, 32 were graded as select structural, 7 as No.1, 13 as No.2, and 6 as Reject as shown in Table 3.7. Beams were graded using the Structural Joists and Planks classification which is for lumber 50 to 100 mm (2″ to 4″) thick and 125 mm (5″) and wider which is applicable for the beams tested in this research. Grading was based on split/checks, knots, slope of grain, and rate of grain. The knots and checks were the most common beam characteristics which led to a decrease in beam grade. Refer to Table 3.8 for the grading criteria for different defects. It should be noted that as the beams dried out, the checks and split sizes increased in the time between grading and actual testing.

Table 3.7: Original Beam Grades

Classification	**SS**	**No.1**	**No.2**	**Reject**	**Total**
C	12	1	3	2	**18**
$1B$	8	1	4	1	**14**
$2B$	4	0	1	1	**6**
$1B-D$	2	2	1	1	**6**
$2B-D$	6	3	4	1	**14**
Total	**32**	**7**	**13**	**6**	**58**

Table 3.8: Grading Criteria for Defects

Grade	**Knot Size**	**Split/Check Length**	**Rate of Growth**	**Slope of Grain**
SS	$2.625''/4'$	$10''$	4 rings/$''$	1:12
No.1	$3.25''/3'$	$10''$	4 rings/$''$	1:10
No.2	$4.25''/2'$	$15''$	NA	1:8
No.3	$5.5''/1'$	$16''$	NA	1:4
Reject	Greater than above criteria			

3.3.3 Reduction of Beam Grade

The timber beams were graded as No.2 and better. GFRP timber strengthening in the field is not practical or economical for high-grade timber stingers because these stringers will likely fail in compression, whereas the GFRP reinforcement increases the tensile strength of the beams. Therefore, providing flexural strengthening to high quality beams will not provide any significant increase in strength [36]. The grade of these beams was reduced in an attempt to observe a significant increase in strength from the control samples to the GFRP strengthened beams and to work with a pool of samples with the same grade. In order to decrease the flexural capacity of these beams, 38 mm (1.5″) diameter holes were drilled through the cross-section of the beams. The beam was divided into 8 – 300 mm (12″) sections. The four sections in the middle of the beam were divided into 20 locations using a grid system. Two holes were drilled at random locations in each section if no other significant defects were present. This procedure was developed based on the NLGA Standard Grading Rules for Canadian Lumber. The grading rule states that for structural joists and planks (50 to 100 mm thick, 125 mm and wider), No.3 grade beams with a nominal width of 250 mm are allowed a 75 mm diameter hole (any cause) or equivalent smaller holes per 300 mm. If knots already exist in the beam, the number of holes in that section may be reduced based on the following criteria that were developed for this project.

1. If knot does not go through the entire beam, it is disregarded

2. If the summation of all knots within the 300 mm zone is less than 1" in diameter on the most critical face of the beam, 2 holes are drilled in that zone

3. If the summation of all knots within the 300 mm zone is between 1" and 2", only one hole is drilled in that zone

4. If the summation of all knots within the 300 mm zone is greater than 2", no holes are drilled in the zone

The holes were drilled using a 38 mm auger bit. The holes located along the edge of the beam were drilled by clamping a 50 mm x 100 mm piece of wood to the side of the beam and drilling the hole half through the 50 mm x 100 mm piece of wood and half through the actual beam, as shown in Figure 3.9. The number of holes in each beam varied between 6 and 8, depending on the number, size, and location of pre-existing knots.

The other criteria that governed the selection of hole locations was the number of holes in any 300 mm section. Since a maximum of 2 holes were added to each 300 mm zone, the number of holes in a 300 mm distance could be more than 2 if adjacent zones have knots located close together. If this occurred, a maximum of 3 holes were allowed in a 300 mm section. If the 4th hole was also within the 300 mm zone, it was shifted horizontal to avoid such a critical zone in the beam. Refer to Figure 3.10 for an example of hole locations.

It should be noted that drilling holes to simulate knots in tension produces similar beam behaviour. The main difference is that the grain naturally "flows" around a knot, while a

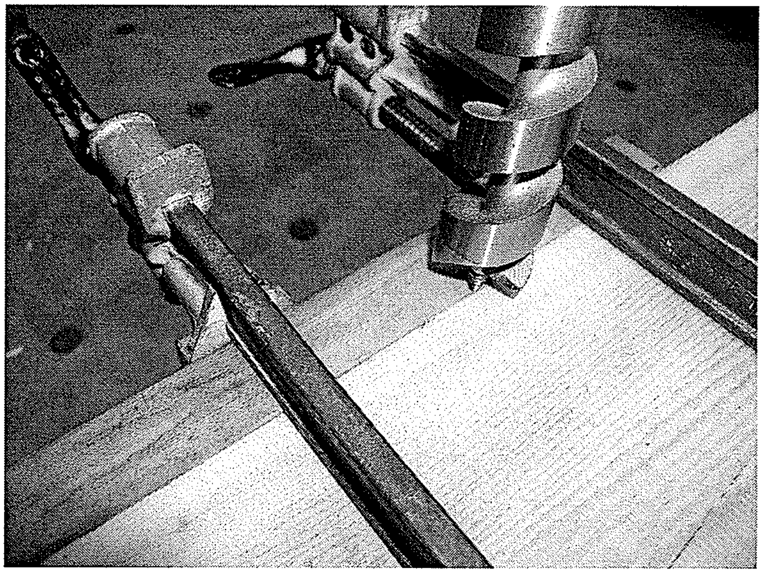

Figure 3.9: Drilling Hole Along Edge of Beam

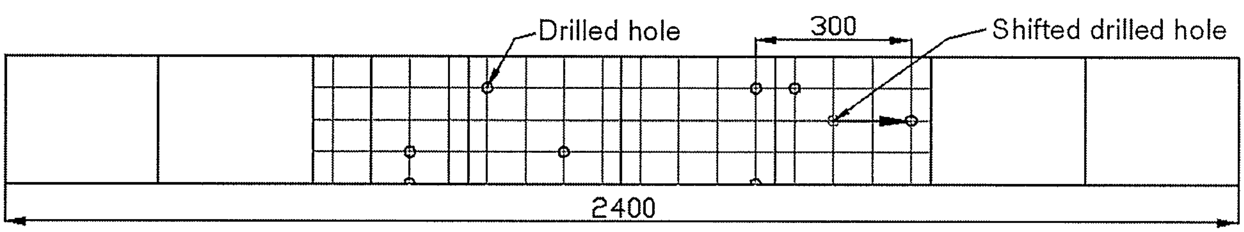

Figure 3.10: An Example of Random Hole Locations

hole cuts through the grain as indicted in Fridley [26]. In compression, it is recognized that there is little similarity in behaviour between knots and holes. The knots are still capable of taking significant compression forces, while holes are not. For this experimental program, this difference is noted. Nevertheless, this method may be used to reduce beam grade and generate beams of similar quality.

3.3.4 Strengthening of Beams

All beams were strengthened at the McQuade Structures Laboratory at the University of Manitoba by a local contractor, Speciality Construction. The beams were turned upside down and a groove was routed along the length. The grooves were cleaned with a brush and vacuum to remove all remaining debris to ensure a satisfactory bond between the timber and the epoxy. Of the 60 original beams, 20 were reinforced with 1–5 mm diameter GFRP Rotafix® rod and 20 were reinforced with 2–5 mm diameter GFRP Rotafix® rods along the bottom of the beam. Refer to Figure 3.11 for the specific groove dimensions and rod locations. It should be noted that for the two-bar strengthening scheme, both bars were placed in the same groove because the beam width was not large enough to accommodate grooves.

A two–part commercially available epoxy called Duralcrete® Gel was used to bond the Rotafix® rods to the timber. The Gel is high modulus epoxy paste adhesive with a 1:1 mix ratio and a moisture insensitive epoxy resin compound with a non-sag, paste consistency.

Refer to Table 3.9 for Duralcrete® Gel properties. The epoxy resin was squeezed into the grooves and the GFRP rods were then inserted into the epoxy. The epoxy was then leveled out so that it was flush with the bottom of the beam. The beam strengthening process is clearly shown in Figures 3.12 to 3.17.

The beams were not tested immediately following the drilling and strengthening process, and therefore suffered from drying out. Large splits developed in some beams that meant this shear strengthening was necessary. Lag bolts were used in an attempt to provide shear resistance to the beams. Four 200 mm (8″) long, 9.5 mm (3/8″) diameter steel lag bolts were drilled into the beam from the top. The lag bolts were spaced 200 mm and 400 mm respectively from each side of the beam. Several washers were use to prevent crushing of the wood. It should be noted that the first two beams tested ($C-13$ and $C-14$) only had one lag bolt. Both these beams failed in shear, which made the adding of two lag bolts to each beam a practical method of avoiding shear failures. Metal straps were also added to five of the later tests ($2B-1$, $2B-2$, $2B-3$, $2B-5$, and $2B-6$) to further increase the shear resistance. The straps were wrapped around the beams at approximately 10 mm and 30 mm from each end of the beam. These straps did not appear to make any significant difference, as 3 out of 5 of the strapped beams still failed in shear.

Ten of the first twenty strengthened beams tested failed in shear. Many of the shear failures occurred through the lag bolts, causing these bolts to bend. The addition of metal straps did not make a significant difference. Since these shear failures were undesirable in order to

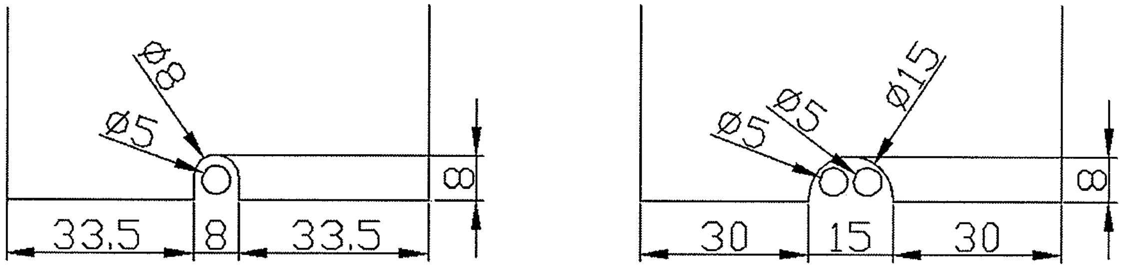

Figure 3.11: GFRP Rod Locations

Table 3.9: Duralcrete®Gel Properties

Ultimate Strength	Elongation at break	Modulus of Elasticity
48.6 MPa	2.5%	3171.9 MPa

Figure 3.12: Routing grooves along bottom of beam

Figure 3.13: Removing loose material with brush

Figure 3.14: Cleaning grooves with vacuum

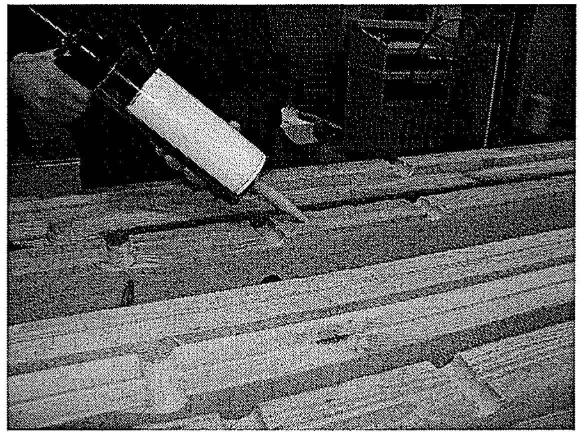

Figure 3.15: Filling grooves with epoxy

Figure 3.16: Inserting GFRP rods into epoxy–filled grooves

Figure 3.17: Smoothing out epoxy resin

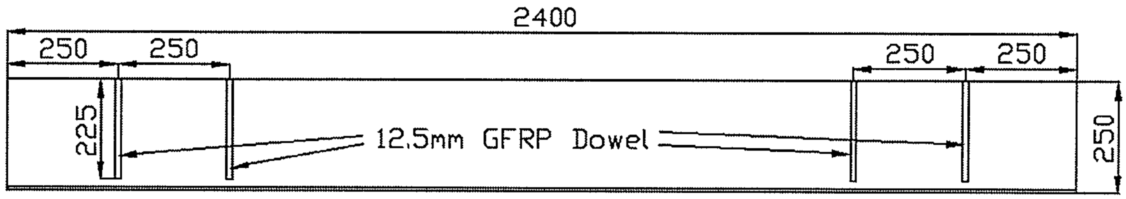

Figure 3.18: GFRP Dowel Locations

Table 3.10: Physical Properties of V-ROD^{TM} GFRP Dowels

Diameter mm	**Area** mm^2	**Tensile Modulus** GPa	**Ultimate Strength** MPa	**Shear Strength** MPa
12.5	126.7	46.4	791	220

investigate the minimum reinforcement ratio for beams in flexure, more shear strengthening was required.

The remaining 20 strengthened beams (6–1B and 14–2B) were strengthened with two 12.5 mm diameter V-ROD^{TM} GFRP dowels at each end, for shear reinforcement. The dowels were spaced a distance, 250 mm from the end of the beam. The dowel holes were drilled at 90° with a 19 mm (3/4″) auger bit to a depth of 225 mm. Refer to Figure 3.18 for the location of the dowels. The holes were cleaned with an air hose to ensure all wood debris was removed from the holes. Duralcrete® Gel was injected into the holes and 215 mm long dowels were inserted into the holes. The epoxy was smoothed out with a trowel. See Figures 3.19 to 3.22 for the strengthening procedure and Table 3.10 for the physical properties of the GFRP dowels.

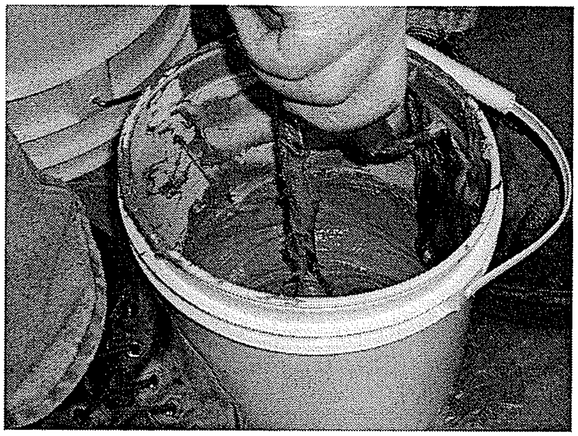

Figure 3.19: Mixing epoxy

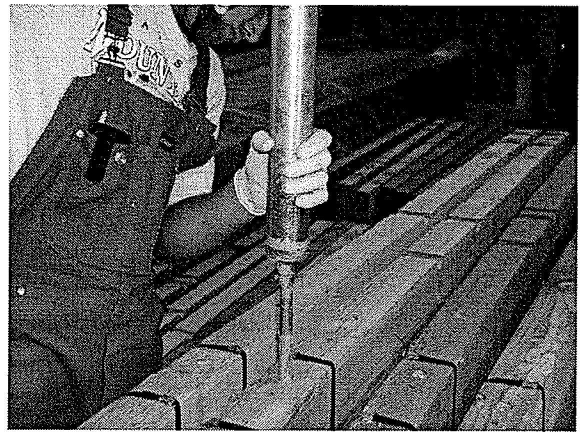

Figure 3.20: Filling grooves with epoxy

Figure 3.21: Inserting GFRP rods into epoxy–filled grooves

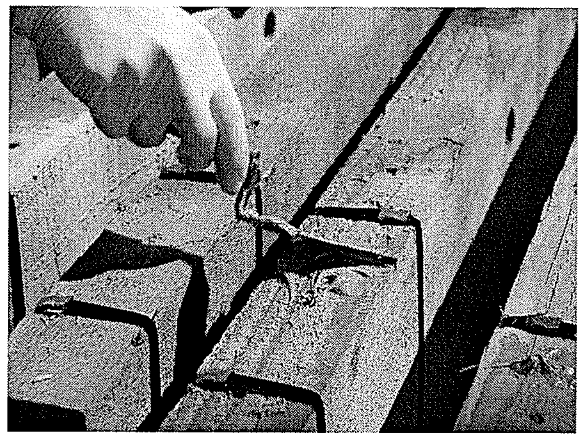

Figure 3.22: Smoothing out epoxy resin

Nine out of ten of the beams that had already failed in shear were re-strengthened in shear with the GFRP dowels with the intent to retest these beams and get flexural failures. Before the dowel holes were drilled, each end of the beam was clamped back together using two bar clamps to close any splits that occurred from the shear failure. Once clamped, two metal straps were placed around the beam at 100 mm and 300 mm respectively from each end of the beam to ensure the splits remained closed after the clamps were removed. The beams were then strengthened using the same procedure as the other 20 beams.

3.3.5 Test Setup

All of the timber beams were tested in the McQuade Structures Laboratory at the University of Manitoba. The beams were simply supported on rollers with a span of 2200 mm and subjected to 3-point bending. Two different testing machines were used for this experimental program due to laboratory equipment availability. A 1000 kN MTS machine was used for the first 38 tests and a 350 kN testing machine was used for the last 29 tests. Both machines applied a monotonically increasing load to the beams using a stoke-controlled load rate of 3 mm/minute in order to achieve the maximum load between 6 and 20 minutes. ASTM D 198–99 [6] states that for static tests of lumber in structural sizes, maximum load should be achieved in about 10 minutes. The maximum load should be reached in not less than 6 minutes and not more than 20 minutes. Bearing lengths of 200 mm were used at the end supports. A 500 mm bearing plate was used to distribute the concentrated load and prevent the crushing of the wood. Lateral support was provided at each end. Refer to Figures 3.23 to 3.26 for photographs of the two test setups.

3.3.6 Beam Instrumentation

Each beam was instrumented with 3 linear variable displacement transducers (LVDT's) to measure deflection at midspan and at quarter spans. LVDT's were attached to screws that were glued to the side face of the beams at mid-height.

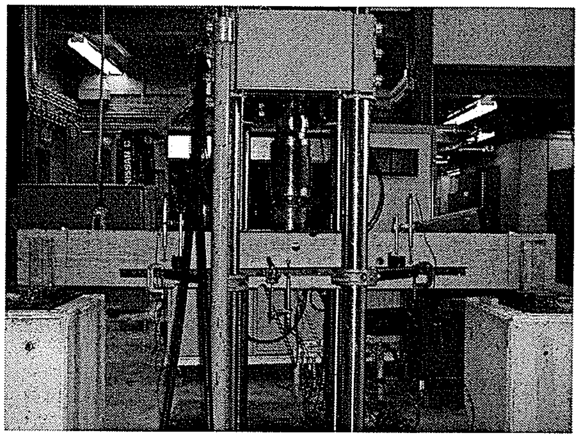

Figure 3.23: View #1 - 1000 kN MTS Machine Test Setup

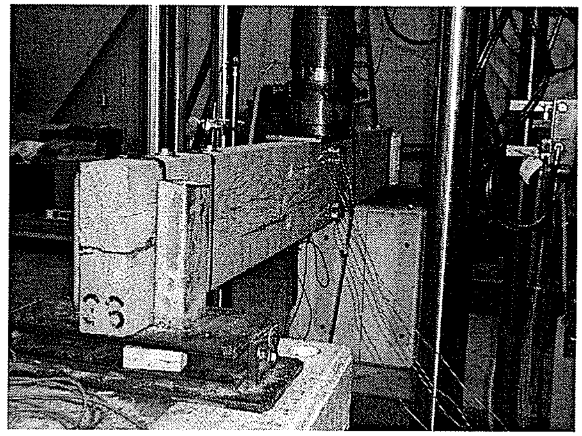

Figure 3.24: View #2 - 1000 kN MTS Machine Test Setup

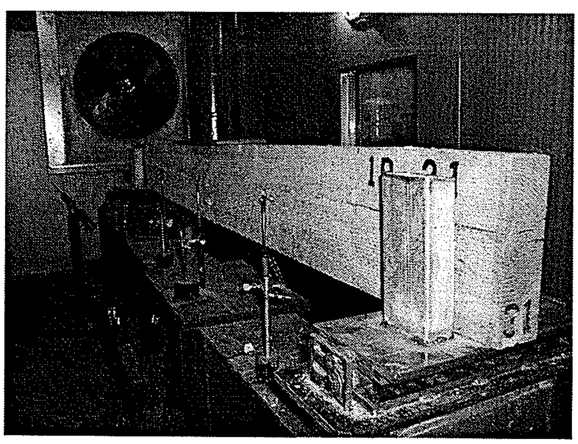

Figure 3.25: View #1 - 350 kN Machine Test Setup

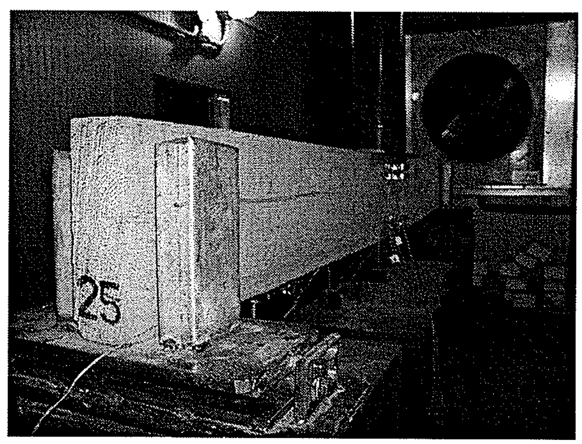

Figure 3.26: View #2 - 350 kN Machine Test Setup

Four 200 mm pi-gauges were used to measure the strains in the beam at midspan at different heights. The four pi-gauges were placed symmetrically 65 mm and 95 mm from the mid-height of the beam.

Of the 40 beams that were strengthened with GFRP rods, 11 were instrumented with one strain gauge at midspan along the rod. These gauges were used to compare the strains in the GFRP to the strain in the timber at midspan. Three beams were instrumented with 5 strain gauges along the GFRP rod to measure the variation in strains along the length of the rod. The gauges were installed at midspan, at quarter spans, and at 100 mm from either end of the rod. The rods were placed in the beams so that the strain gauges were facing the bottom of the beam. One, 50 mm strain gauge was installed on the bottom face of these 3 beams at midspan to measure the strain on the tension face of the timber and compare it to the strain in the rod.

All readings from the LVDT's, pi-gauges, and the machine load and stroke were recorded using a data acquisition system. Refer to Figure 3.27 for LVDT and pi gauge locations.

3.3.7 Moisture Content of Beams

The moisture of each beam was measured immediately after testing to ensure an accurate reading. Measurements were taken using the J-2000 moisture meter (manufactured by Delmhorst Instruments) which utilizes the principle of electrical resistance. Two pins are

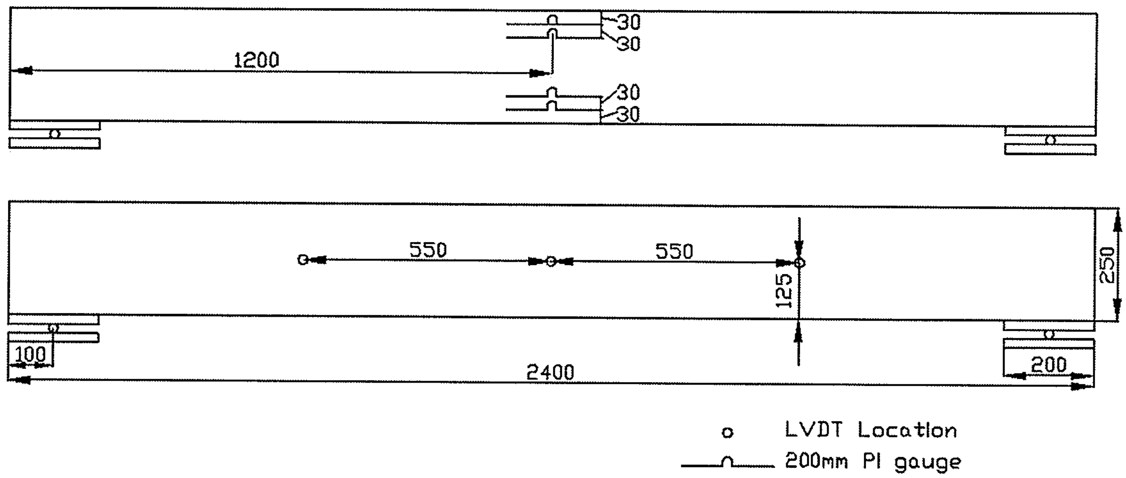

Figure 3.27: Beam Instrumentation

driven into a piece of wood which is capable of conducting electricity. The degree of conductivity varies depending on the moisture content of the wood. The meter allows the user to set the species of wood, the temperature in the room, and can accurately read values between 6% and 40%. Four moisture content readings were taken for each beam at different locations and the values were averaged to obtain an accurate representation of the moisture content.

The moisture content in the tested beam ranged from 15.4 to 34.1%. The major factor influencing the moisture content was the time of testing. As time progressed, the beams dried out and moisture content decreased. The last beam in the first group of beams was tested 85 days before testing began on the second group of beams. Therefore the second group had generally lower moisture contents. Tables 4.9, 4.10, and 4.11 shows the moisture content of the beams.

Chapter 4

Experimental Results and Analysis

4.1 General

This chapter is divided into two sections: (1) durability tests and (2) bending tests. In the first part of this section, results from the shear tests are presented, making comparisons between different strengthening schemes regarding modes of failure, ultimate strength and deflection behaviour, and rigidity. The second part of this section presents results from the bending tests and includes comparisons between the different reinforcement ratio with respect to modes of failure, load – deflection behaviour, rigidity, strains, and neutral axis location.

4.2 Durability Test Results

4.2.1 Accelerated Aging Effects

Cycling the samples for 24 weeks in the environmental chamber did not appear to have any affect on the strength of bond between GFRP and timber. A minimal amount of bleeding of the epoxy was observed on the sheet specimens midway through the cycling process. The dowel specimens did not experience any visible degradation.

4.2.2 Modes of Failure for S Samples

The specimens reinforced with sheets failed by debonding of the GFRP sheets from the timber. In order to understand the failure mechanisms, their possible modes of failure are considered.

1. Bond failure at the interface between the timber and epoxy (interface failure)
2. Failure away from interface in timber (wood failure)
3. GFRP ruptures longitudinally along the sheet

The American Institute of Timber Construction requires a minimum percent wood failure of 80% for dry tests (Barbero [9]). Consequently any samples that had an interface failure of

20% or less were classified as wood failures. The wood failure was divided into two categories, shallow and deep wood failure. A deep wood failure is several to many cells away from the timber-epoxy interface while a shallow wood failure is within the first one or two layers of cells beyond the interface [5].

Non–Treated Samples ($S - NT$)

The most common mode of failure was the interface failure (mode 1). In some cases mode 2 failures were observed. Four out of the eight samples had a wood failure on at least one debonded face, which shows a good bond at the interface between the timber and the GFRP. The mode of failure was not affected by the angle of the reinforcement from the sheets.

Treated Samples ($S - T$)

In the experimental program, failure mode 1 or 2 occurred, with failure mode 3 occurring simultaneously with modes 1 or 2 for several specimens. When the sheets debonded, anywhere from 20% to 90% of the sheet area was attached to timber fibres. There was no noticeable difference between the control samples and the samples that had been cycled in the chamber regarding the sheet surface area which had been covered in wood fibres. Eight of the 15 specimens had a wood failure on one of the two debonded faces. The majority of the samples experienced interface failures. Refer to Figures 4.1, 4.2, 4.3, and 4.4 for typical debonding failures and the variation in the amount of timber fibres that debonded with the

Figure 4.1: Debonded GFRP Sheet

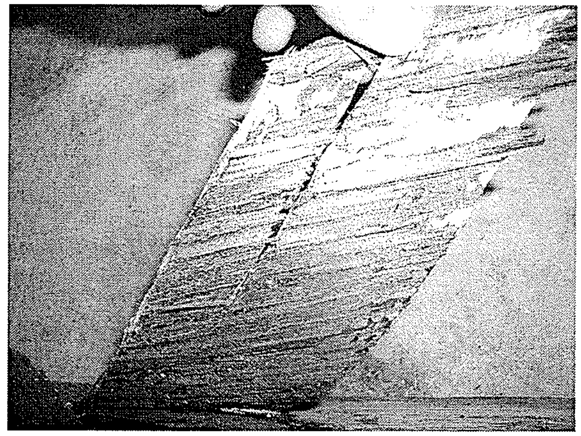

Figure 4.2: Debonded GFRP with Longitudinal Tear

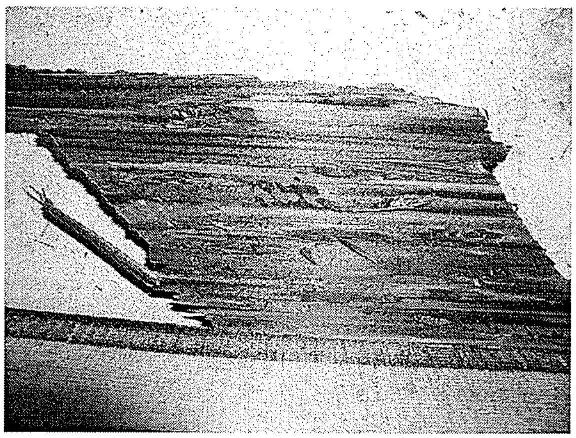

Figure 4.3: Debonded GFRP Sheet with lots of Timber Fibres attached

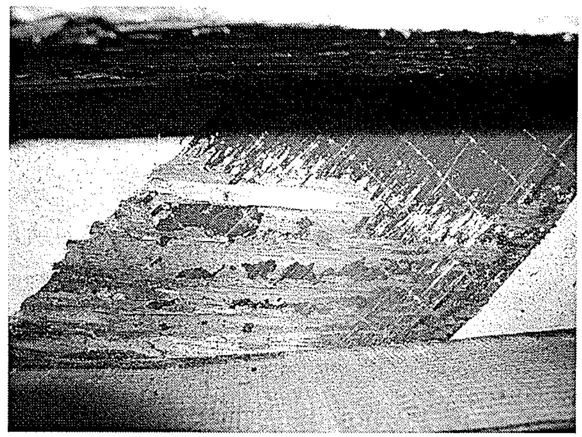

Figure 4.4: Debonded GFRP Sheet with very few Timber Fibres attached

sheets. Tables 4.1 and 4.2 show detailed failure mode observations. It should be noted that 'I' represents an interface failure and 'W' represents wood failure. The trend suggests that the treated samples had 6 to 10% more interface failure than the non-treated samples which suggests that the creosote negatively affects the interface bond. More testing is required to verify these results since a 20% standard deviation was observed.

Table 4.1: Failure Modes – Non-treated Samples

Sample	**Side**	**Wood Failure (%)**		**Interface Failure(%)**	**Failure Classification**
		Deep	**Shallow**		
$S-NT-30°-1$	1	20	50	30	I
	2	60	30	10	W
$S-NT-30°-2$	1	10	30	60	I
	2	-	-	-	-
$S-NT-30°-3$	1	20	20	60	I
	2	10	60	30	I
$S-NT-30°-4$	1	10	80	10	W
	2	-	-	-	-
Mean		**22**	**45**	**33**	
$S-NT-45°-1$	1	50	10	40	I
	2	-	-	-	-
$S-NT-45°-2$	1	0	80	20	W
	2	10	20	70	I
$S-NT-45°-3$	1	0	70	30	I
	2	0	70	30	I
$S-NT-45°-4$	1	0	90	10	W
	2	-	-	-	-
Mean		**10**	**57**	**33**	

Table 4.2: Failure Modes – Treated Samples

Sample	Side	Wood Failure (%)		Interface	Failure
		Deep	Shallow	Failure(%)	Classification
$S-T-C-1$	1	10	80	10	W
	2	0	70	30	I
$S-T-C-2$	1	0	50	50	I
	2	0	30	70	I
$S-T-C-3$	1	0	60	40	I
	2	10	60	30	I
$S-T-C-4$	1	10	40	50	I
	2	0	30	70	I
$S-T-C-5$	1	0	90	10	W
	2	0	70	30	I
Mean		**3**	**58**	**39**	
$S-T-H-1$	1	10	40	50	I
	2	0	60	40	I
$S-T-H-2$	1	10	30	60	I
	2	0	40	60	I
$S-T-H-3$	1	10	70	20	W
	2	10	70	20	W
$S-T-H-4$	1	0	20	80	I
	2	0	50	50	I
$S-T-H-5$	1	50	40	10	W
	2	10	50	40	I
Mean		**10**	**47**	**43**	
$S-T-L-1$	1	10	40	50	I
	2	0	90	10	W
$S-T-L-2$	1	0	70	30	I
	2	0	30	70	I
$S-T-L-3$	1	0	90	10	W
	2	0	50	50	I
$S-T-L-4$	1	0	50	50	I
	2	10	20	70	I
$S-T-L-5$	1	20	60	20	W
	2	-	-	-	-
Mean		**4**	**56**	**40**	

4.2.3 Modes of Failure for D Samples

The dowel reinforced specimens failed by several different failure mechanisms. The likely modes of failure for the dowels in shear are:

1. Pull-out of the dowels from the epoxy
2. GFRP rupture
3. Localized compression failure of the timber around the dowels

Non–Treated Samples ($D-NT$)

All 30° and 45° samples failed by GFRP rupture in shear. The failures were sudden with very little deformation. The 30° samples experienced larger deformations than the 45° samples, possibly due to localized compression failure. The 90° samples failed by localized compressive failure followed by dowel pull-out.

Treated Samples ($D-T$)

Of the 15 tested dowel specimens, 2 failed by a brittle, GFRP rupture (Figure 4.5). The other 13 samples failed in a ductile manner; this type of failure is often difficult to characterize because of its internal nature. Several dowel specimens were cut in half for visual inspection of the dowel. No shear failures of dowels were observed. Localized compression

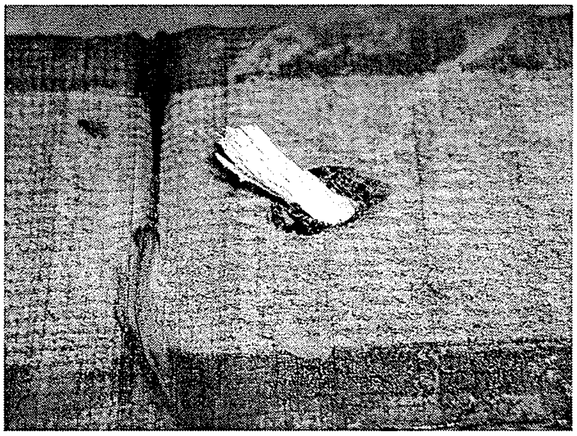

Figure 4.5: Rupture of GFRP dowel

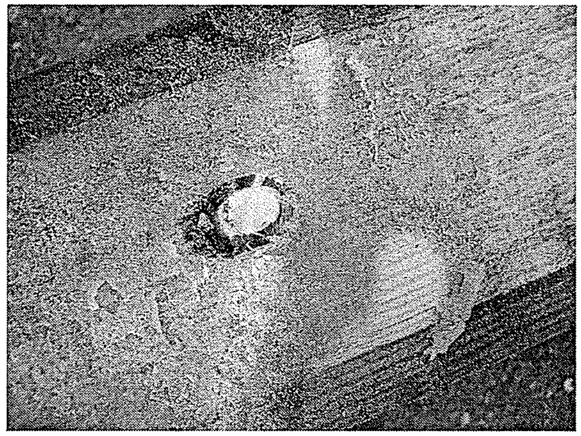

Figure 4.6: Dowel Specimen Failure Mode – Compression of Wood Fibres and Epoxy

failure of the wood around the dowel is the likely mode of failure (Figure 4.6), leading to significant deformation of the specimen from its original position.

If the specimens were loaded considerably beyond the peak load, the GFRP dowels are likely to have ruptured. Specimens 9, 13, 19, 23, and 29 possibly experienced dowel slip prior to failure, as is suggested by the top strain gauge, which stopped working prior to failure, because of the large strains.

4.2.4 Data Analysis

In the following, test results for the untreated samples strengthened with GFRP sheets will be compared with respect to sheet configurations. The untreated samples will be compared to the treated samples and the aged samples will be compared to the control samples. For the GFRP dowels, comparisons will be made for different reinforcement angles, creosote treatment, and environmental exposure.

GFRP Sheets

In most cases the sheets debonded in the middle of the sample, causing the load to drop. The load was then re-distributed and the specimens were able to support a higher load. The ultimate failure always occurred when the sheet completely debonded from the side that was not wrapped around the corner of the specimen as shown in Figure 4.1.

The average ultimate load for the untreated samples was 80.8 kN for the $S-NT-30\,^{\circ}$ samples compared to 57.8 kN for the $S-NT-45\,^{\circ}$ samples. The $S-NT-30\,^{\circ}$ samples carried 28% more load, however they also had a 30% higher reinforcement ratio and used 30% more material compared to the $S-NT-45\,^{\circ}$ samples, making the performance of the reinforcing schemes comparable based on the amount of material used. Therefore the aging tests were performed on the $45\,^{\circ}$ samples that used less material. The $S-NT-30\,^{\circ}$ samples were 38% more ductile than the $S-NT-45\,^{\circ}$ samples, deforming an average of 4.5 mm at ultimate load compared to 2.8 mm for the $S-NT-45\,^{\circ}$ samples.

The average ultimate load for the treated samples ($S-T-C$) that all had a $45\,^{\circ}$ reinforcement scheme was 41.9 kN compared to 57.8 kN for the untreated samples ($S-NT-45\,^{\circ}$). The $S-T-C$ samples had a larger cross-section compared to the $S-NT$ samples which provided a smaller reinforcement ratio compared to the $S-NT$ samples. The area of the sheets used was very similar for the two groups, and since only the sheets resist the load, the reduction in load carrying capacity is only due to the negative impact of the creosote treatment. The treated and untreated samples experienced very similar deformations regardless of treatment history. The $S-T-C$ samples experienced an average deformation of 2.7 mm, which is very similar to what the $S-NT-45^\circ$ samples experienced.

The samples that were aged in the environmental chamber behaved similarly to the control samples and therefore it appears that the accelerated aging did not affect the strength of the samples. The $S-T-H$ specimens had an average ultimate load of 39.4 kN with an average deformation of 2.9 mm, while the $S-T-L$ specimens had an average ultimate load of 41.9 kN with a deformation of 2.4 mm. These results are very similar to the $S-T-C$ results. It should be noted that several LVDT readings from the $S-T-L$ tests appear highly variable due to problems of keeping the LVDT's from freezing up during the tests. Details of these tests are given in Table 4.3.

The strain gauges on the sheets were used to verify the location of debonding. There was always higher strain around the areas that debonded. Therefore strain gauges have applications in the field to monitor the bond between FRP sheets and timber in locations that are difficult to monitor by visual inspection. There are two major drawbacks to the strain gauges:

1. Debonding does not appear to occur at a specific strain, and therefore will vary de-

Table 4.3: Shear Test Results – Sheet Samples

Sample[a]	**Pmax** [kN]	**Deformation** [mm]	**Max Strain** [%]
$S-NT-30°-1$	86	6.6	NA
$S-NT-30°-2$	70	2.8	NA
$S-NT-30°-3$	79	5.8	NA
$S-NT-30°-4$	88	2.8	NA
Average	**80.8**	**4.5**	NA
$S-NT-45°-1$	47	1.6	NA
$S-NT-45°-2$	59	6.1	NA
$S-NT-45°-3$	57	0.9	NA
$S-NT-45°-4$	68	2.6	NA
Average	**57.8**	**2.8**	NA
$S-T-C-1$	43.7	2.1	0.84
$S-T-C-2$	29.6	5.2	0.89
$S-T-C-3$	53.0	2.1	1.46
$S-T-C-4$	47.9	2.4	1.47
$S-T-C-5$	35.3	1.6	0.86
Average	**41.9**	**2.7**	**1.10**
$S-T-H-1$	33.9	2.9	1.34
$S-T-H-2$	45.8	3.5	0.76
$S-T-H-3$	39.9	3.1	0.84
$S-T-H-4$	37.9	2.0	0.68
$S-T-H-5$	39.5	3.1	0.64
Average	**39.4**	**2.9**	**0.85**
$S-T-L-1$	39.3	2.7	0.55
$S-T-L-2$	40.1	6.2	0.75
$S-T-L-3$	35.9	1.4	0.61
$S-T-L-4$	49.5	0.8	1.03
$S-T-L-5$	44.8	0.9[b]	0.83
Average	**41.9**	**2.4**	**0.75**

[a]All non-treated samples tested by Gomez (2006)

[b]LVDT 2 froze up in the chamber, therefore only LVDT 1 was used for deformation.

pending on the physical properties of the timber and the epoxy bond.

2. If the strain gauge is not positioned at the exact location of debonding, the magnitude of the strain gauge reading will be lower.

The average maximum strain for the $S-T-H$ samples was 0.85% and 0.75% for the $S-T-L$ specimens, which are less than the $S-T-C$ value of 1.10%. It is difficult to draw any conclusion from this observation since there were no definite patterns in the readings. Since different testing machines were used for the samples; the rate of loading may have impacted the strains. See Tables A.1, A.2, and A.3 in the Appendix for detailed strain gauge readings.

The results show that the creosote timber affects the bond strength of the GFRP–timber interface. It should be noted that installers had difficulty wrapping the sheets around the corner of the specimens, because of little contact between the sheets and the timber in some areas, possibly leading to the initial de-bonding in the middle of the sheet. The 24-week accelerated aging program did not appear to impact the bond strength of the specimens that were cycled in terms of ultimate load capacity.

GFRP Dowels

The average ultimate load for the $D-NT-30\,^{\circ}$ samples was 40.0 kN compared to 32.5 kN for the $D-NT-45\,^{\circ}$ samples. The samples with a $30\,^{\circ}$ reinforcement angle had 19% more strength and used a 29% higher reinforcement ratio. The $D-NT-30\,^{\circ}$ samples deformed 4.4 mm at ultimate load compared to 4.7 mm for the $D-NT-45\,^{\circ}$ samples.

The average ultimate load taken by the $D-T-C$ samples was 35.8 kN, compared to 32.5 kN for the untreated samples ($D-NT-45\,^{\circ}$). The small variation in strength may be attributed to the 26% greater surface area that the $D-T$ samples had compared to the untreated samples. The small frictional forces on this surface area may have also impacted the strength of the specimens. The deformation of the $D-T-C$ specimens was 4.6 mm, which was comparable to the untreated samples.

The load carrying capacities of the dowel specimens subjected to accelerated aging were slightly less than those of the control specimens. The $D-T-H$ samples carried an average load of 29.0 kN with a deformation of 5.7 mm while the $D-T-L$ samples carried an average of 33.9 kN with a deformation of 3.3 mm. The aged samples carried an average of 12% less load than the control samples. The average maximum strains were 0.72% for $D-T-C$ samples, 1.14% for $D-T-H$ samples, and 0.85% for $D-T-L$ samples. The variability of these strains makes it very difficult to draw any meaningful conclusions. Refer to Table 4.4 for complete results and Figures 4.7 to 4.12 for load-deflection curves for the treated samples. Table 4.5 shows a summary of the results from the shear tests. Tables A.4, A.5, and A.6 in Appendix show detailed strain gauge results for the samples.

Table 4.4: Shear Test Results – Dowel Samples

Sample[a]	Pmax [kN]	Deformation [mm]	Max Strain [%]
$D-NT-30°-1$	37	3.9	NA
$D-NT-30°-2$	40	4.2	NA
$D-NT-30°-3$	43	5.1	NA
Average	**40.0**	**4.4**	NA
$D-NT-45°-1$	29	6.6	NA
$D-NT-45°-2$	35	2.8	NA
$D-NT-45°-3$	33	5.8	NA
$D-NT-45°-4$	33	2.8	NA
Average	**32.5**	**4.5**	NA
$D-NT-90°-1$	27	15.8	NA
$D-NT-90°-2$	32	18.5	NA
$D-NT-90°-3$	27	15.8	NA
$D-NT-90°-4$	27	19.5	NA
Average	**28.3**	**17.4**	NA
$D-T-C-1$	27.4	5.2	0.87
$D-T-C-2$	33.9	3.9	1.45
$D-T-C-3$	45.7	5.2	0.47
$D-T-C-4$	36.3	4.4	0.60
$D-T-C-5$	35.5	4.2	0.21
Average	**35.8**	**4.6**	**0.72**
$D-T-H-1$	31.5	4.7	2.12
$D-T-H-2$	32.8	4.8	0.64
$D-T-H-3$	28.5	6.1	0.99
$D-T-H-4$	28.1	6.6	0.98
$D-T-H-5$	24.0	6.6	0.96
Average	**29.0**	**5.7**	**1.14**
$D-T-L-1$	31.7	3.4	0.16
$D-T-L-2$	36.0	3.9	0.42
$D-T-L-3$	40.3	4.8	1.33
$D-T-L-4$	20.0	1.2	0.27
$D-T-L-5$	41.4	3.4	-2.05[b]
Average	**33.9**	**3.3**	**0.85**

[a]All non-treated samples tested by Gomez (2006)
[b]Absolute strains were used to obtain average values

Table 4.5: Shear Test Results – Summary

Sample	Pmax [kN]	Deformation [mm]	Max Strain [%]
$S - NT - 30\,°$	80.8	4.5	NA
$S - NT - 45\,°$	57.8	2.8	NA
$S - T - C$	41.9	2.7	1.10
$S - T - H$	39.4	2.9	0.85
$S - T - L$	41.9	2.4	0.75
$D - NT - 30\,°$	40.0	4.4	NA
$D - NT - 45\,°$	32.5	4.5	NA
$D - T - C$	35.8	4.6	0.72
$D - T - H$	29.0	5.7	1.14
$D - T - L$	33.9	3.3	0.85
$D - NT - 90\,°$	28.3	17.4	NA

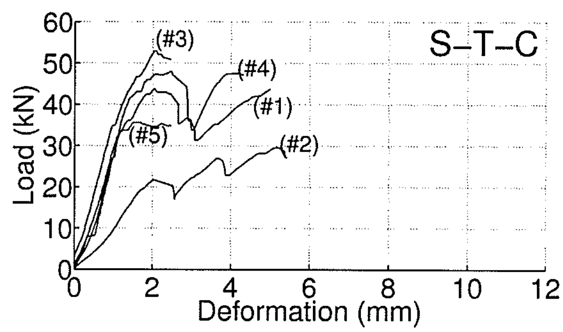

Figure 4.7: Behaviour of control sheet reinforced samples

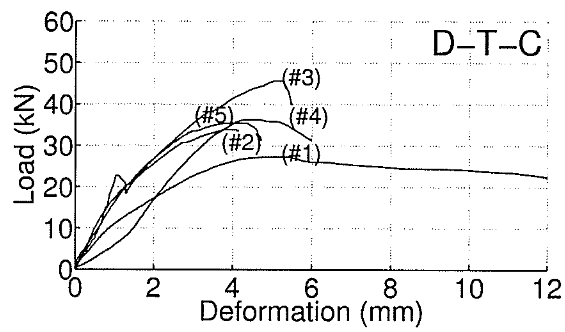

Figure 4.8: Behaviour of control dowel reinforced samples

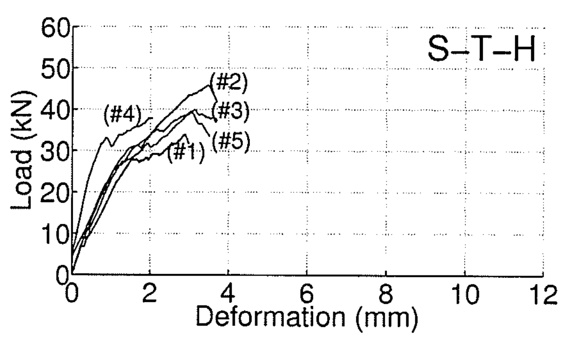

Figure 4.9: Behaviour of sheet reinforced samples subjected to +40 °C

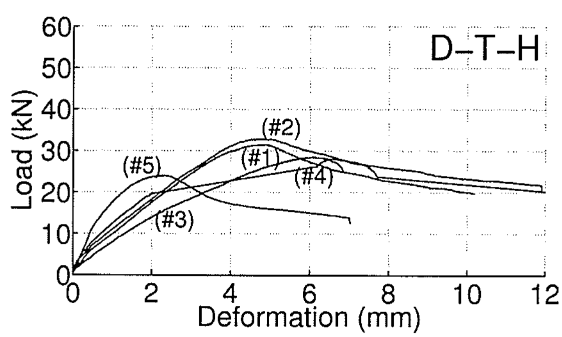

Figure 4.10: Behaviour of dowel reinforced samples subjected to +40 °C

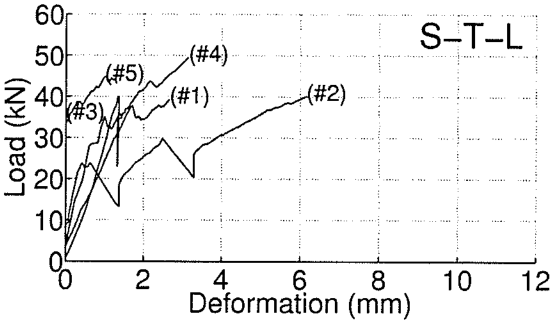

Figure 4.11: Behaviour of sheet reinforced samples subjected to −20 °C

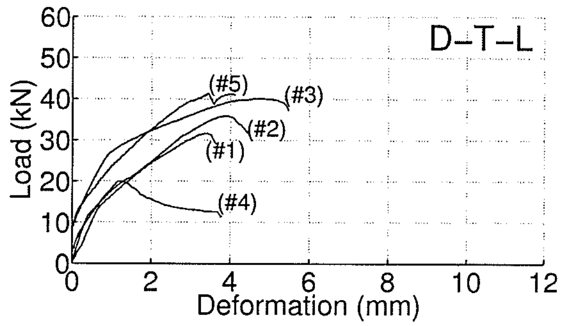

Figure 4.12: Behaviour of dowel reinforced samples subjected to −20 °C

4.2.5 Rigidity of Samples

Rigidity is an important physical property of a timber beam; in particular the stiffness of the specimens determines how effectively the two materials, namely GFRP and timber work together. The average load/deformation ratio was 0.258 kN/m for the $S - NT - 45\,^{\circ}$ samples and varied from 0.022 to 0.069 kN/m for the treated sheet specimens. It can be seen that the creosote treated specimens had an average stiffness of only 16.7% that of the untreated samples, thus indicating the lack of bond between the FRP sheet and the creosote-treated timber. The samples tested at −20 °C behaved more rigidly than the other samples, however there was no conclusive difference between the control samples and samples tested under +40 °C. Refer to Table 4.6 for rigidity results for all of the sheet specimens.

Table 4.7 shows detailed rigidity values for all of the dowel samples as well as average values for the different reinforcement and exposure types. The average rigidity was 0.026 kN/m for the $D - NT - 45\,^{\circ}$ specimens and ranged from 0.013 to 0.026 kN/m for the treated dowel samples. The dowel samples tested at −20 °C behaved more rigidly than the other samples,

Table 4.6: Rigidity of Sheet Samples

Sample	Pmax [kN]	Deformation @ 10kN [mm]	Load/Deformation [kN/m]
$S-NT-30°-1$	86	0.021	0.469
$S-NT-30°-2$	70	0.027	0.375
$S-NT-30°-3$	79	0.019	0.538
$S-NT-30°-4$	88	0.012	0.870
Average	**80.8**	**0.020**	**0.512**
$S-NT-45°-1$	47	0.035	0.282
$S-NT-45°-2$	59	0.030	0.337
$S-NT-45°-3$	57	0.051	0.195
$S-NT-45°-4$	68	0.007[a]	1.395[a]
Average	**57.8**	**0.039**	**0.258**
$S-T-C-1$	43.7	0.502	0.020
$S-T-C-2$	29.6	1.049	0.0095
$S-T-C-3$	53	0.264	0.038
$S-T-C-4$	47.9	0.575	0.017
$S-T-C-5$	35.3	0.406	0.025
Average	**41.9**	**0.559**	**0.022**
$S-T-H-1$	33.9	0.476	0.021
$S-T-H-2$	45.8	0.301	0.033
$S-T-H-3$	39.9	0.360	0.028
$S-T-H-4$	37.9	0.123	0.081
$S-T-H-5$	39.5	0.434	0.023
Average	**39.4**	**0.339**	**0.037**
$S-T-L-1$	39.3	0.304	0.033
$S-T-L-2$	40.1	0.068	0.147
$S-T-L-3$	35.9	0.138	0.072
$S-T-L-4$	49.5	0.422	0.024
$S-T-L-5$	44.8	-0.013[b]	-0.769
Average	**41.9**	**0.233**	**0.069**

[a]Not used in calculations
[b]Not used in calculations

however there was no significant difference between the $D-T-H$ and the $D-T-C$ samples.

Table 4.7: Rigidity of Dowel Samples

Sample	Pmax [kN]	Deformation @ 10kN [mm]	Load/Deformation [kN/m]
$D-NT-30°-1$	37	0.225	0.044
$D-NT-30°-2$	40	0.229	0.044
$D-NT-30°-3$	43	0.233	0.043
Average	**40.0**	**0.229**	**0.044**
$D-NT-45°-1$	29	0.383	0.026
$D-NT-45°-2$	35	0.308	0.032
$D-NT-45°-3$	33	0.446	0.022
$D-NT-45°-4$	33	0.383	0.026
Average	**32.5**	**0.380**	**0.026**
$D-NT-90°-1$	27	0.412	0.024
$D-NT-90°-2$	32	0.594	0.017
$D-NT-90°-3$	27	0.483	0.021
$D-NT-90°-4$	27	0.535	0.019
Average	**28.3**	**0.506**	**0.020**
$D-T-C-1$	27.4	0.887	0.011
$D-T-C-2$	33.9	0.503	0.020
$D-T-C-3$	45.7	0.606	0.017
$D-T-C-4$	36.3	1.489	0.0067
$D-T-C-5$	35.5	0.600	0.017
Average	**35.8**	**0.817**	**0.014**
$D-T-H-1$	31.5	1.062	0.0094
$D-T-H-2$	32.8	0.897	0.011
$D-T-H-3$	28.5	1.347	0.0074
$D-T-H-4$	28.1	0.732	0.014
$D-T-H-5$	24.0	0.435	0.023
Average	**29.0**	**0.895**	**0.013**
$D-T-L-1$	31.7	0.496	0.020
$D-T-L-2$	36.0	0.333	0.030
$D-T-L-3$	40.3	0.060[a]	0.167
$D-T-L-4$	20.0	0.344	0.029
$D-T-L-5$	41.4	0.045[a]	0.222
Average	**33.9**	**0.391**	**0.026**

4.3 Bending Tests

A total of 67 beams were tested in bending. The different strengthening schemes and notations used are as follows: 18 as control beams (C), 14 strengthened with 1 bar ($1B$), 6 strengthened with 2 bars ($2B$), 6 strengthened with 1 bar and dowels ($1B-D$), 14 strengthened with 2 bars and dowels ($2B-D$), and 9 previously tested beams repaired by adding dowels ($F-1B$ or $F-2B$).

4.3.1 Duration of Tests

The target time for the duration of each of the tests was 10 minutes, with a desired range of 6 to 20 minutes. These numbers are based on the time to reach the ultimate load. The load rate of 3 mm/min produced desirable loading times. Table 4.8 lists the average time duration for tests on various beams. The average duration of loading for the tests was between 7 and 8 minutes for all tests with the exception of the $F-1B$ and $F-2B$ beams. The shortest duration of test was 2.5 minutes for $C-18$ and the greatest was 12.9 minutes for $C-1$, demonstrating the large variability of timber beam behaviour.

The $F-1B$ and $F-2B$ beams had less rigidity and more deflection, and therefore the duration of these tests was greater. The average test duration for these beams was 20.4 and 18.1 minutes for the $F-1B$ and $F-2B$ beams respectively. The range in the duration for the failed beams was 13.1 to 29.3 minutes. There was no correlation between the mode of failure and the duration of load. For future testing, the rate of loading could be reduced to 3.5 or 4 mm/min in order to prevent beams from failing in under 6 minutes. The majority of the beams that failed in under 6 minute were control beams and there were only 3 beams that reached their maximum load in under 5 minutes, showing that the rate of loading was sufficient.

Table 4.8: Duration of Tests Summary

Specimen Classification	**Duration [minutes]**
C	7.5
$1B$	7.0
$2B$	8.0
$1B-D$	7.1
$2B-D$	7.8
$F-1B$	20.4
$F-2B$	18.1

4.3.2 Load - Deflection Behaviour

Control Beams

Eighteen control beams were tested as part of this experimental program. Twelve of the beams failed in either tension or compression. These beams had an average ultimate load of 38.6 kN and an average deflection of 22.3 mm. The ultimate loads ranged from 20.6 kN to 58.7 kN, with three beams failing under a load smaller than 25 kN and five under 35 kN.

The six beams that failed in shear are relatively insignificant when drawing conclusions regarding the bending strength of the timber because they failed in shear. It is noted that the average ultimate load for these beams was 40.3 kN, with no beam failing under a load smaller than 30 kN. It is concluded that these beams had a flexural capacity exceeding their shear failure load. Results are shown in Table 4.9 and load-deflection graphs are shown in Figures 4.13 and 4.14 for both tension and shear failures.

Table 4.9: Control Beams - Results

Specimen Classification	**Ultimate Load [kN]**	**Deflection [mm]**	**Stiffness, EI [N-mm^2]**	**Mode of Failure**	**Moisture Content (%)**
$C-1$	44.2	37.4	702	Tension	31
$C-3$	20.6	16.9	503	Compression	26
$C-4$	24.2	27.5	653	Tension	30
$C-7$	34.2	15.1	495	Tension	25
$C-8$	20.7	6.5	728	Tension	28
$C-10$	58.7	50.8	783	Compression	26
$C-11$	37.2	11.5	743	Tension	29
$C-12$	43.2	19.3	805	Tension	26
$C-15$	45.7	29.7	714	Compression	27
$C-16$	49.9	15.7	838	Tension	23
$C-17$	54.4	28.5	695	Tension	24
$C-18$	30.5	9.1	768	Tension	24
Average	**38.6**	**22.3**	**702**		**27**
$C-2$	39.0	20.7	770	Shear	28
$C-5$	50.9	20.6	805	Shear	27
$C-6$	32.7	13.5	556	Shear	30
$C-9$	47.1	22.5	611	Shear	19
$C-13$	34.7	26.6	642	Shear	33
$C-14$	37.5	13.9	752	Shear	27
Average	**40.3**	**19.6**	**689**		**27**

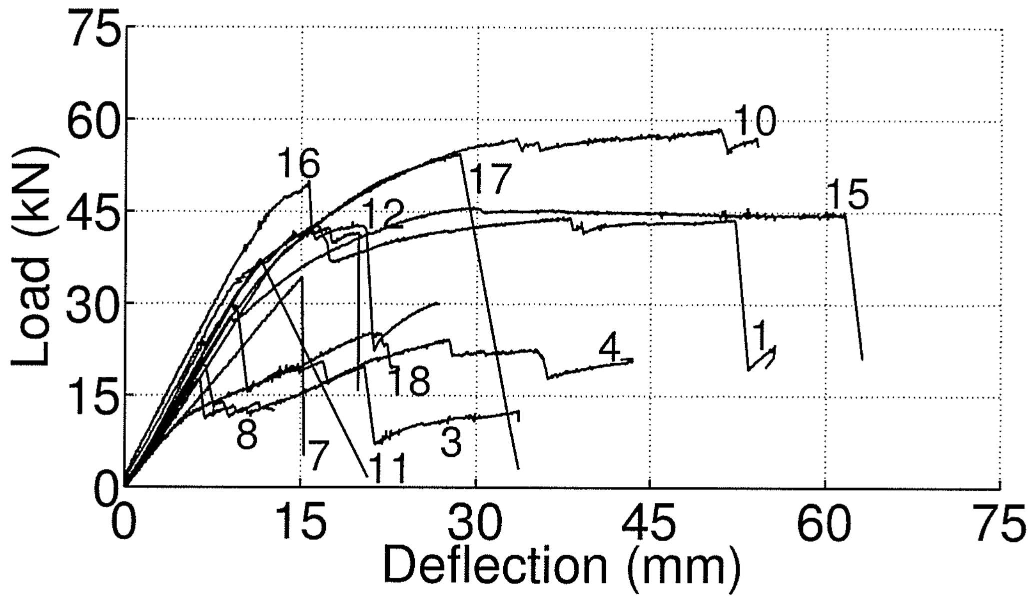

Figure 4.13: Results from control beams that failed in tension

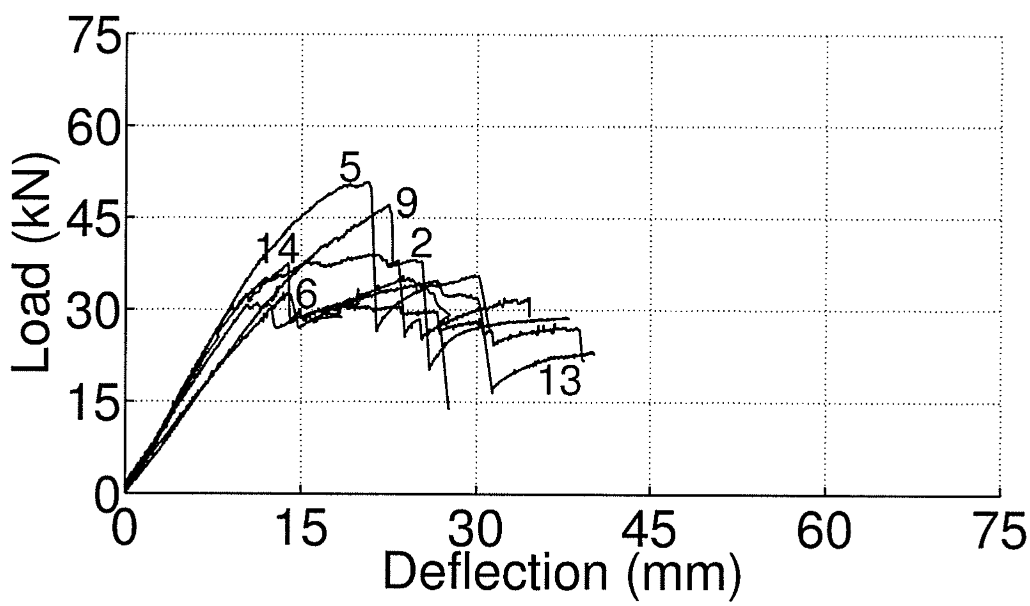

Figure 4.14: Results from control beams that failed in shear

Beams Strengthened for Flexure Only

Twenty beams were strengthened with 1 or 2 GFRP bars for flexural reinforcement. Half of these beams failed in tension and the other half failed in shear. The average ultimate load for the $1B$ and $2B$ beams that failed in tension were 49.8 kN and 48.8 kN respectively, a 29% and 26% respective increase over the control beams. The minimum ultimate load was 41.6 kN, over twice that of the minimum control beam. The $1B$ and $2B$ beams had an average deflection of 18.5 mm and 16.0 mm respectively.

The beams that failed in shear had average ultimate loads of 50.7 kN and 52.7 kN for $1B$ and $2B$ beams respectively. These beams had a minimum load of 36.0 kN. Refer to Table 4.10 for individual beam results and Figures 4.15 to 4.18 for load-deflection curves in which tension and shear failures are separated.

Beams Strengthened for Flexure and Shear

Twenty beams were strengthened with both shear and flexural reinforcement. Six beams had 1 flexural bar and dowels and 14 beams had 2 flexural bars and dowels. There were 2 tension failures for the $1B-D$ beams, while there were 7 tension failures for the $2B-D$ beams. The average ultimate loads were 42.4 kN and 55.0 kN for the $1B-D$ and $2B-D$ beams respectively, with a minimum ultimate load of 42.1 kN. These two sets of beams had an average deflection of 15.9 mm and 19.8 mm respectively. There were only two tension

Table 4.10: Flexural Strengthened Beams - Results

Specimen Classification	Ultimate Load [kN]	Deflection [mm]	Stiffness, EI [N-mm^2]	Mode of Failure	Moisture Content (%)
$1B-2$	55.3	20.6	701	Tension	28
$1B-7$	56.3	24.6	696	Tension	21
$1B-8$	57.0	22.1	670	Tension	24
$1B-10$	41.6	14.3	685	Tension	21
$1B-11$	49.3	14.5	810	Tension	26
$1B-12$	41.9	16.7	651	Tension	26
$1B-14$	47.1	16.4	843	Tension	24
Average	**49.8**	**18.5**	**722**		**24**
$1B-1$	45.9	21.4	576	Shear	34
$1B-3$	54.2	20.5	824	Shear	24
$1B-4$	61.5	19.4	836	Shear	30
$1B-5$	50.6	17.4	724	Shear	28
$1B-6$	55.3	20.9	743	Shear	24
$1B-9$	36.0	17.0	638	Shear	30
$1B-13$	51.2	16.3	758	Shear	25
Average	**50.7**	**19.0**	**728**		**28**
$2B-4$	61.0	18.1	843	Tension	26
$2B-5$	42.9	13.1	763	Tension	25
$2B-6$	42.5	16.9	631	Tension	24
Average	**48.8**	**16.0**	**745**		**25**
$2B-1$	36.5	31.2	601	Shear	29
$2B-2$	62.3	27.8	726	Shear	26
$2B-3$	59.4	22.3	833	Shear	25
Average	**52.7**	**27.1**	**720**		**27**

failures in the $1B-D$ group, therefore no conclusive results could be reported in terms of strength increase in comparison with the control group. However the minimum load was still significantly higher (104%) than the minimum load for the control beams.

The beams that failed in shear had average ultimate loads of 53.3 kN and 55.2 kN for $1B-D$ and $2B-D$ beams respectively. These beams had a minimum load of 39.9 kN and

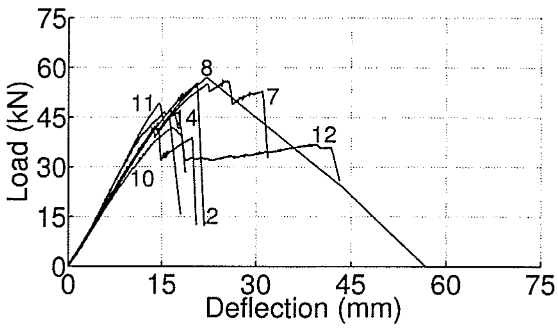

Figure 4.15: Results from $1B$ Beams that failed in tension

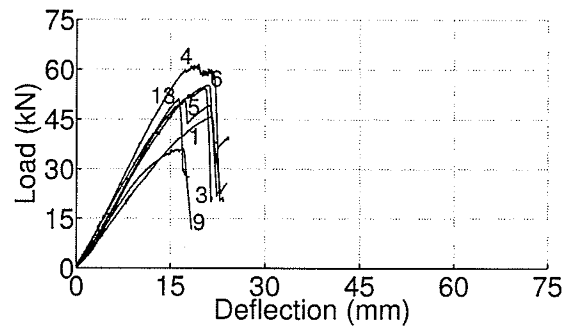

Figure 4.16: Results from $1B$ Beams that failed in shear

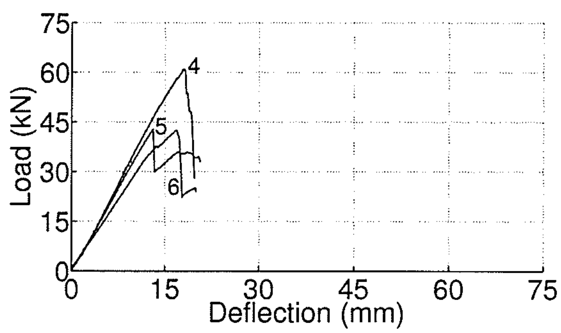

Figure 4.17: Results from $2B$ Beams that failed in tension

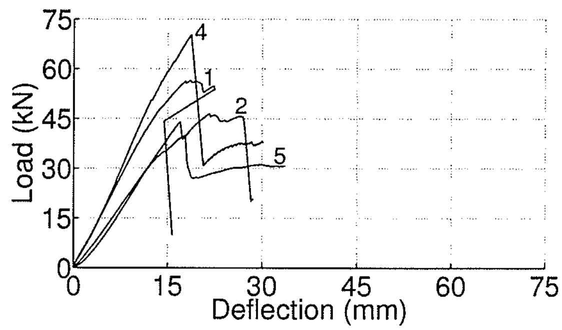

Figure 4.18: Results from $2B$ Beams that failed in shear

a maximum load of 70.2 kN. Detailed results are shown in Table 4.11 and load-deflection graphs for both tension and shear failures are shown in Figures 4.19 to 4.22.

Summary

In this experimental program, flexural reinforcement has been proven to increase the flexural capacity of timber beams. There is a small difference in strength between using 1 or 2 GFRP bars. These results suggest that 2 GFRP bars increase the flexural capacity of the beams by 5 kN in comparison to the flexural capacity of beams with only one GFRP bar. The most

Table 4.11: Flexural and Shear Strengthened Beams - Results

Specimen Classification	Ultimate Load [kN]	Deflection [mm]	Stiffness, EI [N-mm^2]	Mode of Failure	Moisture Content (%)
$1B-D-3$	42.8	15.6	641	Tension	17
$1B-D-6$	42.1	16.1	613	Tension	15
Average	**42.4**	**15.9**	**627**		**16**
$1B-D-1$	56.5	18.6	822	Shear	22
$1B-D-2$	46.5	21.6	655	Shear	23
$1B-D-4$	70.2	18.7	969	Shear	18
$1B-D-5$	39.9	17.8	596	Shear	26
Average	**53.3**	**19.2**	**761**		**22**
$2B-D-1$	46.2	17.6	610	Tension	23
$2B-D-3$	43.9	18.8	581	Tension	21
$2B-D-5$	63.2	24.9	759	Tension	23
$2B-D-6$	67.4	26.2	742	Tension	22
$2B-D-7$	60.3	18.1	759	Tension	18
$2B-D-13$	49.7	19.6	653	Tension	20
$2B-D-14$	54.3	18.5	748	Tension	26
Average	**55.0**	**20.5**	**693**		**22**
$2B-D-2$	66.7	26.4	702	Shear	22
$2B-D-4$	45.5	17.5	650	Shear	23
$2B-D-8$	48.1	16.7	651	Shear	21
$2B-D-9$	46.2	19.8	620	Shear	21
$2B-D-10$	46.6	14.3	798	Shear	22
$2B-D-11$	63.4	19.9	928	Shear	22
$2B-D-12$	69.9	23.8	965	Shear	23
Average	**55.2**	**19.8**	**759**		**22**

important consideration is that both the $1B$ and the $2B$ strengthening schemes perform their function by reducing the variability in the results and increasing the minimum ultimate loads carried by the beams. A results summary is shown in Table 4.12. It should be noted that the tension failures are of main interest for this experimental program which is meant to investigate the flexural strengthening schemes. The results from the shear failures do give an indication that these beams had flexural strengths higher than the ultimate loads, which

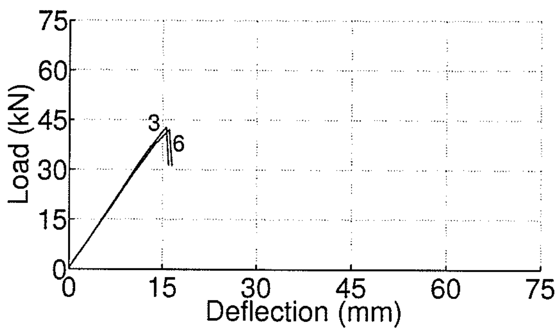

Figure 4.19: $1B - D$ Beams - Tension

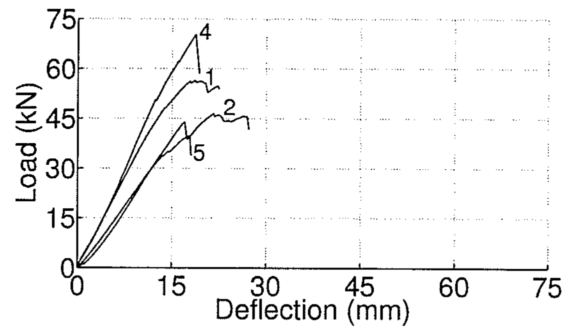

Figure 4.20: $1B - D$ Beams - Shear

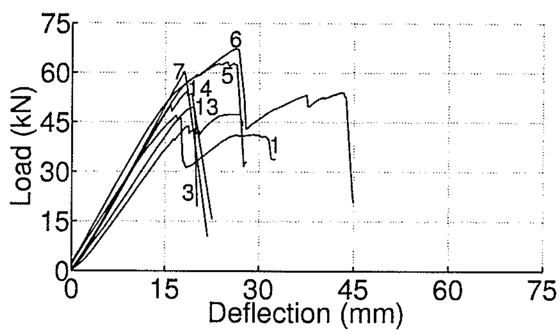

Figure 4.21: $2B - D$ Beams - Tension

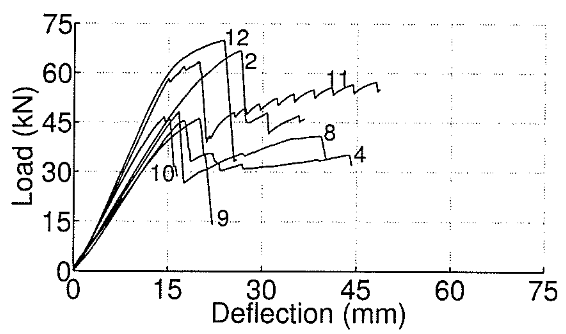

Figure 4.22: $2B - D$ Beams - Shear

confirms the effectiveness of the GFRP bars, which had an average ultimate load greater than 50 kN for all four strengthening schemes.

Beams Repaired after Failure

Nine previously tested beams were strengthened in shear using GFRP dowels. The dowels did not perform as well as anticipated and eight out of the nine beams failed in shear. The only beam that did not fail in shear ($F-1B-1$) still experienced considerable shear deformation along the existing shear plane. The existing shear planes of all nine beams re-opened, and could not be held together by the GFRP dowels.

Table 4.12: Results Summary

Specimen Classification	Ultimate Load [kN]	Deflection [mm]	Sample Size
Tension Failures			
C	38.6	22.3	12
$1B$	49.8	18.5	7
$2B$	48.8	16.0	3
$1B-D$	42.4	15.9	2
$2B-D$	55.0	20.5	7
Shear Failures			
C	40.3	19.6	6
$1B$	50.7	19.0	7
$2B$	52.7	27.1	3
$1B-D$	53.3	19.2	4
$2B-D$	55.2	20.5	7

The $F-1B$ and $F-2B$ beams had average ultimate loads of 40.5 kN and 37.1 kN respectively. The GFRP dowels were not effective in shifting the failure mode of the beams and the ultimate load was not able to surpass the ultimate load for the corresponding beams in the previous tests. The ultimate loads were still higher than for the control beams, which show that the GFRP strengthening is working to increase the load carrying capacity. The minimum ultimate load was 27.0 kN, which was still a 24% increase from the lowest strength of control beam.

The average deflections were over 50 mm for both the $F-1B$ and $F-2B$ beams, which was 100% more than in the previous tests. The addition of GFRP dowels did not enhance the stiffness of these beams. The average stiffness was 311 N-mm^2 and 352N-mm^2 for the $F-1B$ and $F-2B$ beams respectively. Refer to Table 4.13 for complete results and Table 4.14 for a comparison of the $F-1B$ and $F-2B$ beams to the original test results for these beams.

Load-deflection curves are shown in Figures 4.23 and 4.24.

Table 4.13: Previously Failed Beams - Results

Specimen Classification	Ultimate Load [kN]	Deflection [mm]	Stiffness, EI [N-mm^2]	Mode of Failure	Moisture Content (%)
$F-1B-1$	35.9	49.6	267	Tension	16
$F-1B-2$	40.0	59.3	289	Shear	19
$F-1B-3$	45.6	35.7	536	Shear	18
$F-1B-4$	44.5	67.7	237	Shear	18
$F-1B-5$	27.0	47.0	206	Shear	17
$F-1B-6$	48.7	73.0	350	Shear	21
Average	**40.5**	**55.4**	**314**		**18**
$F-2B-1$	39.0	20.7	232	Shear	20
$F-2B-2$	50.9	20.6	386	Shear	20
$F-2B-3$	32.7	13.5	468	Shear	16
Average	**37.1**	**52.4**	**329**		**19**

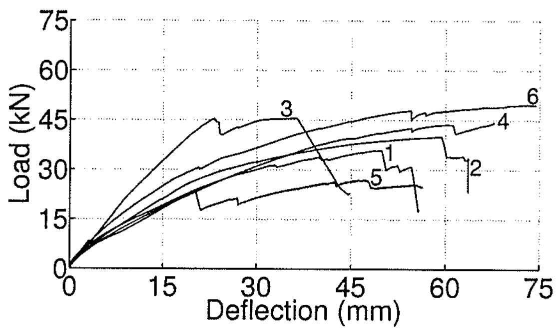

Figure 4.23: $F-1B$ Beams

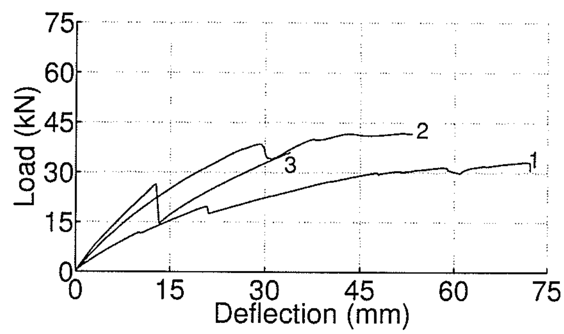

Figure 4.24: $F-2B$ Beams

4.3.3 Beam Stiffness

The stiffness of the beams was calculated by solving Equation 4.1 for EI within the linear portion of its load – deflection graph. For simplicity, linear beam behaviour was assumed to be from 25 - 50% of maximum load for all 58 beams. For the 9 repaired beam, linear beam

Table 4.14: Results Comparison - Restrengthened, Failed Beams to Original Beam Tests

Specimen Classification	**Repaired Beams - % of Original Value**		
	Ultimate Load	**Deflection**	**Stiffness, EI**
$F-1B-1$	78%	232%	46%
$F-1B-2$	74%	289%	35%
$F-1B-3$	74%	184%	64%
$F-1B-4$	88%	389%	32%
$F-1B-5$	49%	225%	28%
$F-1B-6$	97%	448%	46%
Average	**77%**	**294%**	**42%**
$F-2B-1$	91%	229%	39%
$F-2B-2$	67%	186%	39%
$F-2B-3$	61%	152%	56%
Average	**73%**	**189%**	**45%**

behaviour was assumed to be from 20 - 35% since these beam had a lower stiffness as shown in Figures 4.23 and 4.24.

$$\Delta = \frac{P\ell^3}{48EI} \tag{4.1}$$

The control beams had an average stiffness of 698 N-mm, whereas all of the strengthened beams had an average stiffness of 726 N-mm for the $1B$, $2B$, $1B-D$, and $2B-D$ beams combined. This constituted an increase of 4% compared to the control beams which is relatively insignificant. The addition of dowels to the beams did not increase the stiffness of the beams. The failed beams that were re-strengthened had a considerably lower average stiffness of 319 N-mm for $F-1B$ and $F-2B$ combined results. The current FRP strengthening technique is not effective for increasing beam stiffness. The small area of the FRP and the fact that timber area is removed to make room for the FRP means that the beam area is not changing, and therefore FRP strengthening does very little to improve the timber stiffness. Table 4.15 shows a summary of the average beam stiffness for all tested samples for each strengthening scheme. The stiffness was not separated for different modes of failure because beam stiffness is based on linear-elastic beam behaviour.

Table 4.15: Beam Stiffness Summary

Specimen Classification	**Stiffness, EI [N-mm^2]**	**Sample Size**
C	698	18
$1B$	725	14
$2B$	733	6
$1B - D$	716	6
$2B - D$	726	14
$F - 1B$	314	6
$F - 2B$	329	3

4.3.4 Strains

Strain in GFRP reinforcement is an important indicator of beam performance. Fourteen strengthened beams were instrumented with a strain gauge on each GFRP bar. Figure 4.25 shows the load vs. strain plots for these bars. There is no significant difference between the two reinforcement ratios. The strains in the bars were linear until a load of at least 35 kN in all beams with the exception of one of the $1B$ specimens. The noticeable increase in GFRP bar strain could be attributed to either higher strain than the strain gauges were capable of measuring or yielding of the timber, which would produce higher strains in the bars.

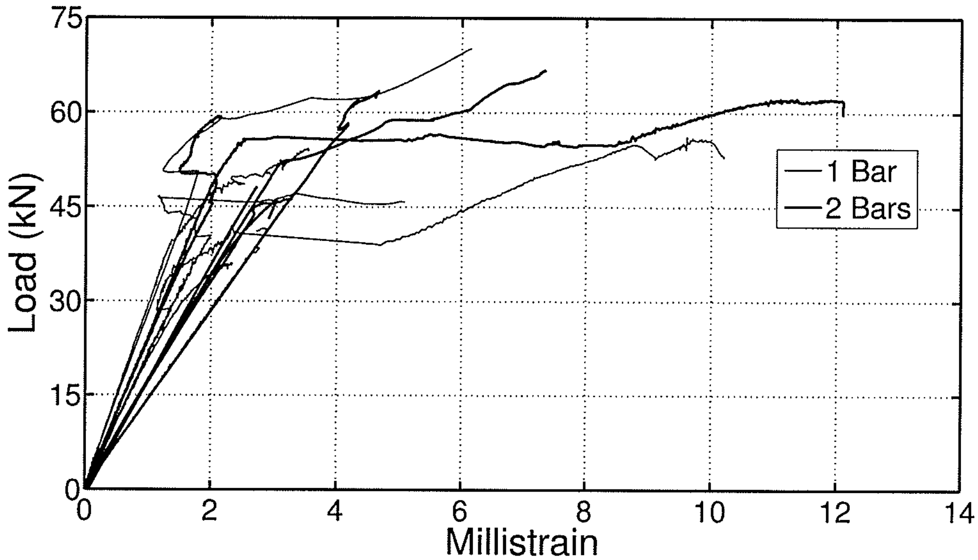

Figure 4.25: Load vs. Strain for GFRP Bars

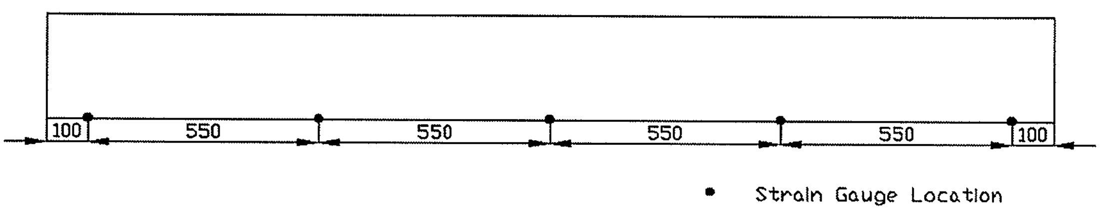

Figure 4.26: Strain Gauge Locations Along Length of Beam on GFRP Bar

Three beams were instrumented with 5 strain gauges along the GFRP bar and 1–50 mm strain gauge on the bottom face of the timber at midspan. This instrumentation was to determine if the strain in the bars varied linearly along the length of the bars. Strain gauges 1 to 5 were located at 100 mm, 650 mm, 1200 mm, 1750 mm, and 2300 mm respectively along the beam as shown in Figure 4.26. It should be noted the several of the gauges were not working properly and were therefore left out from the results.

For beam $1B - D - 4$, strain gauge 4 was not working, while the gauge readings from the remaining locations corresponded quite well to each other. Strains 1 and 5 were relatively similar, especially below the load of 30 kN. Strain 3 and the timber gauge were very similar up to 50 kN when there was a small crack in the tension face of the beam, that caused the strains in the GFRP to increase more rapidly. The timber gauge showed smaller strain due to the fact that the timber with the strain gauge may have been separated from the rest of the beam due to a crack, as shown in Figure 4.27. Figure 4.28 shows a relatively linear increase in load until ultimate load is reached. There are small changes in the slope of the graph at 50 kN and again at 62 kN, which are corresponding to the changes in strain shown in Figure 4.27.

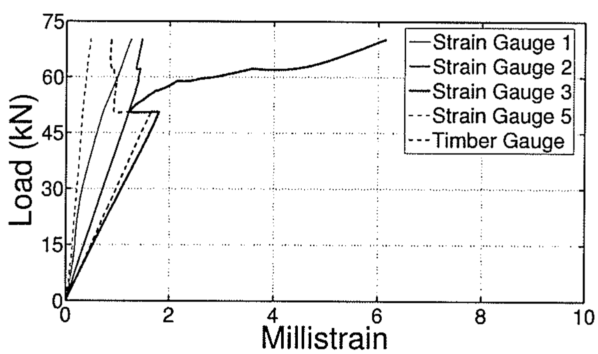

Figure 4.27: Strain Gauge Readings in GFRP Bar for Beam $1B - D - 4$

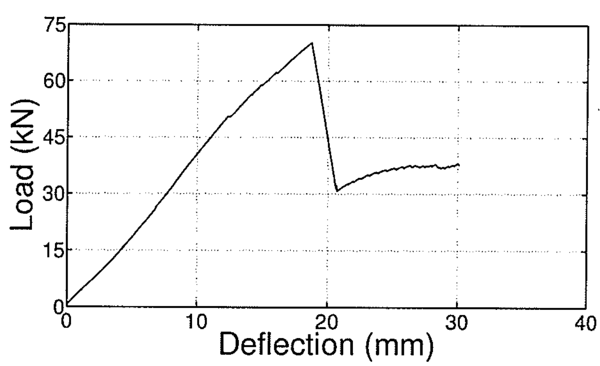

Figure 4.28: Load vs. Deflection for $1B - D - 4$

Figure 4.29 shows the neutral axis (N.A) location at 25%, 50%, 75%, and 100% of ultimate load. The N.A. remains relatively constant throughout loading and drops slightly as the load approaches the ultimate. The pi gauge readings correspond very well to the best fit line used to determine the N.A. for each graph.

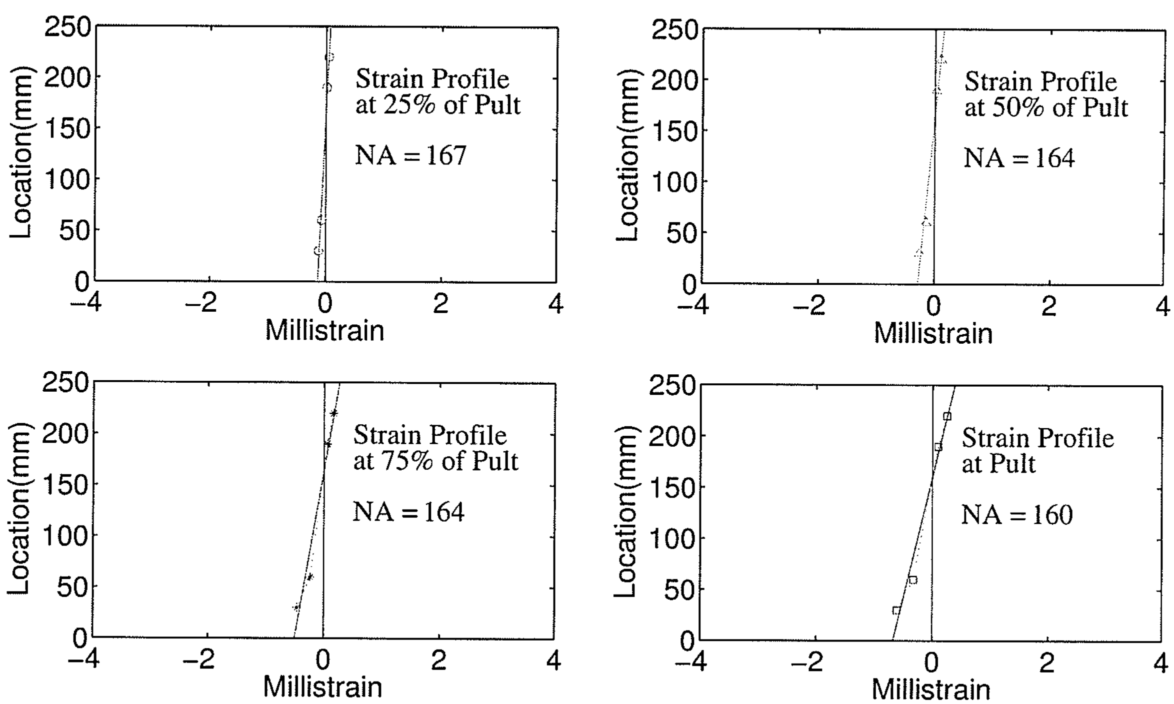

Figure 4.29: Strain Profile at Midspan for $1B - D - 4$ at Various Loads

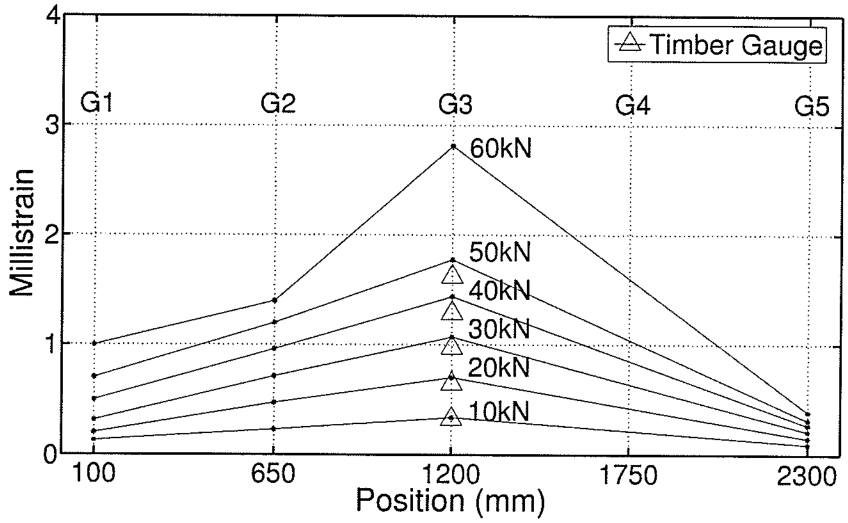

Figure 4.30: Strain Profile in GFRP Bar for Beam $1B - D - 4$

The strain profile along the length of the beam shows a linear relationship along the beam, with the highest strains near the middle of the beam and a large jump in strain between 50 kN and 60 kN. There is more strain near the 100 mm position in comparison to the 2300 mm position as shown in Figure 4.30. This beam failed in shear at the 100 mm side of the beam, which corresponds to the higher strains on this side of the beam.

Beam $1B-D-6$ had several strain gauges that were not working. Both gauges at the ends of the beams did not work. Because these gauges were over the supports, the supports may have damaged the gauges. The timber strain gauge was also defective and did not provide any readings. Strains 2 and 4 at the quarter spans corresponded very well to each other as shown in Figure 4.31. The slightly higher values of strain 2 compared to strain 4 was due to the tension failure of the beam, which originated from a tension crack very close to the location of strain gauge 2. Strain 3 produced the largest strains as expected and the strains increased linearly until ultimate load. The load vs. deflection plot in Figure 4.32 shows that the load increased relatively linearly until failure at around 42 kN.

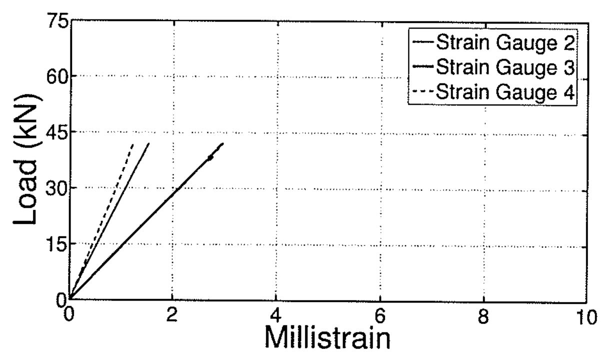

Figure 4.31: Strain Gauge Readings in GFRP Bar for Beam $1B-D-6$

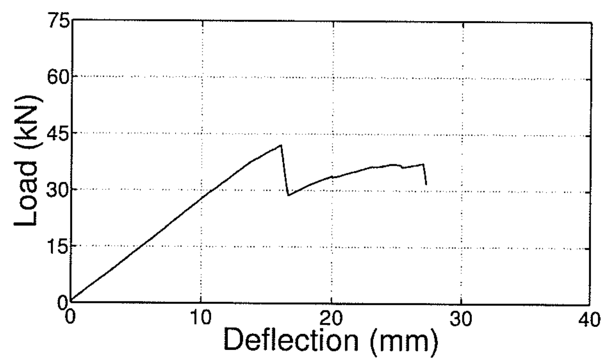

Figure 4.32: Load vs. Deflection for $1B-D-6$

The strain profiles at midspan as depicted in Figure 4.33 show very little movement of the N.A. as the load is increased. The N.A. drops slightly as the loading approaches the ultimate load. The strain profile along the length of the beam is shown in Figure 4.34 and shows the highest strains at midspan along the beam.

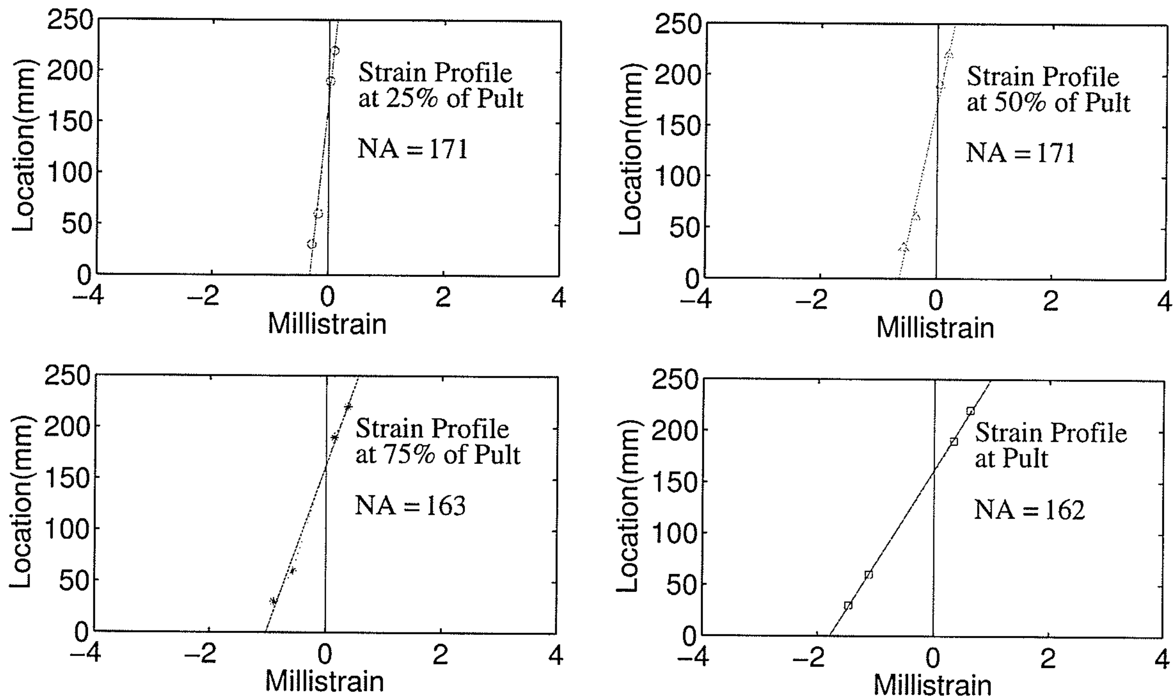

Figure 4.33: Strain Profile at Midspan for $1B - D - 6$ at Various Loads

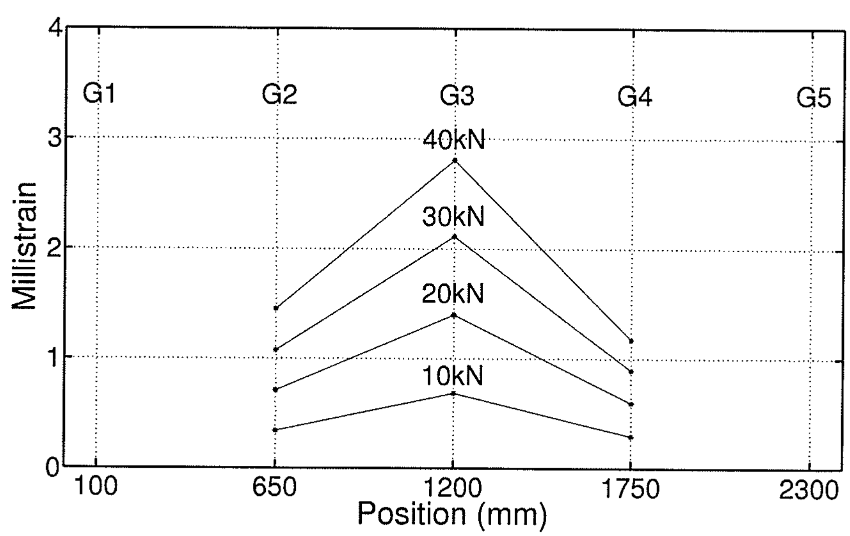

Figure 4.34: Strain Profile in GFRP Bar for Beam $1B - D - 6$

Beam $2B-D-2$ shows similar results to the other beams and had one malfunctioning strain gauge (G2). Strain gauge 3 and the timber gauge had very similar strains until the load was just over 50 kN, as shown in Figure 4.35. This beam failed in shear on the side with gauge 5. Therefore the higher strain gauge reading at location 5 compared to location 1 is in agreement with the results. The load vs. deflection graph in Figure 4.36 shows a linear response with respect to the load until it is just under 60 kN, beyond which load level there is small decrease in slope on the graph which corresponds to the abrupt changes in strain in gauges 3 an the timber gauge.

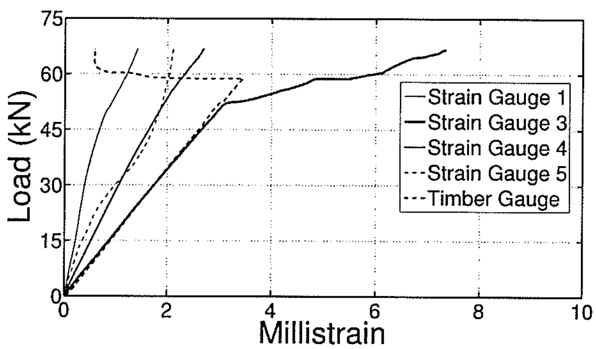

Figure 4.35: Strain Gauge Readings in GFRP Bar for Beam $2B-D-2$

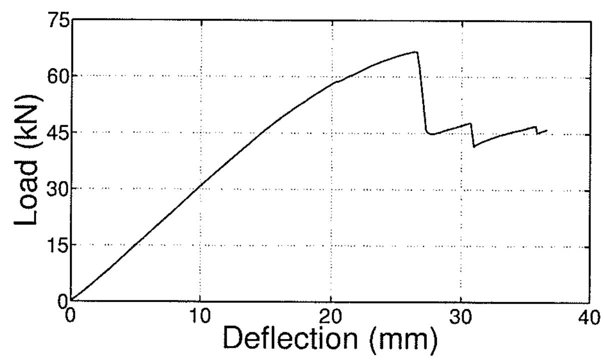

Figure 4.36: Load vs. Deflection for $2B-D-2$

The strain profile of the beam at midspan in Figure 4.37 shows a constant neutral axis height as the load increases. The N.A. height may be decreasing, however strains in pi gauge 1 does not increase at the same rate as the strains in other pi gauges, which effects the best fit line. The non-linear strain profile from locations 3 to 5 in Figure 4.38 suggests that as load increased above 20 kN, strains near the support increased more rapidly due to shear stresses that eventually led to failure.

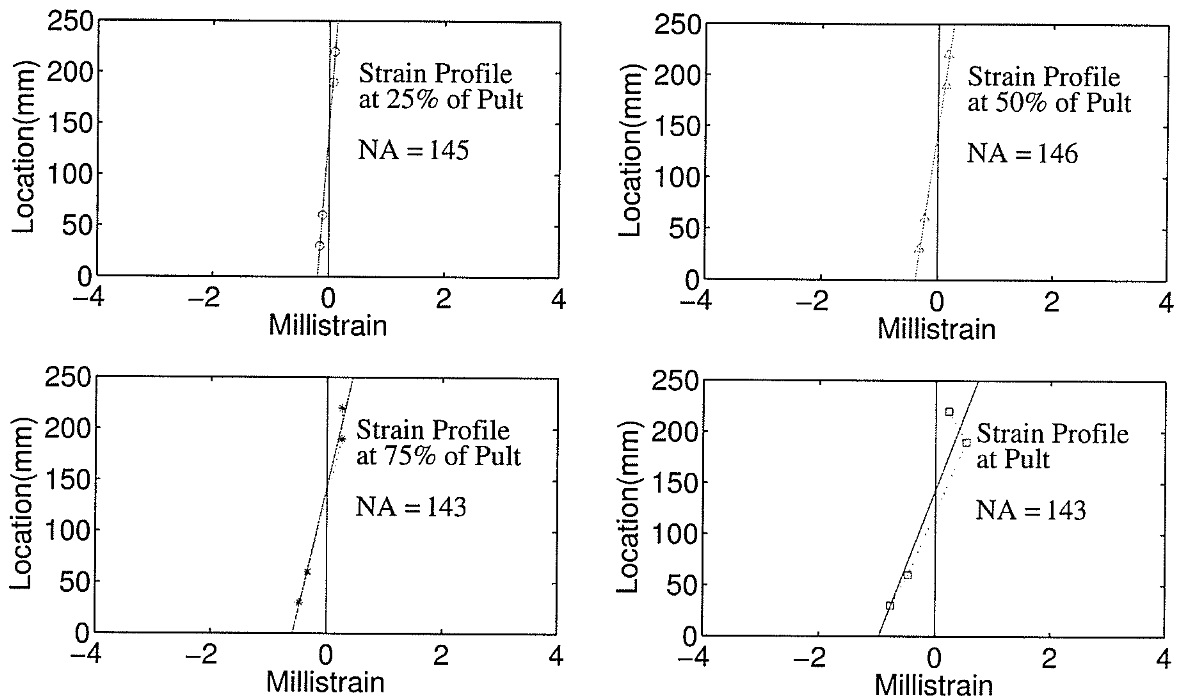

Figure 4.37: Strain Profile at Midspan for $2B - D - 2$ at Various Loads

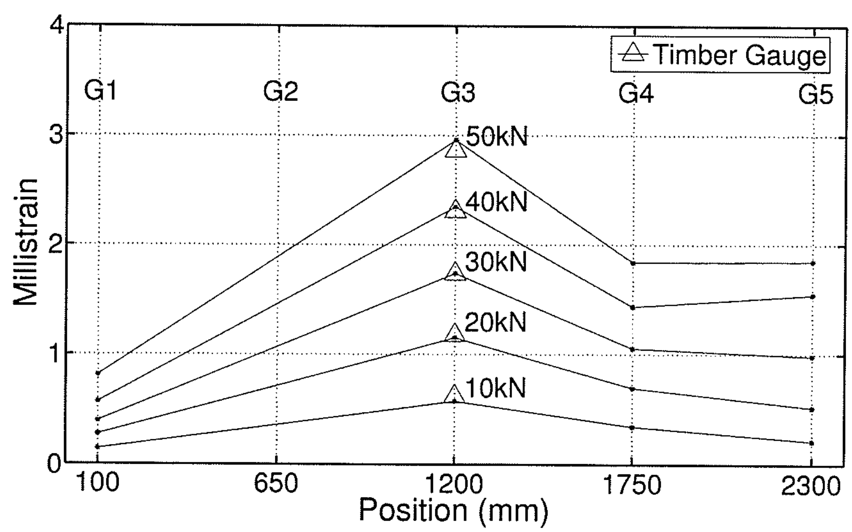

Figure 4.38: Strain Profile in GFRP Bar for Beam $2B - D - 2$

4.3.5 Neutral Axis Location

Each beam was instrumented with four pi gauges at midspan to determine the strains in the cross-section. The gauges were placed near the top and bottom of the beam as shown in Figure 3.27. The maximum strains theoretically occur at the extreme fibres and the N.A. (location of zero strain) is usually located at mid-height. If a beam is failing in tension, strains on the tension face will increase more rapidly than the strains on the compression face of the beam. Therefore the N.A. will theoretically shift upwards. On the other hand, when the beam is failing in compression, the N.A. will shift downwards. An analysis of the strains at each pi gauge location, the load – deflection curve, and the relationship between N.A. position and load were studied simultaneously to determine whether failure mode could be predicted simply by analyzing this information.

Control Beams

Eighteen control beams were analyzed. Figure 4.39 shows the movement of the N.A. as the $C-16$ beam is subjected to load. The N.A. position shifts upwards from initial loading until around 35 kN when there is a small drop in the N.A. position caused by decreased strains in the tension zone. There were some shear cracks developing at this load which probably have impacted the drop in N.A position. The beam ultimately failed in tension, which is shown by the "jump" in N.A. position at the end of the test as strains near the bottom of the beam were increasing rapidly.

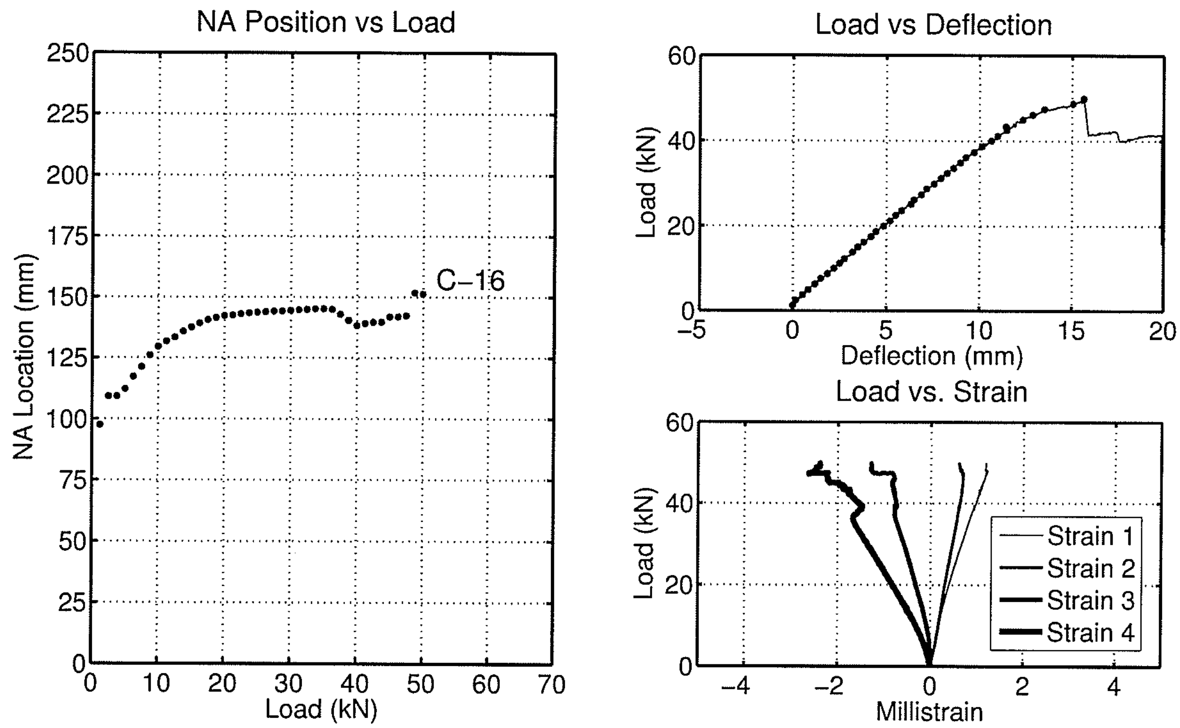

Figure 4.39: Neutral axis location from bottom face of beam for $C-16$

Table 4.16 summarizes the N.A positions for the control beams failing in tension. The N.A position at 50% of ultimate load is relatively close for all beams with an average location of 133 mm and a standard deviation of 14. As the load increases, the variability in the N.A location changes and is difficult to predict. Some beams experience upward neutral axis shift in accordance with theory, however there are also several beams that experienced decreases in the height of the N.A.

Three of the eighteen control beams failed in compression. The N.A location of these beams was expected to move towards the bottom face of the beam as more and more compression occurred. Table 4.17 confirms this finding. These beams had little variability in neutral axis

Table 4.16: Neutral Axis Summary - Control Beams failing in Tension

Specimen	**Neutral axis location from bottom face of beam [mm]**		
	50% of Ultimate	**90% of Ultimate**	**Ultimate**
$C-1$	126	120	163
$C-4$	150	56	57
$C-7$	131	132	132
$C-8$	104	89	88
$C-11$[a]	148	150	151
$C-12$	132	130	103
$C-16$	144	142	151
$C-17$	128	109	98
$C-18$	137	138	138
Average	133	118	120
Standard Deviation	14	30	35

[a]Strain gauge 3 was not used to calculate NA location

at 50% of maximum load and the N.A. position decreased as the load increased. Figure 4.40 shows the N.A. position for beam, $C-15$. The position is constant at just over 130 mm until the load reached 30 kN, when the N.A. begins to drop linearly from 135 mm to under 100 mm. The strain at the top of the beam in the compression zone increased much more rapidly than the strain in the tension zone. The load vs. deflection curve in Figure 4.40 shows a typical compression failure curve, with a constant load, but increasing deflection as the beam continues to deflect without being able to carry additional load.

Figure 4.41 corresponds to a typical shear failure that often had large variation in the N.A. location because the beam is often not behaving as one solid beam, but rather as a beam separated into several beams by the longitudinal shear cracks, thus making it difficult to predict the beam behaviour. This particular beam failed in shear very close to the bottom

Table 4.17: Neutral Axis Summary - Control Beams failing in Compression

Specimen	Neutral axis location from bottom face of beam[mm]		
	50% of Ultimate	90% of Ultimate	Ultimate
$C-3$[a]	142	116	103
$C-10$	147	165	138
$C-15$[a]	134	97	90
Average	141	126	110
Standard Deviation	7	35	25

[a]Strain gauge 2 was not used to calculate NA location

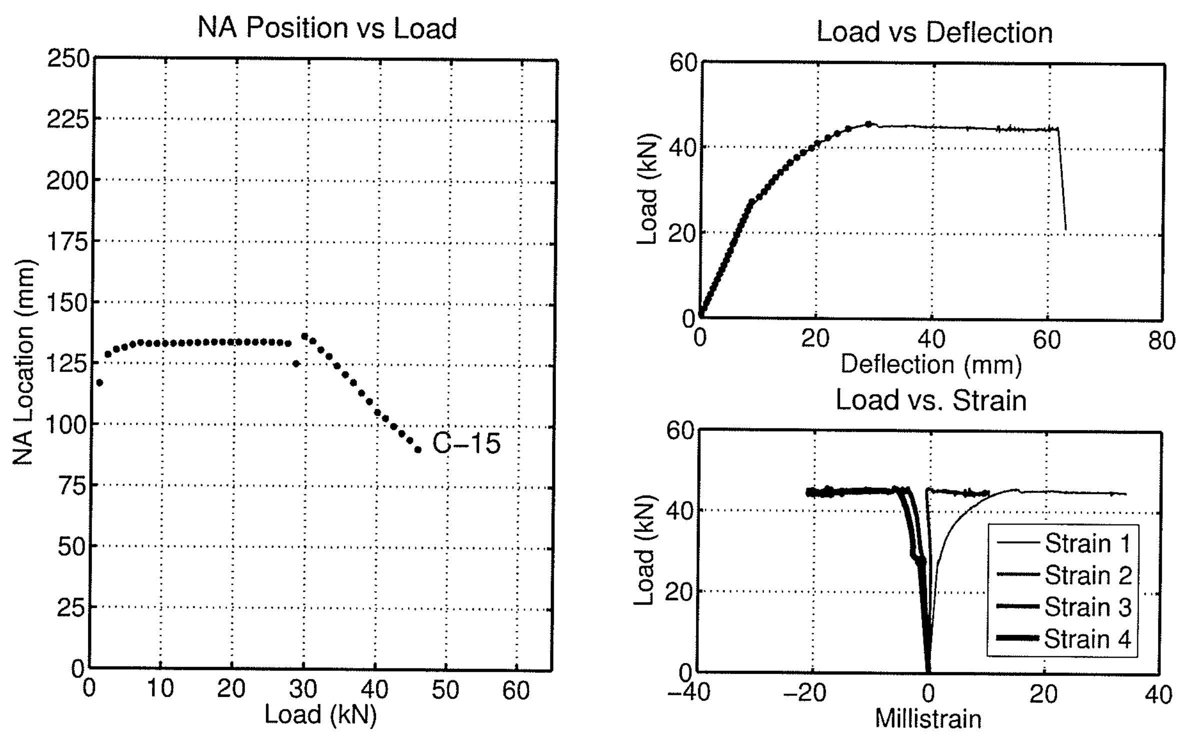

Figure 4.40: Neutral axis location from bottom face of beam for $C-15$

of the beam. The load vs. deflection curve shows a relatively linear pattern until the load reached around 30 kN when the strains near the top of the beam begin to increase much more rapidly than those near the bottom of the beam. The low strains at the bottom of the beam may be caused by the shear crack, which splits the beam and causes a small portion of the beam to act independently of the rest of the beam, thereby causing the neutral axis location to be quite different than that for a typical beam in bending with a N.A. at 125 mm.

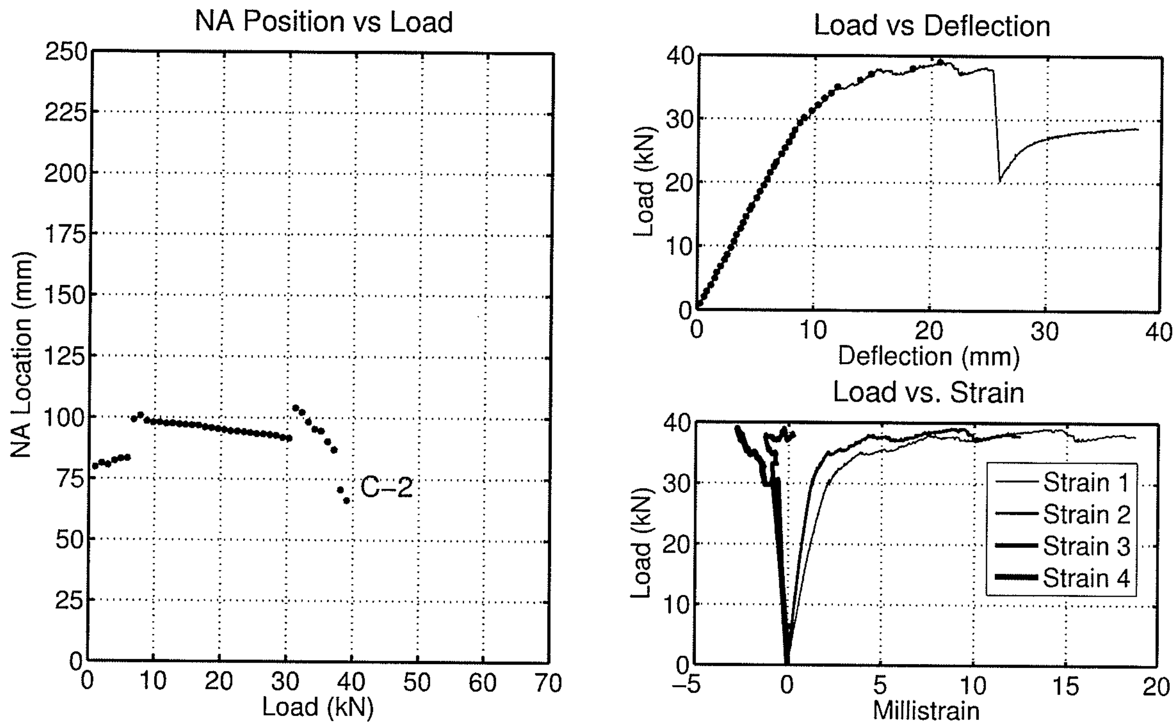

Figure 4.41: Neutral axis location from bottom face of beam for $C-2$

Table 4.18 summarizes the N.A. location for the control beams that failed in shear. There is considerable variability in the results. The standard deviation for these results are higher than for the tension and compression failures and several beams have a N.A. located well above the mid-height of the beam while several beams have a N.A. below mid-height. This could be a result of unreliable measurements from pi-gauges that were subjected to numerous incidents of cracking and therefore may not be providing reliable results.

Table 4.18: Neutral Axis Summary - Control Beams failing in Shear

Specimen	**Neutral axis location from bottom face of beam[mm]**		
	50% of Ultimate	**90% of Ultimate**	**Ultimate**
$C-2$	95	87	66
$C-5$	129	136	128
$C-6$	144	150	150
$C-9^a$	145	171	171
$C-13$	95	46	44
$C-14$	107	34	46
Average	119	104	101
Standard Deviation	23	57	56

[a]Strain gauge 2 was not used to calculate NA location

Strengthened Beams

The neutral axis locations were also analyzed for the strengthened beams. The results are summarized in Table 4.19. The neutral axis shifts upwards as expected due to the addition of flexural reinforcement. It should be noted that there is a lot of variability in the results, however this variability tends to decrease slightly in beams near ultimate loads in comparison to the control beams as determined by comparing the standard deviations. The strengthened beams that failed in shear had on average significantly higher N.A. positions compared to those in the control beams. The difference was 20 to 30 mm on average, depending on the percentage of ultimate load. There was also less movement in the N.A. as the load approached the ultimate load. This pattern was especially noticeable in beams strengthened with dowels. Refer to Tables A.8 and A.9.

Figure 4.42 shows a typical N.A. profile for a strengthened beam failing in tension. Initially,

Table 4.19: Neutral Axis Summary - Strengthened Beams

Failure Mode	**Neutral Axis Location [mm]**		
Tension	**50% of Ult. Load**	**90% of Ult. Load**	**Ultimate Load**
Average	143	139	138
Standard Deviation	18	19	20
Shear	**50% of Ult. Load**	**90% of Ult. Load**	**Ultimate Load**
Average	138	149	144
Standard Deviation	20	26	27

the N.A. position is above the mid-height of the beam. Then it drops slightly and remains constant until the beam begins to crack at a load of about 50 kN. The N.A. then rises again as the load approaches ultimate. The load vs. deflection curve shows this cracking with a slight drop in load at 50 kN and the load vs. strain curve shows the significant increases/decreases in strain near the bottom of the beam as the beam fails which could be caused the the pi-gauges which are no longer functioning properly due to the tension failure.

The typical N.A profile for a shear failure in shown in Figure 4.43. In this profile, the N.A. position is relatively constant, with a slight increase in height as the beam approaches its ultimate load. The load vs. deflection curve remains linear until around 60 kN at which point it starts to level out. The strains in the beam at the top and bottom of the beam begin to deviate from their previously linear behaviour at around 60 kN as well. This is likely because the beam is under considerable shear stress, causing the beam to act as two smaller beams, separated by the shear plane.

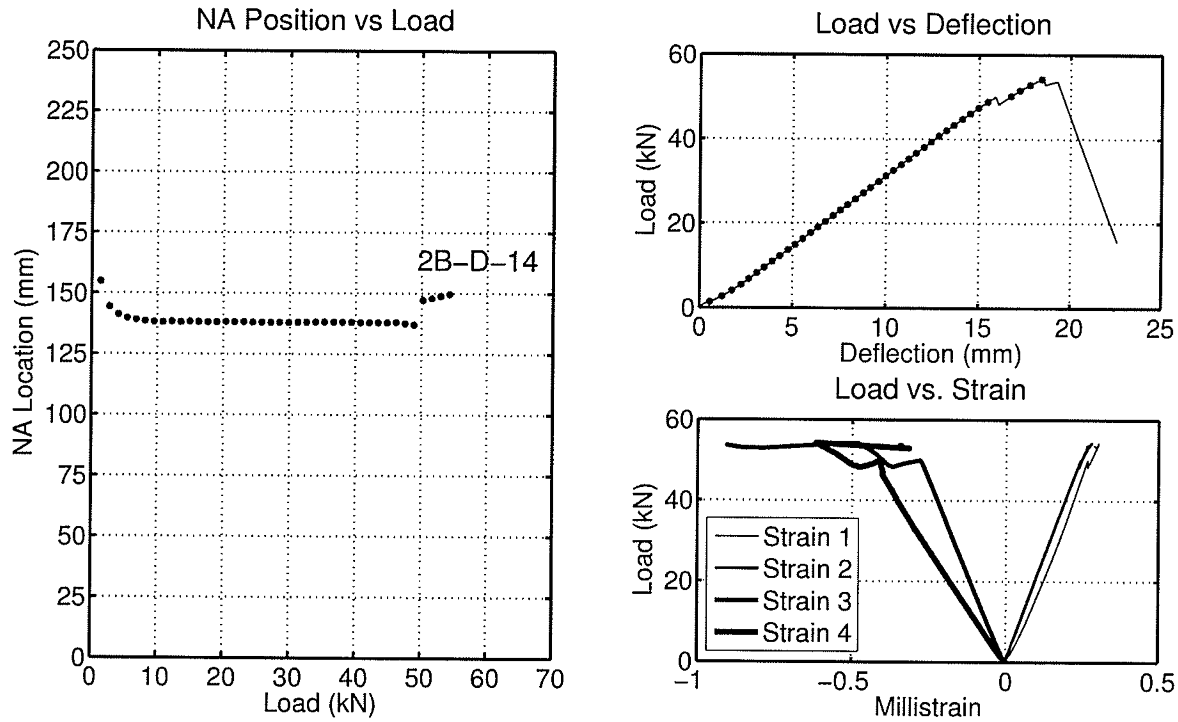

Figure 4.42: Neutral Axis Location for $2B - D - 14$

Summary

The position of the neutral axis of a timber beam with increasing load provides useful data regarding the beam behaviour and its failure mode. By analyzing beam strains, it is often possible to get an indiction of where the maximum stresses are acting and determine likely failure modes. By adding reinforcement to beams, the neutral axis often shifts upwards, and the variability in N.A. position often decreases, making beam behaviour more predictable. This also demonstrates itself in an overall decrease in variability of stiffness and ultimate loads.

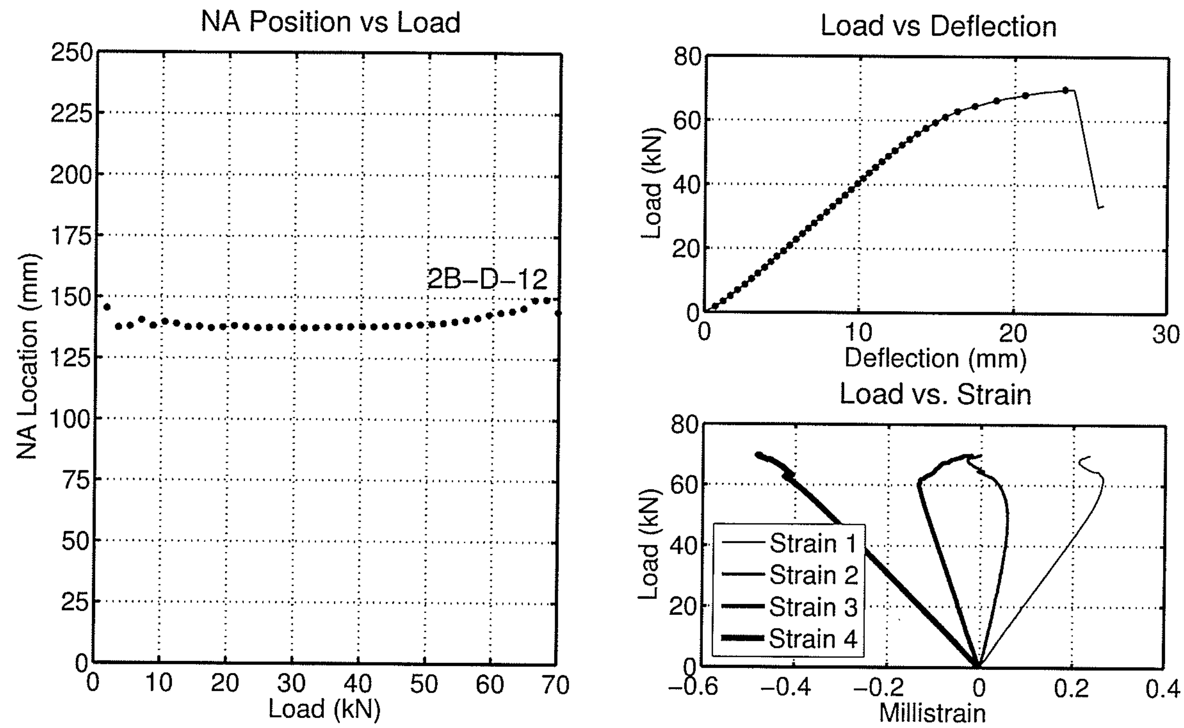

Figure 4.43: Neutral Axis Location for $2B - D - 12$

4.3.6 Modes of Failure

The timber beams failed by a number of different failure modes:

1. Tension parallel to the grain
2. Shear parallel to the grain
3. Compression
4. Tension perpendicular to the grain

The common modes of failure were tension parallel to the grain and shear parallel to the grain. Approximately half of the beams failed in tension with the other half failing in shear. Figure 4.44 and 4.45 show relatively severe tension failures for a control beam and a strengthened beam respectively. Nine control beams failed in tension, of which 7 of the failures originated from a drilled hole along the bottom surface of the beam, 1 from a knot at the bottom of the beam (see Figure 4.46), and 1 failed without a noticeable defect. The tension cracks propagated upwards and often went through some of the drilled holes. The strengthened beams that failed in tension usually experienced some cracks in the epoxy along the bottom surface of the beam. The cracking usually originated around drilled hole locations as shown in Figure 4.47. The strengthened beams never experienced GFRP rupture. The beams that failed in tension underwent cracking of the epoxy around the bars as flexural stresses increased. The cracking of the epoxy is always accompanied by tension failures.

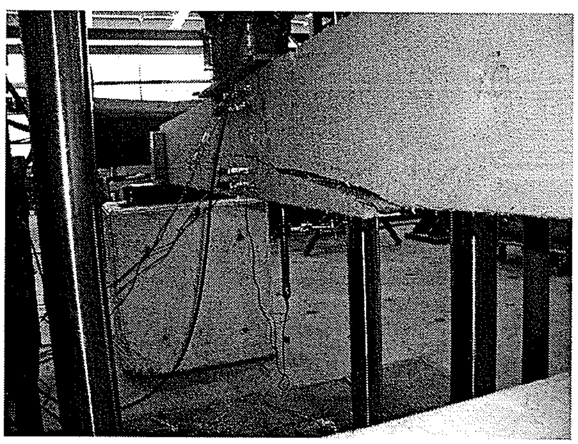

Figure 4.44: Tension Failure Originating from Drilled Hole ($C-4$)

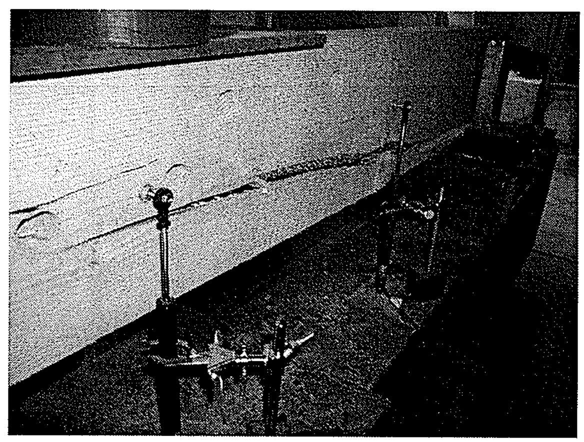

Figure 4.45: Tension Failure with 2 GFRP Bars ($2B-D-7$)

Shear failures were a common mode of failure. The timber beams were freshly cut (green) when they were purchased and therefore had a high original moisture content of around

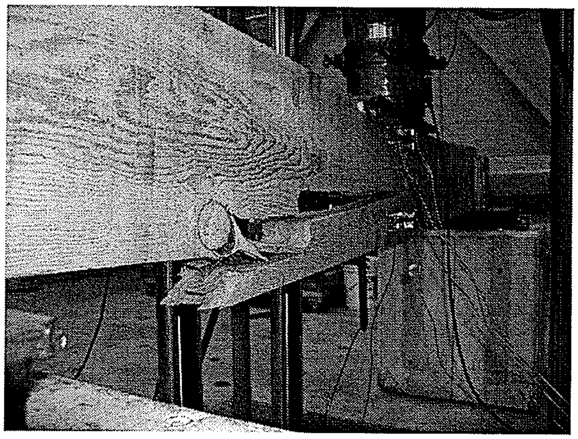

Figure 4.46: Tension Failure Originating from Knot $(C-17)$

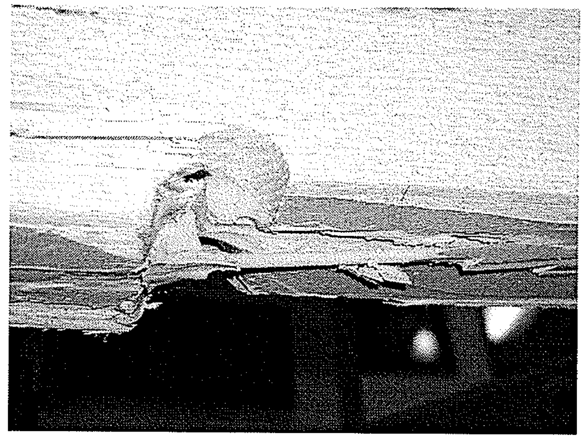

Figure 4.47: Tension Failure with 1 GFRP Bar $(1B-2)$

30%. The untreated beams were susceptible to rapid drying. Many of the beams had large checks near their ends caused by varying drying rates of the outer surface relative to that of the middle of the beam. This caused many of the checks and splits to become more severe between time of delivery and the time of testing. The beams were left outside the majority of the time to reduce the rate of drying that would occur in a relatively dry indoor environment. Shear failures were also triggered by the relatively short shear span of the beams. ASTM D198–99, Standard Test Methods of Statics Tests of Lumber in Structural Sizes [6] states that a shear span of less than 5 will produce a high percentage of shear failures. For this experimental program, the shear span was calculated according to Equation 4.2.

$$\frac{a}{h} = \frac{1100}{250} = 4.4 \tag{4.2}$$

Figure 4.48 depicts a shear failure through the GFRP dowels and Figures 4.49 and 4.50 shows a shear failure occurring below the GFRP dowels. Most of the shear failures occurred along existing check or splits and often went through some of the drilled holes (see Figure 4.51). The shear strengthening used to increase the shear strength of the beams such as the lag bolt, metal strapping, and even the GFRP dowels were relatively ineffective. The lag bolts would often bend, the metal strapping would slip, and the dowels would bend or pull out. This dowel action was common and small hairline cracks developed through the dowels. Figure 4.52 shows a dowel failure for beam $1B-D-5$ which was cut through the dowel along the failed shear plane. The GFRP dowels did not appear to rupture, however hairline cracks suggest that a larger number of dowels or a larger diameter dowel would be more suitable for future testing. The shear failures often occurred below the lag bolts or dowels, bypassing the reinforcement. Due to the flexural reinforcement, extending the shear reinforcement deeper into the beams was not an option. The relatively short shear span allowed for a greater number of beams for testing, however a shear span, a/h, greater than 5 and more prompt testing if treated beams are used is recommended for future testing to shift the shear failures to tensile failures.

Twenty, non-tested beams were strengthened with GFRP dowels and eleven failed in shear, showing that the dowels were not very effective in preventng shear failures. Of these 11 failures, 7 were through the dowels and 4 occurred below the dowels.

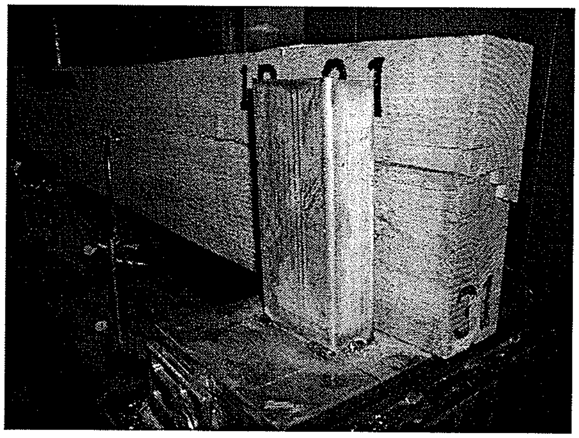

Figure 4.48: Shear Failure Parallel to Grain through Dowel ($1B-D-5$)

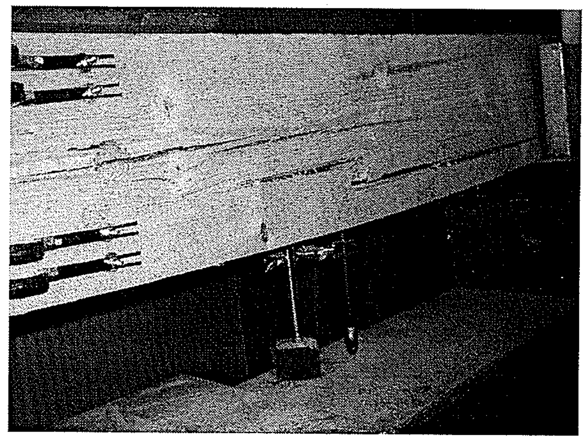

Figure 4.49: Shear Failure Parallel to Grain below Dowel ($F-2B-3$)

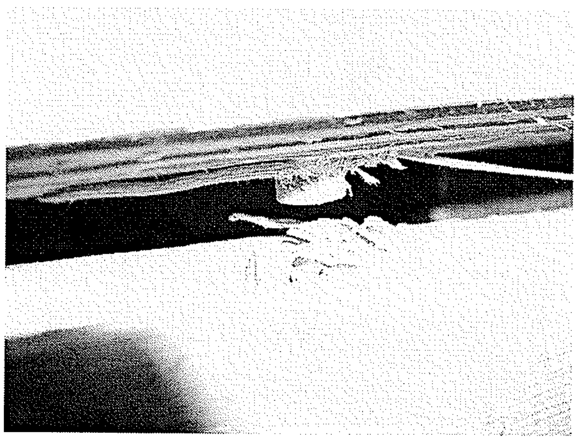

Figure 4.50: Close up of Shear Failure below Dowel ($F-2B-3$)

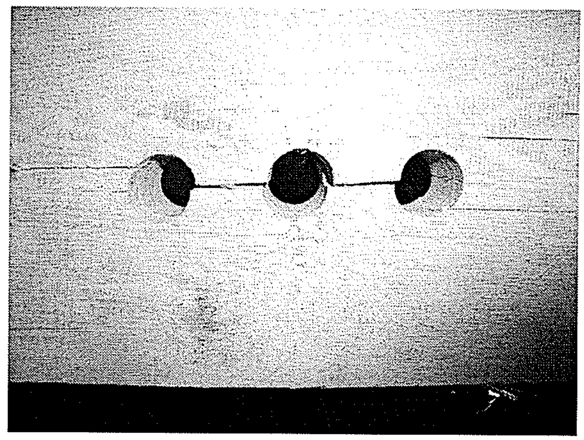

Figure 4.51: Shear Failure through Drilled Holes ($1B-D-2$)

Nine previously tested beams were restrengthened with GFRP dowels and retested. All these beams had failed in shear, and therefore the pre-existing shear planes had been significantly weakened, making it difficult for other modes of failure to govern. Out of the nine beams, only one failed in tension ($F-1B-1$), with the other eight failing in shear. All of these previously failed beams experienced shear slippage along the same planes that they had previously failed along, including $F-1B-1$. Six of these beams experienced a shear

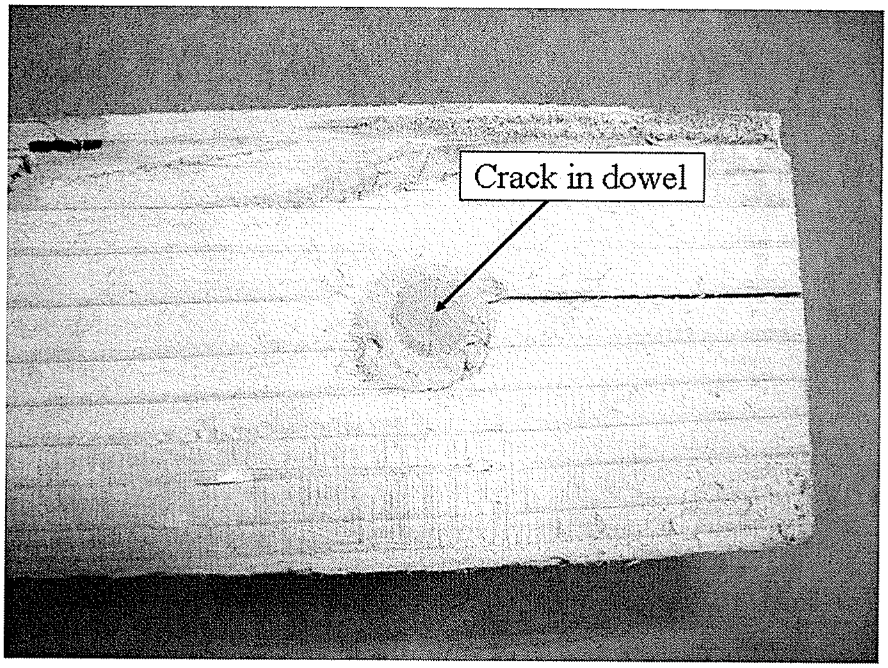

Figure 4.52: Dowel Action Shown by Cut Through Failed Beam ($1B - D - 5$)

failure through the dowels, indicating that the dowels were not able to shift the failure mode from shear to tension (see Figure 4.53). Beam $F - 1B - 1$, which ultimately failed in tension experienced significantly high shear forces, which led to a lower stiffness and the dowels were unable to increase the shear strength of the beam. Several of these beams experienced significant compression strains, but shear was the ultimate mode of failure due to the considerable amount of movement in the shear plane. All of these re-tested beams experienced a significant amount of deflection.

Three of the control beams failed in compression (see Figure 4.54). These three beams were grouped with the tension failures when analyzing the results since the objective of this experimental program is to investigate the minimum reinforcement ratio for timber beams

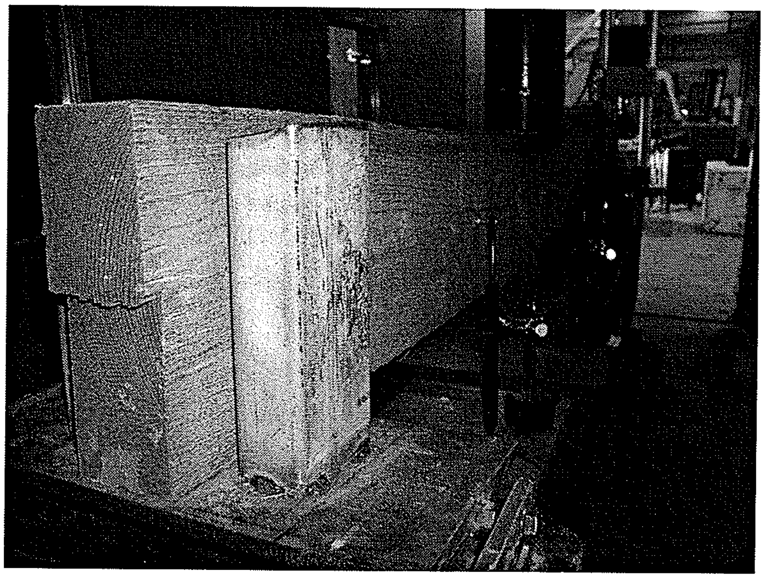

Figure 4.53: Shear Failure Parallel to Grain through Dowel ($F-1B-4$)

in bending. Shear strength was not the focus of this research and therefore beams that failed in shear were not useful for determining the flexural capacity of the beams. Several beams experienced some tension perpendicular to the grain; however this was not the ultimate mode of failure. Figure 4.55 shows beam $2B-D-3$ that experienced tension perpendicular to the grain and the cracking failure can be clearly seen on the figure. Table 4.20 provides a summary of the modes of failure based on the various strengthening schemes.

Table 4.20: Modes of Failure Summary

Specimen Classification	Critical Mode of Failure		
	Tension // to Grain	Shear // to Grain	Compression
C	9	6	3
$1B$	7	7	0
$2B$	3	3	0
$1B-D$	2	4	0
$2B-D$	7	7	0
$F-1B$	1	5	0
$F-2B$	0	3	0

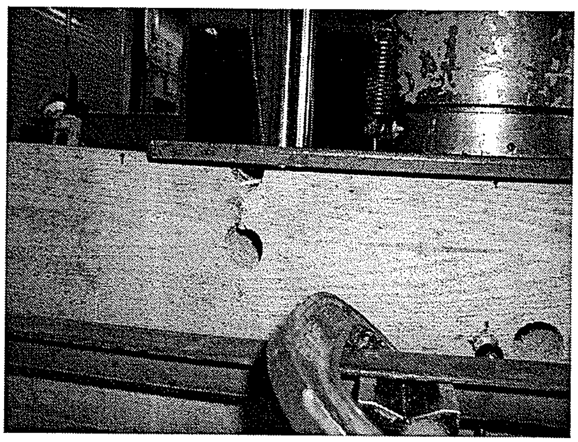

Figure 4.54: Compression Failure ($C-10$)

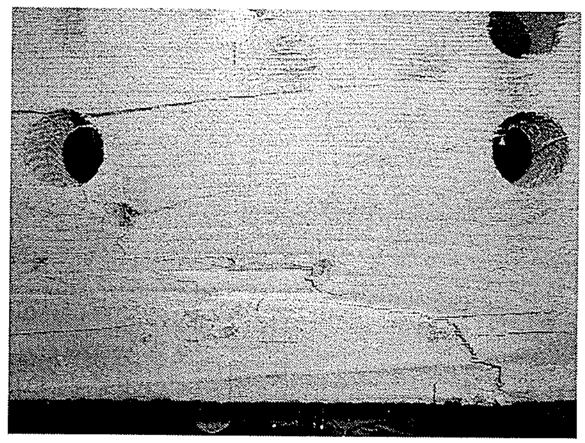

Figure 4.55: Tension Failure Perpendicular to Grain ($2B-D-3$)

Chapter 5

Analysis of Variance

5.1 General

Analysis of variance (ANOVA) was used to analyze the variance produced by more than two groups of means and determine whether genuine differences exist among the means of a dependent variable as a result of an independent variable [17]. In this analysis, the dependent variable used was ultimate load and the independent variable was the strengthening scheme.

Table 5.1: Groups of Data Used for ANOVA

Group Number	Strengthening Scheme	Number of Beams
1	C	18
2	$1B$	14
3	$2B$	6
4	$1B-D$	6
5	$2B-D$	14

5.2 Bending Tests

5.2.1 Analysis of Variance – 5 Groups

Analysis of variance was preformed using 5 groups of data from the experimental program, as summarized in Table 5.1. The mean values for each of the five groups was calculated using Equation 5.1.

$$\bar{X} = \frac{\sum X}{N_T} \tag{5.1}$$

where:

$\sum X$ = the summation of the ultimate loads from each test

N_T = the number of beams tested

Therefore, $\bar{X}_C = 39.2$ kN, $\bar{X}_{1B} = 50.2$ kN, $\bar{X}_{2B} = 50.8$ kN, $\bar{X}_{1B-D} = 49.6$ kN,

$\bar{X}_{2B-D} = 55.1$ kN

The sums of squares between groups and within groups are calculated in Equations 5.2 and 5.3 respectively.

$$SS_{BG} = N_C\bar{X}^2{}_C + N_{1B}\bar{X}^2{}_{1B} + N_{2B}\bar{X}^2{}_{2B} + N_{1B-D}\bar{X}^2{}_{1B-D} + N_{2B-D}\bar{X}^2{}_{2B-D} - N_T\bar{X}^2{}_T = 2235.0 \tag{5.2}$$

$$\begin{aligned} SS_{WG} &= (\sum X^2{}_C - N_C\bar{X}^2{}_C) + (\sum X^2{}_{1B} - N_{1B}\bar{X}^2{}_{1B}) + (\sum X^2{}_{2B} - N_{2B}\bar{X}^2{}_{2B}) \\ &+ (\sum X^2{}_{1B-D} - N_{1B-D}\bar{X}^2{}_{1B-D}) + (\sum X^2{}_{2B-D} - N_{2B-D}\bar{X}^2{}_{2B-D}) = 5266.0 \end{aligned} \tag{5.3}$$

The total sum of squares is shown in Equation 5.4.

$$SS_T = SS_{BG} + SS_{WG} = 2235.0 + 5266.0 = 7501.0 \tag{5.4}$$

Once the sums of squares are calculated, the mean squares between groups and within groups were determined using Equations 5.5 and 5.6.

$$MS_{BG} = \frac{SS_{BG}}{k-1} = \frac{2235.0}{5-1} = 558.8 \tag{5.5}$$

where k is the number of groups.

$$MS_{WG} = \frac{SS_{WG}}{N_T - k} = \frac{5266.0}{58-5} = 99.4 \tag{5.6}$$

The F statistic was used to do a hypothesis test to determine if there were significant differences between means of different groups. Equation 5.7 was used for the F statistic.

$$F = \frac{MS_{BG}}{MS_{WG}} = \frac{558.8}{99.4} = 5.6 \tag{5.7}$$

The higher the F statistic, the more likely that there is a significant difference between groups. The Tukey Method was used to evaluate differences among pairs of means as shown in Equation 5.8 [10]. If F is large enough, we can reject the hypothesis that the difference between the two means is due only to sampling error and conclude that the difference between the specific mean is significant.

$$F = \frac{\bar{X}_L - \bar{X}_S}{\sqrt{\frac{MS_{WG}}{2}(\frac{1}{N_L} + \frac{1}{N_S})}} \tag{5.8}$$

where:

$\bar{X}_L$ = the larger of the two means

$\bar{X}_S$ = the smaller of the two means

N_L = the size of the group with the larger mean

N_S = the size of the group with the smaller mean

The F_p – values are used to compare the F statistic and are shown in Table 5.3. The F statistic was calculated in Equation 5.7 and was compared to the value of F at a designated confidence as denoted by p. All of the beams that were strengthened using various strengthening schemes are very similar to one another and do not have any significant variation as summarized in Table 5.1. The control beams have significant difference in mean when compared to any of the strengthened beans, demonstrating that the GFRP reinforcement significantly increases the ultimate loads of the beams. They are significantly different from the $1B$ and $2B-D$ schemes with a 99.5% confidence and from the $1B-D$ and $2B$ schemes with a 97.5% confidence. This minor difference is attributed to the small number of beams tested using the $1B-D$ and $2B$ schemes. When comparing the different strengthening schemes to one another, there is no significant difference at the lowest confidence level of 90%.

Table 5.4 shows a summary of the MATLAB ANOVA results which includes sums of squares, degrees of freedom, mean squares, F statistic, and p-value. Figure 5.1 and 5.2 show the

Table 5.2: ANOVA Results for 5 groups

Groups Compared	**F**	**Difference**
C vs. $1B$	4.40	Significant, $p < 0.005$
C vs. $2B$	3.48	Significant, $p < 0.025$
C vs. $1B - D$	3.15	Significant, $p < 0.025$
C vs. $2B - D$	6.34	Significant, $p < 0.005$
$1B$ vs. $2B$	0.16	Not significant, $p > 0.100$
$1B$ vs. $1B - D$	0.17	Not significant, $p > 0.100$
$1B$ vs. $2B - D$	1.83	Not significant, $p > 0.100$
$2B$ vs. $1B - D$	0.28	Not significant, $p > 0.100$
$2B$ vs. $2B - D$	1.26	Not significant, $p > 0.100$
$1B - D$ vs. $2B - D$	1.59	Not significant, $p > 0.100$

Table 5.3: $F_p(4, 53)$ at different confidence levels

F_p	p	**Confidence Level**
2.06	0.100	90%
2.56	0.050	95%
3.05	0.025	97.5%
3.71	0.010	99%
4.22	0.005	99.5%

Table 5.4: ANOVA Table - From MATLAB

Source	SS	df	MS	F	Prob>F
Groups	2235.27	4	558.82	5.63	0.0008
Error	5263.03	53	99.30		
Total	7498.31	57			

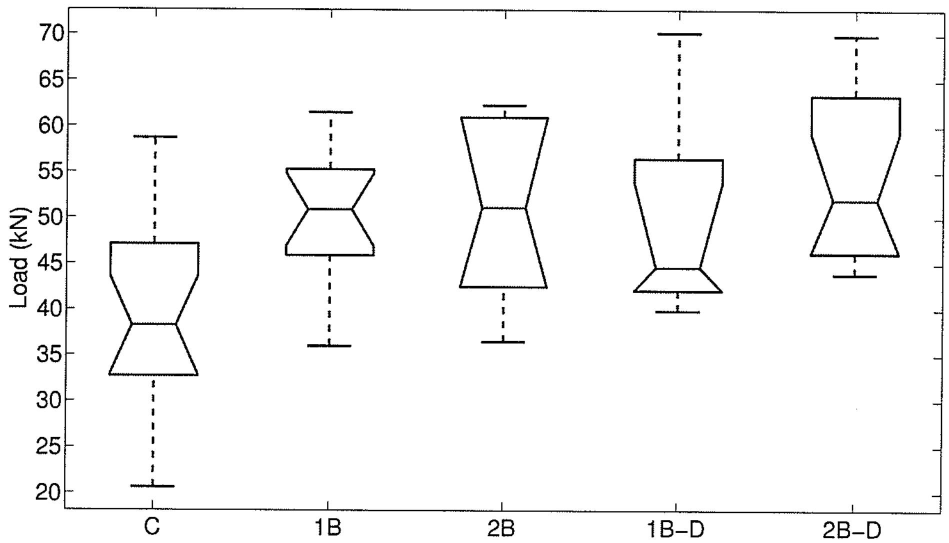

Figure 5.1: Box Plots of Ultimate Loads for 5 Strengthening Schemes

results graphically. The only disagreement in the results from the procedure outlined in Equations 5.1 to 5.7 and the MATLAB analysis are the significance of the control beams compared to the $1B - D$ and $2B$ beams. Figure 5.2 states that there is not a significant difference between C and $1B - D$ and C and $2D$. The bars on these graphs slightly overlap, however based on the above procedure, it is assumed that these groups are significantly different. The overlap is attributed to the small sample size for the $1B - D$ and $2B$ groups, which makes the results more sensitive to the number of samples. All F_p are obtained from Mendenhall [41].

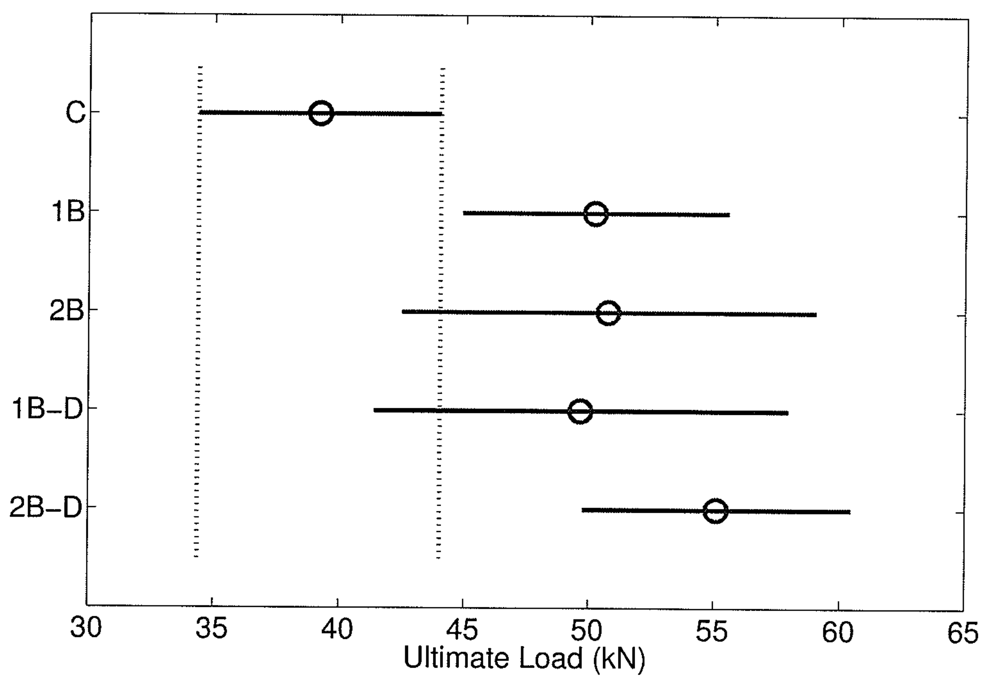

Figure 5.2: Multiple Comparison of Ultimate Loads for 5 Strengthening Schemes

Table 5.5: Groups of Data Used for ANOVA

Group Number	Strengthening Scheme	Number of Beams
1	Control	18
2	1 Bar	20
3	2 Bars	20

Table 5.6: ANOVA Summary

Groups Compared	F	Significance
C vs. $1B$	4.80	Significant, $p < 0.025$
C vs. $2B$	6.45	Significant, $p < 0.005$
$1B$ vs. $2B$	1.70	Not significant, $p > 0.100$

5.2.2 Analysis of Variance – 3 Groups

Analysis of variance was preformed using 3 groups of data from the experimental program in order to increase the sample size of each group from the initial 5-group analysis, as summarized in Table 5.5.

Table 5.6 shows a summary of the calculated F –values for different pairs of means. It is shown that the control beams vary significantly for the strengthened beams, while the strengthened beams vary from each other due to sampling errors and therefore are very comparable data sets. The $F_p(2, 55)$ are shown in Table 5.7. The control beams vary from the strengthened beams significantly with a 97.5% confidence for the C vs. $1B$ and a 99.5% confidence for the C vs. $2B$. The $1B$ and $2B$ schemes are not significantly different.

ANOVA was also performed in MATLAB using a 95% confidence interval. The p-value is extremely small, which strongly indicates that the ultimate loads from the different strength-

Table 5.7: $F_p(2, 55)$ at different confidence levels

F_p	p	**Confidence Level**
2.40	0.100	90%
3.17	0.050	95%
3.96	0.025	97.5%
5.03	0.010	99%
5.86	0.005	99.5%

Table 5.8: ANOVA Table - From MATLAB

Source	**SS**	**df**	**MS**	**F**	**Prob>F**
Groups	2155.08	2	1077.54	11.09	$8.97656e^{-5}$
Error	5343.23	55	97.15		
Total	7498.31	57			

ening schemes are significantly different. These results are in agreement with the procedure used in Equations 5.1 to 5.7.

Figure 5.3 illustrates the distribution of the data in each group. Figure 5.4 shows a multiple comparison of the various groups of data. It graphically shows that group C is significantly different from group $1B$ and $2B$ using a 95% confidence interval.

These three strengthening schemes were also analyzed by removing all of the shear failures from the results and just considering the flexural failures. This reduced the sample size to 12 control beams, 9 beams strengthened with 1 bar, and 10 beams strengthened with 2 bars. By doing a multiple comparison using these smaller sample groups, there was no longer a significant difference between the control beams and the beams strengthened with 1 bar. There is a small amount of overlap as shown in Figure 5.5. This is caused by the small sample size and the increased uncertainty that must be accounted for. There is still

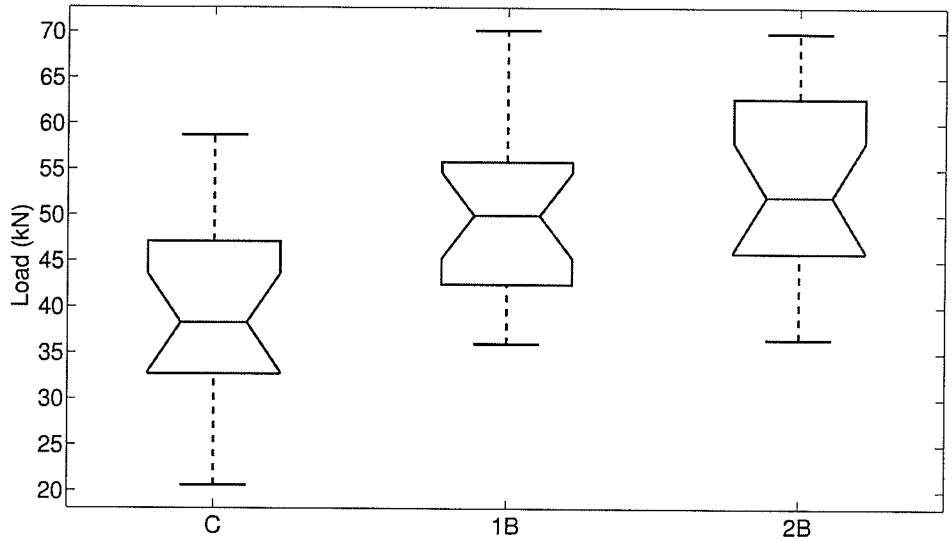

Figure 5.3: Box Plots of Ultimate Loads for 3 Strengthening Schemes

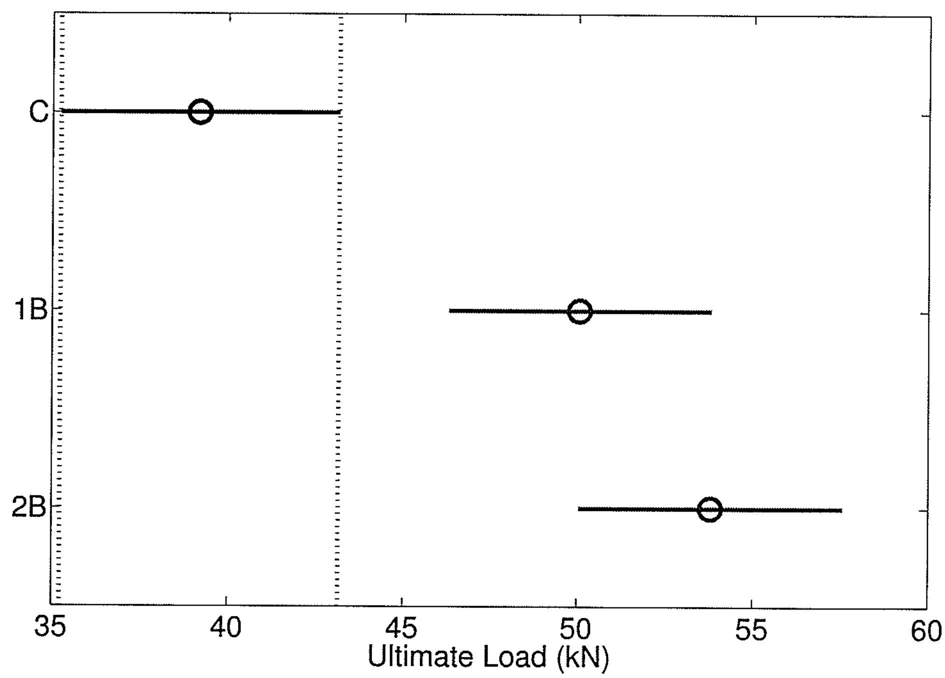

Figure 5.4: Multiple Comparison of Ultimate Loads for 3 Strengthening Schemes

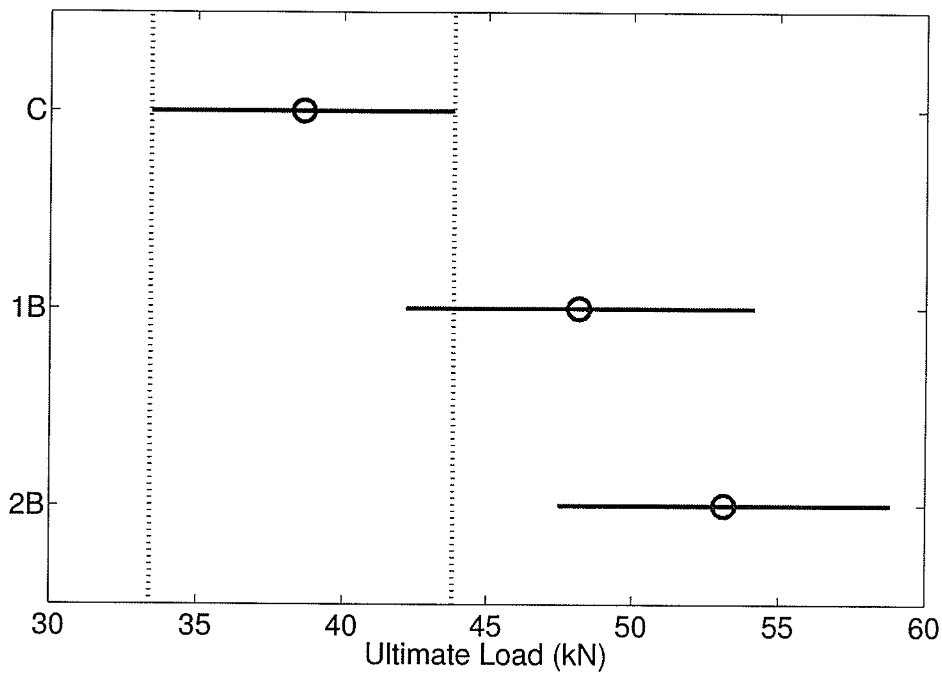

Figure 5.5: Multiple Comparison of Ultimate Loads for 3 Strengthening Schemes (Tension Failures Only)

no significant difference between the $1B$ and $2B$ groups.

5.2.3 Analysis of Variance – 2 Groups

Analysis of variance was preformed again using only 2 groups of data from the experimental program. The groups were the control beams and the strengthened beams and are shown in Table 5.9.

Table 5.10 shows the calculated F –value for the control beams vs. the strengthened beams. The control beams vary significantly for the strengthened beams with a F – value of 20.6.

Table 5.9: Groups of Data Used for ANOVA

Group Number	Strengthening Scheme	Number of Beams
1	Control	18
2	1 Bar or 2 Bars	40

Table 5.10: ANOVA Summary

Groups Compared	F	Significance
C vs. $1B/2B$	20.6	Significant, $p < 0.025$

The $F_p(1, 56)$ values for different levels of confidence are shown in Table 5.11.

An ANOVA summary using MATLAB generated the following results as shown in Table 5.12. The p – value is extremely small, which strongly indicates a significant difference between the groups.

Figure 5.6 illustrates the distribution of the data in each group and Figure 5.7 shows a multiple comparison of the various groups of data. It graphically shows that group C is significantly different from group $1B/2B$ using a 95% confidence interval.

The analysis was broken down one step further by only analyzing the beams that failed in tension. All of the strengthened beams were grouped together. The two groups consisted

Table 5.11: $F_p(1, 56)$ at different confidence levels

F_p	p	Confidence Level
2.80	0.100	90%
4.02	0.050	95%
5.32	0.025	97.5%
7.13	0.010	99%
8.56	0.005	99.5%

Table 5.12: ANOVA Table - From MATLAB

Source	**SS**	**df**	**MS**	**F**	**Prob>F**
Groups	2015.2	1	2015.2	20.58	$3.06573e^{-5}$
Error	5483.1	56	97.91		
Total	7498.31	57			

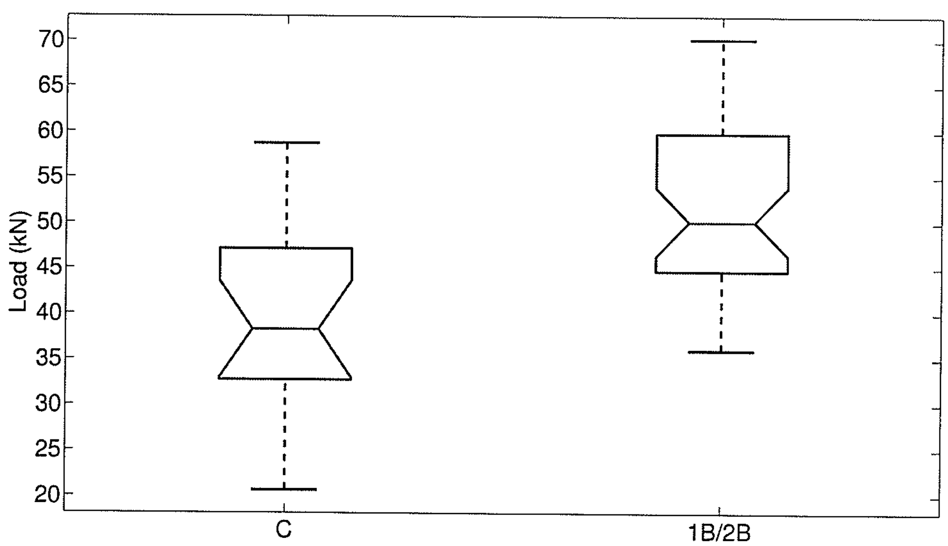

Figure 5.6: Box Plots of Ultimate Loads for 2 Strengthening Schemes

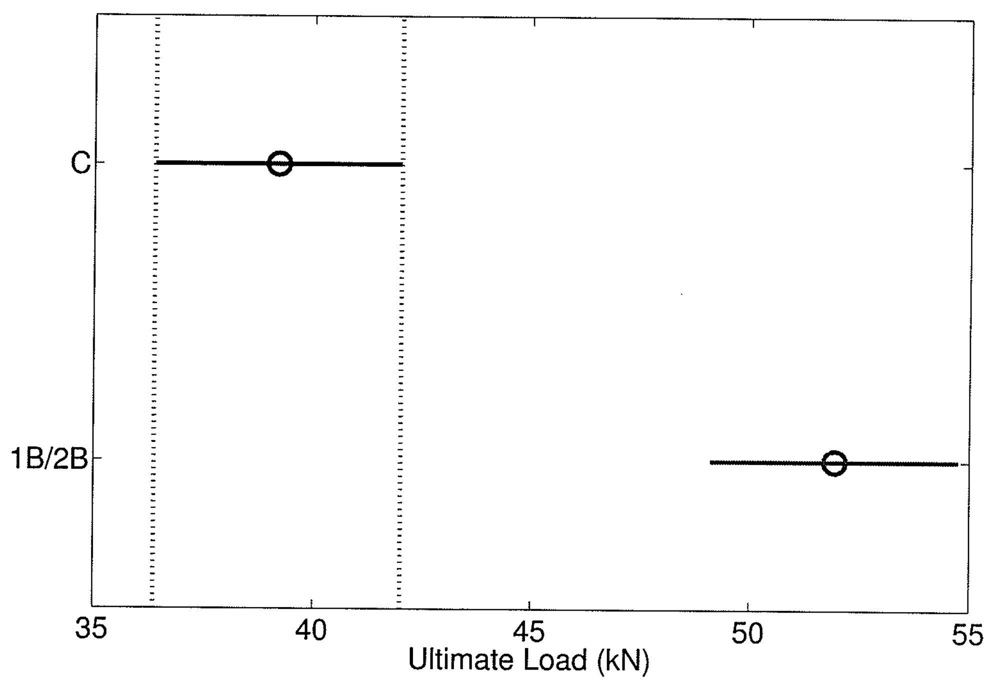

Figure 5.7: Multiple Comparison of Ultimate Loads for 2 Strengthening Schemes

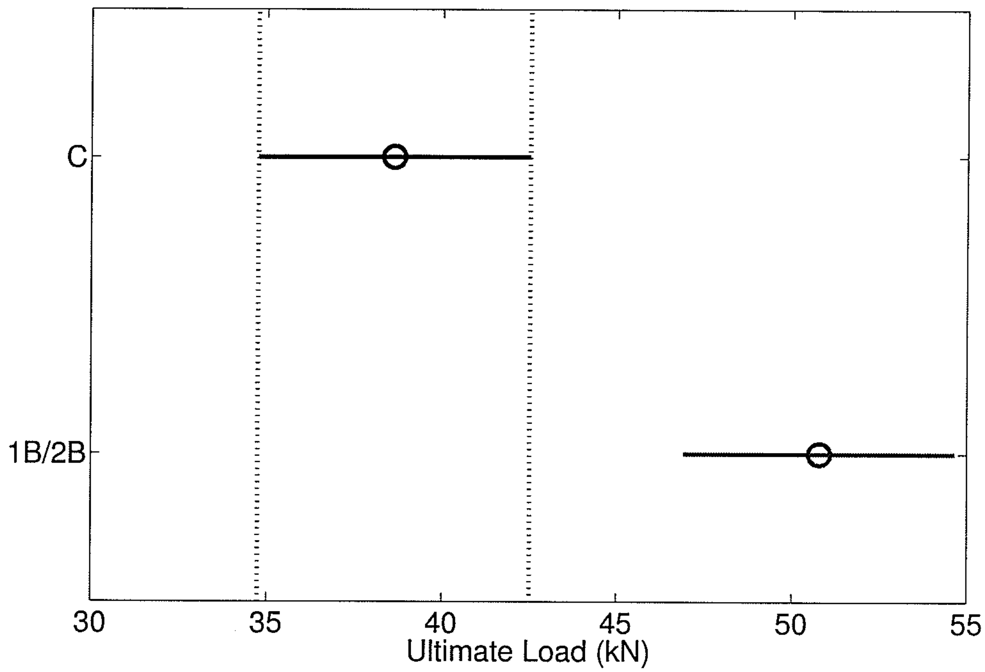

Figure 5.8: Multiple Comparison of Ultimate Loads for 2 Strengthening Schemes (Tension Failures Only)

of 12 control beams and 19 strengthened beams. There was a significant difference found between the two groups as shown in Figure 5.8. By increasing the size of the groups, the length of the lines on the Figure can be decreased since there is more certainty in the results.

Table 5.13: ANOVA Table - From MATLAB - Sheet Samples

Source	**SS**	**df**	**MS**	**F**	**Prob>F**
Groups	899.25	3	299.75	5.87	0.0074
Error	765.94	15	51.06		
Total	1665.19	18			

5.3 Durability Tests

An analysis of variance was performed on ultimate loads from the durability tests to determine if the results were significantly different from one group to another. All of the 45° configurations were compared.

Table 5.13, Figure 5.9, and Figure 5.10 show the results of the MATLAB ANOVA procedure for the 45° sheet samples. The groups compared were the non-treated samples tested by Gomez [32] and all of the treated samples, which included the control samples, the high temperature samples, and the low temperature samples. Figure 5.10 shows that there is a significant difference in the results between the $S - NT - 45°$ group and the other groups, which solidifies the negative impact of creosote treatment on FRP–timber bond strength. There was no significant difference between any of the $S - T$ groups, which shows that there was no significant impact of the accelerated aging program on the strength of the FRP–timber bond.

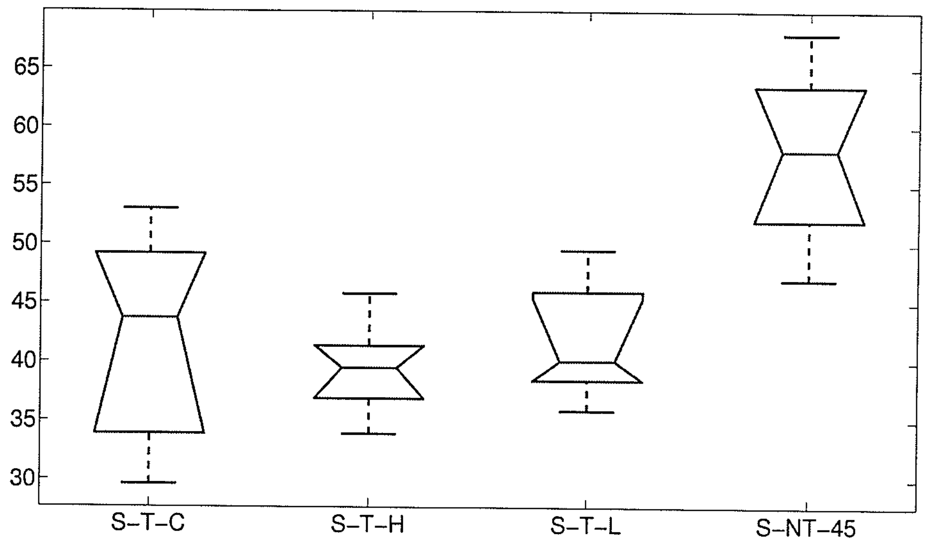

Figure 5.9: Box Plots of Ultimate Loads for Different Sheet Schemes

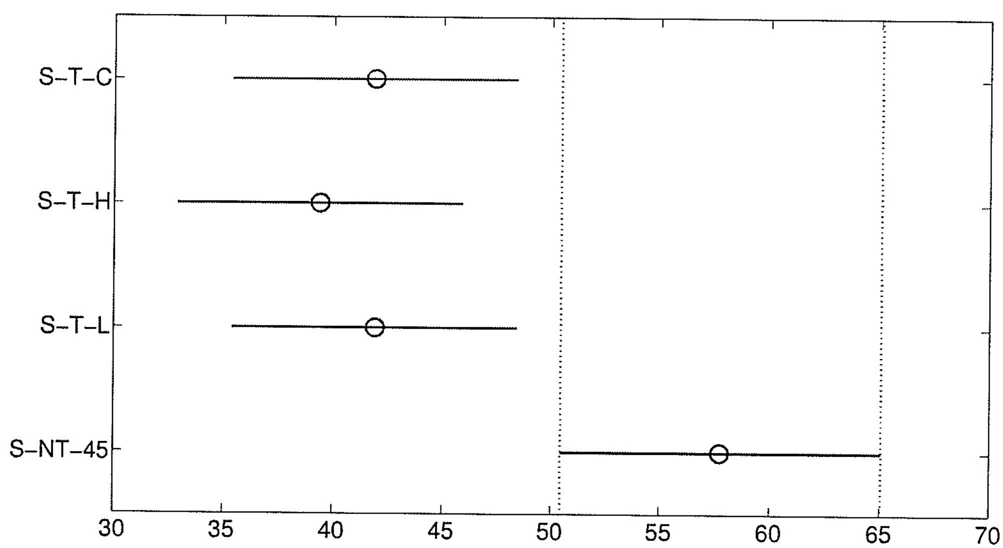

Figure 5.10: Multiple Comparison of Ultimate Loads for Different Sheet Schemes

Table 5.14: ANOVA Table - From MATLAB - Dowel Samples

Source	**SS**	**df**	**MS**	**F**	**Prob>F**
Groups	122.96	3	40.99	1.14	0.3638
Error	537.93	15	35.86		
Total	660.90	18			

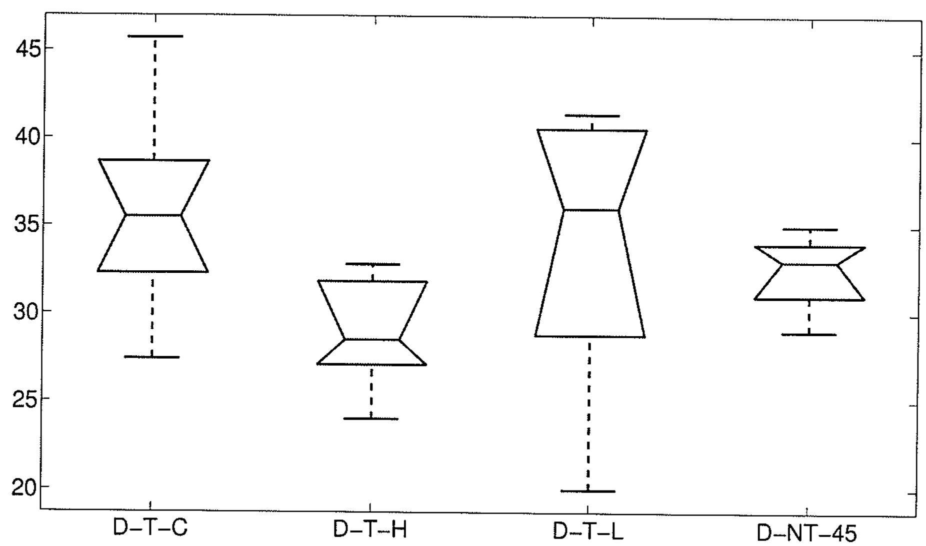

Figure 5.11: Box Plots of Ultimate Loads for Difference Dowel Schemes

Table 5.14, Figure 5.11, and Figure 5.12 show the results of the MATLAB ANOVA procedure for the 45 ° dowel samples. Figure 5.10 shows that there is not a significant difference in the results between any of the groups and therefore the dowels specimens were not suspectable to bond degradation caused by the accelerated aging process. The creosote treatment had no impact on the bond strength of the internal GFRP dowels.

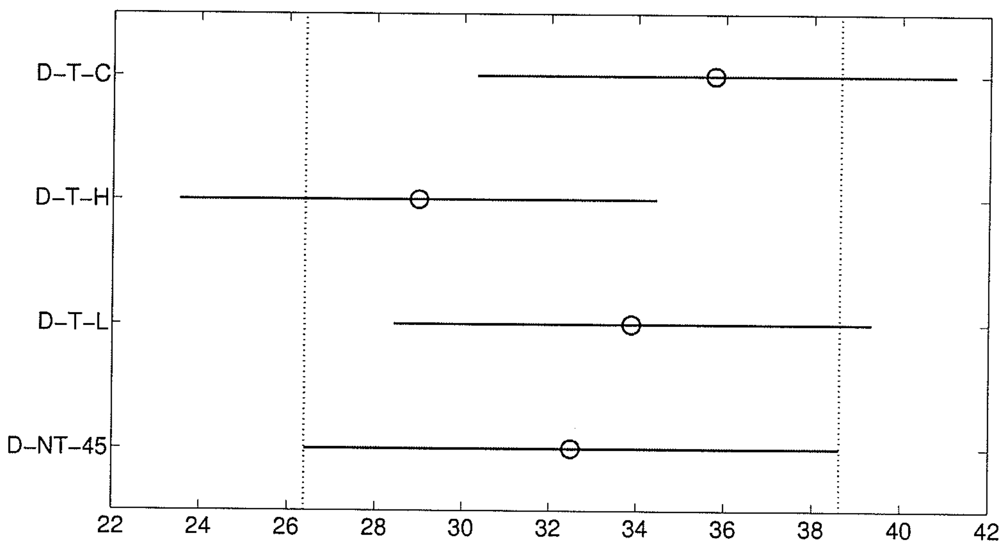

Figure 5.12: Multiple Comparison of Ultimate Loads for Difference Dowel Schemes

Chapter 6

Finite Element Analysis

6.1 Linear Analysis

FEA is difficult to use because of the heterogeneity of timber. Linear FEA was used in this program only to verify the position of the neutral axis for beams with artificial defects. This analysis was not used to find ultimate capacity, nor deflection of timber beams. The timber beams were modeled using TEKSAP, a linear finite element analysis program. The dimensional capabilities are 1000 nodes and 6000 degrees of freedom [43].

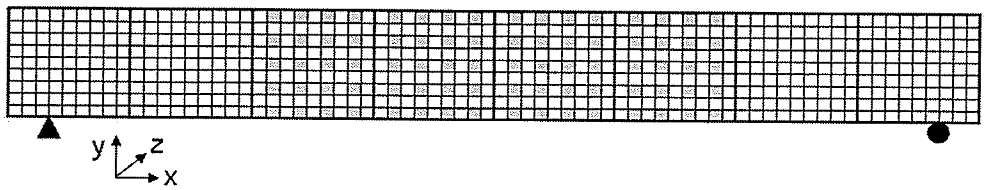

Figure 6.1: Mesh Layout

6.1.1 Mesh Size

The beam had a 75 x 250 mm cross-section and was 2400 mm long. To lower the grade of the beam, 37.5 mm diameter holes were drilled. The mesh size used for analysis reflected the size of the holes. For simplicity, a rectangular mesh was used. The mesh had 730 nodes and 648 elements, each of 33.33 mm wide and 27.78 mm high, producing an element area of 926 mm^2. This was comparable to the area of the holes which was 1104 mm^2. Plate and shell elements were used to model the beam and all elements were given a thickness of 75 mm to reflect the dimensions of the beam. Refer to Figure 6.1 for the mesh layout. The gray elements represent possible hole locations. If a hole was drilled at one of these locations, the element properties were set to zero, so that the element would behave like a hole.

6.1.2 Boundary Conditions

The beam under consideration is in plane stress, meaning that there is no translation or rotation permitted in the z-direction. The simply supported beam was modeled by restraining node 4 in the x and y directions and node 70 in the y-direction, as shown in Figure 6.1.

6.1.3 Beam Properties

For simplicity, it was assumed the beam was made of a homogenous material. The modulus of elasticity was assumed to be equal to 11500 MPa, which is reflective of coastal Douglas-fir timber with a moisture content of approximately 20% [25]. Poisson's ratio was taken as 0.449 [25]. For this model, a 10 kN point load was applied at midspan, thus ensuring linear behaviour of the beam.

6.1.4 Program Verification

The program was verified by comparing the results for deflection and stress calculation with hand calculations. The maximum deflection, Δ, in the beam occurs at midspan when a single point load is applied at midspan, and is given by:

$$\Delta = \frac{P\ell^3}{48EI} = \frac{(10000N)(2200mm)^3}{(48)(11500MPa)(9.766x10^7mm^4)} = 1.98mm \tag{6.1}$$

where $I = \frac{bh^3}{12} = 9.766x10^7mm^4$

The stress at midspan of the beam will vary linearly throughout the member depth. At mid-height, the stress is zero. The stresses at the extreme fibres of the beam are determined

Table 6.1: Comparison of FEM and Theoretical Results

	FEM Result	**Theoretical**	**Percent Error**
Deflection, Δ $[mm]$	2.02	1.98	2.3%
Stress, σ $[MPa]$	6.71	7.04	4.7%

using Equation 6.2:

$$\sigma = \frac{My}{I} = \frac{(5.5x10^6Nmm)(125mm)}{(9.766x10^7mm^4)} = 7.04MPa \tag{6.2}$$

where $M = \frac{P\ell}{4} = \frac{(10000N)(2200)}{4} = 5.5x10^6Nmm$

The results from these hand calculations are compared to FEM results in Table 6.1. Acceptable accuracy was found. Therefore the use of the program for the purpose of locating the neutral axis of the beam is feasible, provided the material remains elastic.

6.1.5 Neutral Axis Position

Due to the heterogeneity of timber, it is difficult to predict the location of the neutral axis of a timber beam in bending. If timber is assumed to be homogenous throughout, the neutral axis would be located at mid-height, which is 125 mm from the bottom of the beam. By introducing 6 to 8 – 1.5″ diameter holes into the beam using a statistically random process, the neutral axis may shift, depending on the hole locations. If more holes are located near

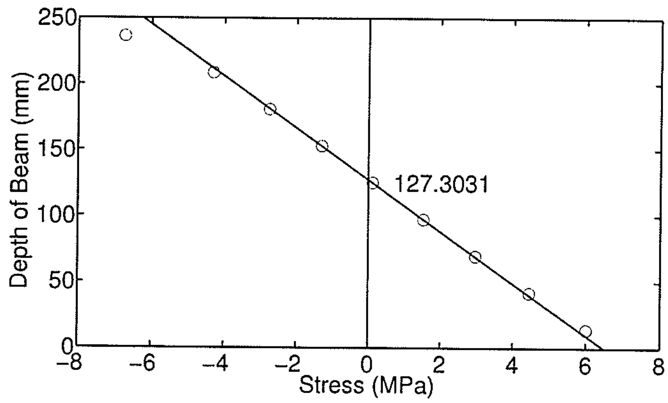

Figure 6.2: Control Beam - Neutral Axis Location

the top of the beam, the compression zone decreases, which in turn would shift the neutral axis downwards. If more holes are located near the bottom of the beam, the neutral axis is expected to shift upwards.

The FEM model was used to verify the above hypothesis and also quantitatively assess the impact of the holes on beam behaviour. The FEM model was run using a control beam with no holes. The neutral axis location was determined to be located at 127.3 mm from the bottom of the beam at a load of 10 kN. Refer to Figure 6.2. The slight variation from 125 mm is caused by the increased stresses that the applied point load transfers to the elements near the point load.

When a number of holes are positioned near the top of the beam as depicted in Figure 6.3, the neutral axis shifts downwards as noted above. Figure 6.4 shows the neutral axis to be 115.8 mm above its bottom face. It is noted that this position of the neutral axis was arrived at by using a best fit line through the middle 3 elements. The 9 points on the graph represent

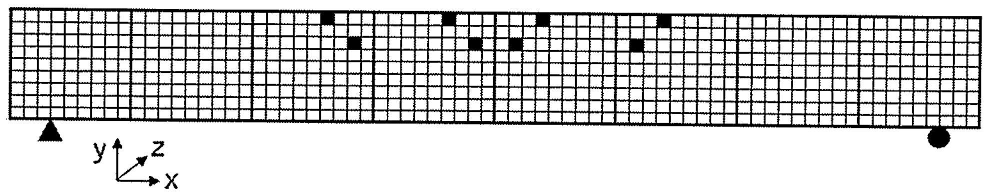

Figure 6.3: Holes Located Near Top of Beam

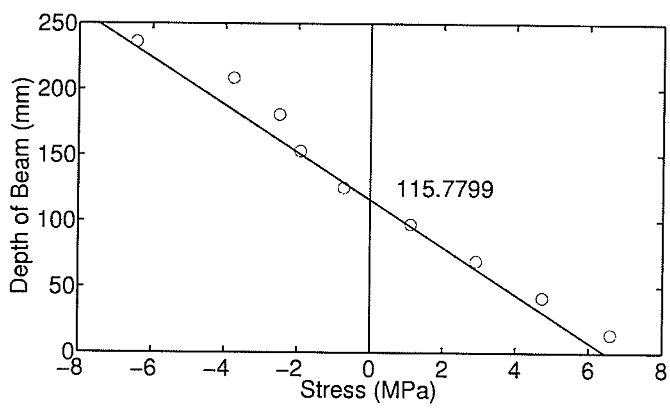

Figure 6.4: Beam with Holes near Top - Neutral Axis Location

the stresses in the 9 central elements from the top to bottom of the beam.

The FEM model shows an upward shift in the neutral axis when the holes are positioned near the bottom of the beam. Refer to Figure 6.5. The neutral axis is estimated to be 138.7 mm above the bottom face, as shown in Figure 6.6. These results confirm the earlier hypothesis on shift in N.A. location due to defects in the section. It should be noted that the heterogenous nature of timber makes beam behaviour difficult to predict.

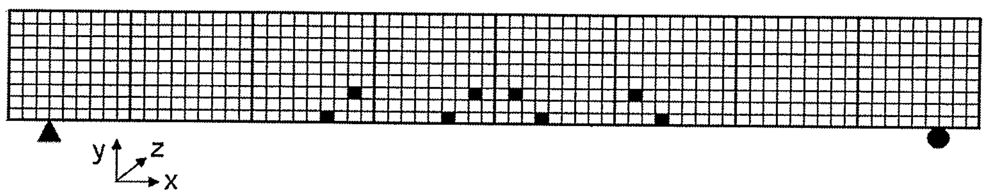

Figure 6.5: Holes Located Near Bottom of Beam

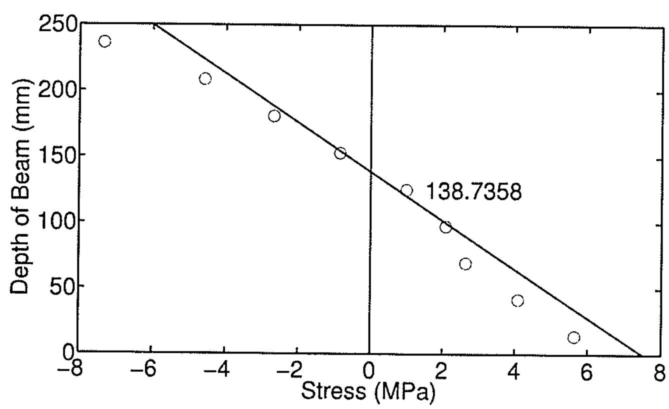

Figure 6.6: Beam with Holes near Bottom - Neutral Axis Location

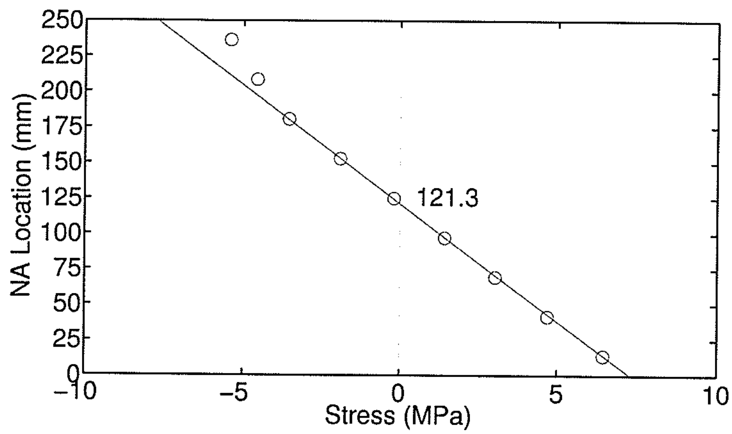

Figure 6.7: NA Position for Beam $C-2$ Determined by FEA

6.1.6 Comparison with Experimental Results

Three of the control beams were modeled using FEM. The beams chosen were $C-2$, $C-15$, and $C-16$. The NA positions of these beams have already been determined with the pi gauge readings in Figures 4.41, 4.40, and 4.39. The comparison of the neutral axis location from the experimental results (pi gauge readings) to the FEM model were taken at a load of 10 kN to ensure that the beam is still behaving linearly in order for the FEM to be valid.

Beam $C-2$ failed in shear and had an initial position of N.A. 100 mm above the bottom face at 10 kN, compared to the FEA model prediction of 121.3 mm. This prediction is relatively good, since it predicts a NA location below the mid-height of the beam. Figure 6.7 shows the NA location as predicted by the FEM model and each plotted point represents the stress in the x-direction in an element along the midspan of the beam.

Beam $C-15$ failed in compression. The NA location at 10 kN was 132 mm above the bottom

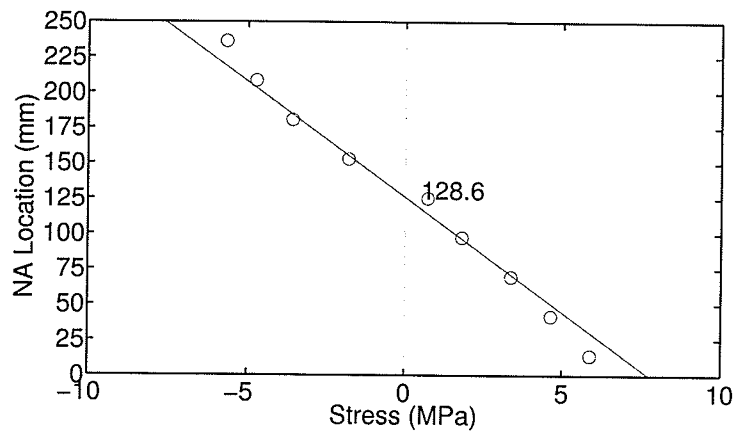

Figure 6.8: NA Position for Beam $C-15$ Determined by FEA

face, which is in good agreement with the FEM model prediction of 128.6 mm. Refer to Figure 6.8 for a plot of the NA position.

Beam $C-16$ experienced a tensile failure. The NA location was 130 mm above the bottom face at 10 kN, being relatively close to 135 mm above the bottom face, predicted in the FEM. It should also be noted that the NA location rose to as high as 145 mm before cracking, demonstrating that the FEM model was able to predict the general location of the beams neutral axis as shown in Figure 6.9.

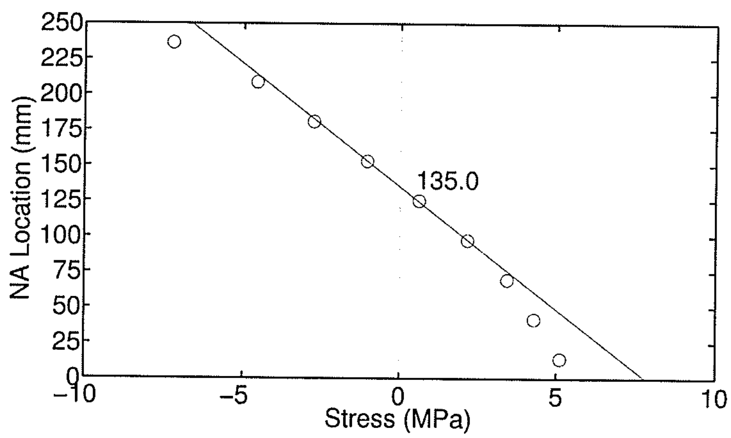

Figure 6.9: NA Position for Beam $C - 16$ Determined by FEA

Chapter 7

Economic Considerations

7.1 Shear Reinforcement

A cost estimate for comparing GFRP bars to GFRP sheets was done with price estimates from Vector Construction Group. The costs of the two reinforcing options were calculated for 10 full-scale beams, each with a cross-section of 100 x 400 mm and a length of 7000 mm. The beams were assumed to have single spans and the reinforcement would be installed at 45 ° at a spacing of 300 mm. The cost for the bars (9 mm Aslan 100 Rods) is $8–10/bar for material and $27–30/bar for labour/equipment/general conditions. The material costs associated with the sheets (MBrace EG900 GFRP U wraps) are $12–14/U wrap and $23–26/U wrap for labour/equipment/general conditions. The sheets would be installed similar

Table 7.1: Cost Comparison – GFRP Sheets vs. Bars

	GFRP Sheets	GFRP Bars
Materials	\$12–14	\$8–10
Labour/Equipment/General Conditions	\$23–26	\$27–30
Total Cost	\$35–40	\$35–40

to the method used for the shear specimens tested, with the two bottom pieces overlapping each other at the bottom of the beam. It should be noted that all costs are bid prices. The prices of each option are very similar with a range of \$35-40/unit, however the installation of the rods is more labour–intensive while the sheets involve higher material costs. Table 7.1 shows a summary of the cost analysis.

These costs for the two options are very similar, requiring judgement by the designer. The accessibility to the site, accessibility to the actual girders, number of beams, amount of reinforcement and required disposal of creosote-contaminated debris if any, are all factors that must be considered.

7.2 Shear and Flexural Reinforcement – GFRP bars

Pricing for GFRP bar strengthening was obtained from Specialty Construction. For a bridge strengthening project, there is often a large variation in prices that depend on:

1. Material cost (type and quantity of reinforcement and epoxy)
2. Size of project (larger projects will have lower unit costs)

3. Bridge location (travel time and transportation costs)

4. Site accessibility (method of access to underside of bridge such as hanging scaffold or scaffold on frozen water)

5. Environmental concerns (containment of creosote-contaminated waste)

An estimated strengthening cost for a timber stringer ranges from $110 to 200/m. A bridge strengthened with both dowels for shear and near surface mounted GFRP rods for flexure would cost approximately $160/m, assuming the bridge is less than an hour away from the contractor's setup and is relatively accessible. Material costs for this project are around $40 to 50/m which is a fairly small percentage of the overall project cost.

Chapter 8

Conclusions and Recommendations

An experimental program was undertaken to investigate the strengthening of timber stringers using GFRPs. Durability tests and bending tests were carried out in this research.

The durability tests were composed of two components. The first involved subjecting 20 of the 30 specimens to an accelerated aging process to simulate extreme environmental conditions. This was a 24-week program, with three rotating cycles, including a humid cycle (85% R.H.), a hot cycle ($40\,^{\circ}C$), and a drying cycle. The second part was direct shear tests preformed on 30 - 100 x 200 x 770 mm creosote-treated, Douglas-fir samples with a predefined shear plane. Ten of the samples were tested at $-20\,^{\circ}C$, ten at $+40\,^{\circ}C$, and ten were control samples tested at room temperature and did not undergo the accelerated aging.

The bending tests involved the testing of 58 - 75 x 250 x 2400 mm Douglas-fir beams in three point bending. Artificial defects were introduced into the beams using a statically random process to lower the grade of the beams. Of the beams tested, 18 were control beams, 20 were strengthened in the tensile zone with one 5 mm diameter GFRP bar, and 20 were strengthened with two 5 mm diameter GFRP bars in the tensile zone. Shear strengthening was also provided in the form of 12.5 mm GFRP dowels to prevent shear failures, however this was not the focus of this investigation.

8.1 Conclusions

The following conclusions were drawn from this experimental program.

1. The creosote treated shear samples strengthened with GFRP sheets at 45° carried an average load of 41.9 kN, compared to 57.8 kN for the non-treated samples, a strength loss of 27.5%. The non-treated specimens strengthened with 30° sheets carried 80.8 kN, a 28% increase in strength for a 30% increase in reinforcement ratio compared to the 45° sheets.

2. The creosote treated samples had 6 to 10% more interface failure than the untreated samples which shows that the creosote negatively impacts bond strength.

3. There was sufficient bond durability observed in the GFRP–timber interface for the shear specimens. The accelerated aging program did not produce any noticeable decrease in bond strength for either the sheet or dowel samples compared to their respec-

tive control specimens. Based on the results of the statistical analysis using ANOVA, creosote treatment significantly lowers the load-carrying capacity of the samples.

4. The minimum reinforcement ratio, ρ, specified in the CHBDC S6–06 can be lowered from 0.2% to 0.1% without a significant loss in the bending strength. Providing reinforcement in timber beams leads to less variability in comparison to the control beams. This was achieved by bridging existing natural and artificial defects that were present in the beams.

5. The control and strengthened beams carried an average load of 38.2 kN and 50.8 kN respectively, representing an increase of 31.6%. The minimum failure load increased from 20.6 kN to 41.6 kN, a 102% increase, demonstrating the ability of the GFRP to effectively increase the beam strength for beams with lower strength.

6. An analysis of variance was used to compare the ultimate loads of the different strengthening schemes. There was no significant difference in the results between the two reinforcement ratios, however the control beams carried considerably less load and there was a statistically significant difference in load carrying capacity between these beams and the strengthened beams.

7. The FEA model was capable of accurately modeling a timber beam while the beam was acting linearly. The FEA model predicted the neutral axis position relative to the mid-height of the beam fairly accurately based on the location of artificial defects. It was shown that beam failing in tension have their N.A. above the mid-height, while

beams failing in compression have their axis below mid-height. This simple check can potentially be used to determine appropriate strengthening schemes on existing timber bridges.

8.2 Recommendations

This experimental program shows favorable results regarding the strengthening of timber with GFRP, however a number of recommendations have been outlined for future research.

1. Test full scale, creosote-treated timbers with the CHBDC S6-06 minimum reinforcement ratio of $\rho = 0.2\%$. Test beams with $\rho = 0.1\%$ to verify the results of this experimental program and consider reducing the reinforcement requirements of the CHBDC S6–06.

2. Investigate the behaviour of FRP-strengthened timber beams under cyclic and dynamic loading under long-term environmental exposures.

3. Provide shear reinforcement at a minimum angle of $45\,^{\circ}$ in the critical shear zones.

4. Investigate the bond between the GFRP rods and the epoxy resin for beams in bending, as cracking in epoxy during loading has the potential to negatively effect the bond between the two materials.

5. The bond strength between the GFRP and the timber needs to be further investigated.

References

[1] American Institute of Timber Construction. (1994). Timber Construction Manual. 4th Edition. John Wiley & Sons Inc., New York, U.S.

[2] ASTM (1998). Standard Test Method for Heat and Moisture Resistance of Wood-Adhesive Joints, ASTM D4502-92. American Society for Testing and Materials, West Conshohocken, PA.

[3] ASTM (1994). Standard Methods of Testing Small Clear Specimens of Timber, ASTM D143-94. American Society for Testing and Materials, West Conshohocken, PA.

[4] ASTM (1996). Standard Practice for Developing Accelerated Tests to Aid Prediction of the Service Life of Building Components and Materials, ASTM E632-82 (Reapproved 1996). American Society for Testing and Materials, West Conshohocken, PA.

[5] ASTM (1999). Standard Practice for Estimating the Percentage of Wood Failure in Adhesive Bonded Joints. ASTM D5266-99. American Society for Testing and Materials, West Conshohocken, PA.

[6] ASTM (1999). Standard Test Methods of Static Tests of Lumber in Structural Sizes, ASTM D198-99. American Society for Testing and Materials, West Conshohocken, PA.

[7] Abdel-Magid, B., Dagher, H., and Kimball, T. (1994). "The Effect of Composite Reinforcement on Structural Wood." Proceedings of the 3rd ASCE Material Engineering Conference on Infrastructure: New Materials and Methods of Repair. K.D. Basham, Editor, ASCE, New York, N.Y., pp.417-424.

[8] Amy, K. and Svecova, D. (2004). "Strengthening of Dapped Timber Stringers using Glass Fibre Reinforced Polymer Bars." Canadian Journal of Civil Engineering, 31(6): 943–955.

[9] Barbero, E., Davalos, J., and Munipalle, U. (1994). "Bond Steength of FRP-Wood Interface." Journal of Reinforced Plastics and Composites. 13(9): 835-854.

[10] Bartz, A. (1999). Basic Statistical Concepts, 4th edition. Prentice-Hall, Inc. Upper Saddle River, United States.

[11] Battles, E., Dagher, H., and Abdel-Magid, B. (2000). "Durability of Composite Reinforcement for Timber Bridges." Transportation Research Record 1696. Paper No. 5B0111.

[12] Boon, E. (2000). "GFRP Dowel for Strengthening of Timber Structures: Direct Shear Tests." Bachelor of Science in Civil and Geological Engineering undergraduate thesis presented to University of Manitoba, Winnipeg, Manitoba, Canada.

[13] Borri, A., Corradi, M, and Grazini, A. (2004). "A Method for Flexural Reinforcement of Old Wood Beams with CFRP Materials." Composites: Part B 36: 143-153.

[14] Brooks, K. (2000). "Assessment of the Environmental Effects Associated with Wooden Bridges Preserved with Creosote, Pentachlorophenol, or Chromated Copper Arsenate." Res. Pap. FPL-RP-587. Madison, WI, USA. Department of Agriculture, Forrest Services, Forest Products Laboratory.

[15] Buchanan, A. (1990)."Bending strength of lumber." Journal of Structural Engineering, ASCE, 116(5): 1213–1229.

[16] Buchanan, A. (1984). "Strength Model and Design Methods for Bending and Axial Load Interaction in Timber Member." Doctor of Philosophy in Civil Engineering thesis. University of British Columbia, Vancouver, British Columbia, Canada.

[17] Coolidge, F. (2006). Statistics – A Gentle Introduction, 2nd edition. Sage Publications, Inc. Thousand Oaks, United States.

[18] CSA. (2006). Canadian Highway Bridge Design Code. Standard S6.1-06. Canadian Standards Association, Toronto, Ont.

[19] Dagher, H. and Lindyberg. (2001). "Development of AASHTO Design Specifications for FRP-Glulam Bridges."

[20] Davalos, J., Qiao, P., and Trimble, B. (2000). "Fiber-Reinforced Composite and Wood

Bonded Interfaces: Part 1. Durability and Shear Strength." Journal of Composites Technology & Research, JCTRER, 22(4): 224–231.

[21] Davis, G. (1997). "The Performance of Adhesive Systems for Structural Timbers." International Journal of Adhesion and Adhesives, 17(3): 247–255.

[22] Deppe, H. (1981). "Long-term Comparative Tests Between Natural and Accelerated Weathering Exposures of Coated and Uncoated Wood-based Material." Proceedings of the Washington State University International Symposium on Particleboard, 79–100.

[23] Duwadi, S. and Ritter, M. (1995). Research on Timber Bridges and Related Topics. Federal Highway Administration.

[24] Falk, R. et al. (2003). "Effect of Drilled Holes on the Bending Strength of Large Dimension Douglas-fir Lumber." Forest Products Journal, 53(5): 55–60.

[25] Forest Products Laboratory. (1999). Wood handbookWood as an Engineering Material. Gen. Tech. Rep. FPLGTR113. Madison, WI: U.S. Department of Agriculture, Forest Service, Forest Products Laboratory. 463 p.

[26] Fridley, K., Williams, J., and Cofer, W. (2001). "Reliability of Reused Sawn Lumber: Effect of Fastener Holes." Journal of Structural Engineering. 127(4): 412–417.

[27] Gardner, D., Wolcott, M., and Munipahle, U. (1992). "Wood Reinforced with Pultruded Fibre Reinforced Composites." Pacific Rim Bio-Based Composites Symposium, Rotorua, New Zealand. 263–269.

[28] Gentile, C., Svecova, D., and Rizkalla, S. (2002). "Timber Beams Strengthened with GFRP Bars: Development and Applications." Journal of Composites for Construction. 6(1):, 11–20.

[29] Ghosh, P. and Bose, N. (1995). "FRP Composites Based on Different Types of Glass Fibers and Matrix Resins: A Comparative Study." Journal of Applied Polymer Science, 58: 2177–2184.

[30] Gilfillan, J., Gilbert, S., and Patrick, G. (2003). "The Use of FRP Composites in Enhancing the Structural Behaviour of Timber Beams." Journal of Reinforced Plastics and Composites, 22(15): 1373-1388.

[31] Gillespie, R. 1965. "Accelerated Aging of Adhesives in Plywood-type Joints." Proceeding of the 19th Annual Meeting of the Forest Products Research Society, New York City, June 29, 1965.

[32] Gomez, S. (2006). "Performance of Timber Stringers Reinforced with GFRP Wraps." Master's of Science in Civil Engineering thesis. University of Manitoba, Winnipeg, Manitoba, Canada.

[33] Hay, S. (2005). "Shear Strengthing of Timber Stringers using GFRP Sheets." Master's of Science in Civil Engineering thesis. University of Manitoba, Winnipeg, Manitoba, Canada.

[34] Herzog, B. (2004). "Effect of creosote and copper naphthenate preservative treatments

on properties of FRP composite materials used for wood." Journal of Advanced Materials, 36(4): 25–33.

[35] Hirasawa, H., Oikawa, A., and Kobayashi, A. (2006). "Loading Tests of Glulam Beams Reinforced by CFRP Sheets and Plates." Proceeding of the 9th World Conference on Timber Engineering, Portland, OR, USA.

[36] Johns, K. and Lacroix, S. (2000). "Composite Reinforcement of Timber in Bending." Canadian Journal of Civil Engineering, 27(5), 899–906.

[37] Johns, K. and Racine, P. (2001). "Composite Reinforcement of Timber in Bending." 29th Annual Conference of the Canadian Society for Civil Engineering, Victoria, Canada.

[38] Lopez-Anido, R., Gardner, D., and Hensley, J. (2000). "Adhesive Bonding of Eastern Hemlock Glulam Panels with E-Glass/Vinyl Ester Reinforcement." Forrest Products Journal, 50(11/12): 43–47.

[39] Lyons, J. and Ahmed, M. (2005). "Factors Affecting the Bond Between Polymer Composites and Wood." Journal of Reinforced Plastics and Composites, 24(4): 405–412.

[40] Madsen, B. (1992). Structural Behaviour of Timber. Timber Engineering Ltd. North Vancouver, Canada.

[41] Mendenhall, W. (1993). Beginning Statistics : A to Z. Wadsworth, Inc. Belmont, United States.

[42] Micelli, F., Scialpi, V., and La Tegola, A. (2005). "Flexural Reinforcement of Glulam Timber Beams and Joists with Carbon Fiber-Reinforced Polymer Rods." Journal of Compsites for Construction, 9(4): 337–347.

[43] Mufti, A. (2005). TEKSAP User Manual Free Format Version. ISIS Canada Research Network - Technical Report.

[44] National Lumber Grades Authority. 2003. Standard Grading Rules for Canadian Lumber. National Lumber Grading Authority, New Westminster, B.C.

[45] Plevris, N and Triantifillou, T. (1992). "FRP-Reinforced Wood as Structural Material." Journal of Materials in Civil Engineering, ASCE. 4(3): 300-317.

[46] Raknes, E. 1997. "Durability of Structural Wood Adhesives After 30 Years Aging." Holz als Roh- und Werkstoff 55 (1997) 83–90.

[47] Ritter, M. (1997). Timber Bridges: Design, Construction, Inspection, and Maintenance. U.S. Department of Agriculture, Forrest Services, August, 1992, EM 7700-8.

[48] Rizkalla, S. (2001). Reinforcing Concrete Structures with Fibre Reinforced Polymers. ISIS Design Manual No.3. ISIS Canada, Winnipeg, Canada.

[49] Sonti, S., GangaRao, H., and Talakanti, D. (1996). "Accelerated Aging of Wood-Composite Members." Proceeding of 41st International SAMPE Symposium and Exhibition. 41(2): 1632–1641.

[50] Svecova, D. and Eden, R. (2004). "Flexural and Shear Strengthing of Timber Beams using Glass Fibre Reinforced Polymer Bars - An Experimental Investigation." Canadian Journal of Civil Engineering, 31: 45–55.

[51] Svecova, D. and Mota, C. (2002). "Durability of Rotafix CB10T Slowset Epoxy with Creosoted Timber." University of Manitoba, Winnipeg, Canada, October 2002.

[52] Tascioglu, C., Goodell, B., and Lopez-Anido, R. (2003). "Bond Durability Characterization of Preservative Treated Wood and E-Glass/Penolic Composite Inferfaces." Composites Science and Technology, 63: 979–991.

[53] Triantafillou, T. and Deskovic, N. (1992). "Prestressed FRP sheets as external reinforcement of wood members." Journal of Structural Engineering, ASCE. 118(5): 1270–1284.

[54] Triantafillou, T. (1997). "Shear Reinforcement of Wood Using FRP Materials." Journal of Materials in Civil Engineering, ASCE. 9(2): 65–69.

[55] Vick, C. (1997) "More Durable Epoxy Bonds to Wood With Hydroxymethylted Resorcinol Coupling Agent." Adhesive Age. 40(8): 24–29.

[56] Vick, C. and Okkonen, E. (1998). "Strength and Durbility of One-Part Polyurethane Adhesive Bonds to Wood." Forrest Products Journal, 48(11/12): 71–76.

[57] Wegner, L. and Gasmo, W (2000). "The Behaviour of Damaged Timber Beams Repaired with Glass Fibre-Reinforced Polymer Laminates." 2000 Annual Conference - Canadian Society for Civil Engineering, pp. 259.

Appendix A

Table A.1: Shear Test Results from Control Specimens (Sheets)

Sheets @ 45 °			Strain @ Pmax (%)			
Test #	Pmax (kN)	Deformation (mm)	Strain 1	Strain 2	Strain 3	Strain 4
6	43.7	2.1	0.60	0.84	0.61	0.44
12	29.6	5.2	0.23	0.84	0.63 [a]	0.89
18	53	2.1	0.25	1.46 [b]	0.70	0.73
24	47.9	2.4	1.15	1.27	0.45	1.47
30	35.3	1.6	0.22	0.86	0.67	0.22
Average	41.9	2.7	0.49	1.06	0.61	0.75

[a] 0.63 was the strain taken at 27kN, 1 minute, 55 seconds before ultimate load. This was the last accurate strain gauge reading.

[b] 1.46 was the strain taken at 52.7kN, 2 seconds before ultimate load. This was the last accurate strain gauge reading.

Table A.2: Shear Test Results from Specimens tested @ +40 °C (Sheets)

Sheets @ 45 °			Strain @ Pmax (%)			
Test #	Pmax (kN)	Deformation (mm)	Strain 1	Strain 2	Strain 3	Strain 4
4	33.9	2.9	1.34	0.41	0.56	0.10
10	45.8	3.5	0.59	0.34	0.76	0.27
16	39.9	3.1	0.84	0.27	0.45	0.46
22	37.9	2.0	0.17	0.68	0.44	0.13
28	39.5	3.1	0.64	0.31	0.57	0.52
Average	39.4	2.9	0.72	0.40	0.55	0.30

Table A.3: Shear Test Results from Specimens tested @ $-20\,^{\circ}$C (Sheets)

Sheets @ 45 °			Strain @ Pmax (%)			
Test #	Pmax (kN)	Deformation (mm)	Strain 1	Strain 2	Strain 3	Strain 4
2	39.3	2.7	0.52	0.05	0.55	0.07
8	40.1	6.2	0.22	0.23[a]	0.60	0.75
14	35.9	1.4	0.35	0.40	0.61	0.11
20	49.5	0.8	1.03	0.26	0.35	0.74
26	44.8	0.9[b]	0.16	0.83	0.57	0.52
Average	41.9	2.4	0.46	0.35	0.54	0.44

[a]0.23 was the strain taken at 24.0kN, 4 minutes, 47 seconds before ultimate load. This was the last accurate strain gauge reading.

[b]LVDT 2 froze up in the chamber, therefore only LVDT 1 was used for deformation.

Table A.4: Shear Test Results from Control Specimens (Dowels)

Dowels @ 45 °			Strain @ Pmax (%)		
Test #	Pmax (kN)	Deformation (mm)	Strain 1	Strain 2	Strain 3
5	27.4	5.2	0.42	0.87	0.21
11	33.9	3.9	0.37	1.45	0.19
17	45.7	5.2	0.47	-0.11[a]	0.24
23	36.3	4.4	0.38 [b]	0.60	0.09
29	35.5	4.2	0.21 [c]	0.005[d].	0.10
Average	35.8	4.6	0.37	0.97	0.17

[a]This negative strain was not included in the average strain calculations. It was likely caused by local compression of the dowel.

[b]0.38 was the strain at 35.8kN, 16 seconds before ultimate load. This was the last accurate strain gauge reading.

[c]0.21 was the strain at 27.7kN, 3 minutes, 5 seconds before ultimate load. This was the last accurate strain gauge reading

[d]This strain was not included in the average strain calculations. It was likely caused by local compression of the dowel, causing the strain to decrease (become less povitive)

Table A.5: Shear Test Results from Specimens tested @ +40 °C (Dowels)

Dowels @ 45 °			Strain @ Pmax (%)		
Test #	Pmax (kN)	Deformation (mm)	Strain 1	Strain 2	Strain 3
3	31.5	4.7	0.39	2.12	0.10
9	32.8	4.8	0.33[a]	0.64[b]	0.17
15	28.5	6.1	0.28	0.99[c]	0.29
21	28.1	6.6	-[d]	0.98[e]	-
27	24.0	6.6	0.04	0.96	0.20
Average	29.0	5.7	0.26	1.14	0.19

[a] 0.33 was the strain at 32.1kN, 29 seconds before ultimate load. This was the last accurate strain gauge reading.

[b] 0.64 was the strain at 32.5kN, 20 seconds before ultimate load. This was the last accurate strain gauge reading.

[c] 0.99 was the strain at 26.4kN, 1 minute, 32 seconds before ultimate load. This was the last accurate strain gauge reading.

[d] Gauges were damaged at time of GFRP rod installation

[e] 0.98 was the strain at 19.4kN. Technical problems with the DAQ resulted in an incomplete data file. This was the last accurate strain gauge reading.

Table A.6: Shear Test Results from Specimens tested @ −20 °C (Dowels)

Dowels @ 45 °			Strain @ Pmax (%)		
Test #	Pmax (kN)	Deformation (mm)	Strain 1	Strain 2	Strain 3
1	31.7	3.4	0.16	0.09	0.07
7	36.0	3.9	0.42	0.20	0.11
13	40.3	4.8	0.98[a]	1.33[b]	0.26
19	20.0	1.2	0.15 [c]	0.27	0.01
25	41.4	3.4	0.53	-2.05[d]	0.14
Average	33.9	3.3	0.45	0.47	0.12

[a] 0.98 was the strain at 39.5kN, 48 seconds before ultimate load. This was the last accurate strain gauge reading.

[b] 1.33 was the strain at 24.36kN, 3 minutes, 53 seconds before ultimate load. This was the last accurate strain gauge reading.

[c] 0.15 was the strain at 16.3kN, 31 seconds before ultimate load. This was the last accurate strain gauge reading.

[d] This negative strain was not included in the average strain calculations. It was likely caused by local compression of the dowel.

Table A.7: Beam Grades

Beam #	**Grade**	**Details**
$C-1$	SS	
$C-2$	Reject	Check exceeds 16" at end of beam
$C-3$	SS	
$C-4$	SS	
$C-5$	No.2	Check exceeds 10" at end of beam
$C-6$	SS	
$C-7$	SS	
$C-8$	No.1	Knots greater than 2.625" in critical section
$C-9$	SS	
$C-10$	SS	
$C-11$	SS	
$C-12$	SS	
$C-13$	SS	
$C-14$	No.2	Check exceeds 10" at end of beam
$C-15$	SS	
$C-16$	Reject	Check exceeds 16" at end of beam

Continued on next page

Table A.7 – continued from previous page

Beam #	Grade	Details
$C-17$	No.2	Check exceeds 10" at end of beam Knots greater than 2.625" in critical section
$C-18$	SS	
$1B-1$	Reject	Check exceeds 16" at end of beam
$1B-2$	SS	
$1B-3$	No.2	Check exceeds 10" at end of beam
$1B-4$	SS	
$1B-5$	SS	
$1B-6$	No.1	Knots greater than 2.625" in critical section
$1B-7$	SS	
$1B-8$	SS	
$1B-9$	No.2	Knots greater than 3.25" in critical section
$1B-10$	SS	
$1B-11$	SS	
$1B-12$	No.2	Check exceeds 10" at end of beam Knots greater than 2.625" in critical section
$1B-13$	SS	
$1B-14$	No.2	Check exceeds 10" at end of beam

Continued on next page

Table A.7 – continued from previous page

Beam #	Grade	Details
$2B-1$	Reject	Check exceeds 16" at end of beam
$2B-2$	SS	
$2B-3$	SS	
$2B-4$	SS	
$2B-5$	SS	
$2B-6$	No.2	Check exceeds 10" at end of beam
$1B-D-1$	SS	
$1B-D-1$	SS	
$1B-D-3$	No.1	Knots greater than 2.625" in critical section
$1B-D-4$	No.2	Knots greater than 3.25" in critical section
$1B-D-5$	Reject	Check exceeds 16" at end of beam
$1B-D-6$	No.1	Knots greater than 2.625" in critical section
$2B-D-1$	SS	
$2B-D-2$	SS	
$2B-D-3$	No.2	Knots greater than 3.25" in critical section
$2B-D-4$	Reject	Check exceeds 16" at end of beam
$2B-D-5$	No.2	Check exceeds 10" at end of beam Knots greater than 2.625" in critical section

Continued on next page

Table A.7 – continued from previous page

Beam #	**Grade**	**Details**
$2B-D-6$	No.1	Knots greater than 2.625" in critical section
$2B-D-7$	No.1	Knots greater than 2.625" in critical section
$2B-D-8$	SS	
$2B-D-9$	No.1	Knots greater than 2.625" in critical section
$2B-D-10$	No.2	Check exceeds 10" at end of beam
$2B-D-11$	SS	
$2B-D-12$	No.2	Check exceeds 10" at end of beam
$2B-D-13$	SS	
$2B-D-14$	SS	

Table A.8: Neutral Axis Summary - Strengthened Beams failing in Tension

Specimen	**Neutral axis location from bottom face of beam [mm]**		
	50% of Ult. Load	**90% of Ult. Load**	**Ultimate Load**
$1B-2$	154	138	133
$1B-7$	151	171	180
$1B-8$	130	122	123
$1B-10$	146	139	136
$1B-11$	132	127	126
$1B-12$	167	153	153
$1B-14$	155	122	122
$1B-D-3$	132	132	132
$1B-D-6$	171	164	162
$2B-4^a$	167	167	166
$2B-5$	128	127	128
$2B-6$	110	116	116
$2B-D-1$	151	147	147
$2B-D-3$	129	115	107
$2B-D-5$	133	141	141
$2B-D-6$	111	109	108
$2B-D-7^b$	170	164	164
$2B-D-13$	142	136	135
$2B-D-14$	138	148	150
Average	143	139	138
Standard Deviation	18	19	20

[a]Strain gauge 3 was not used to calculate NA location
[b]Strain gauge 2 was not used to calculate NA location

Table A.9: Neutral Axis Summary - Strengthened Beams failing in Shear

Specimen	**Neutral axis location from bottom face of beam [mm]**		
	50% of Ult. Load	**90% of Ult. Load**	**Ultimate Load**
$1B-1$	157	165	166
$1B-3$	135	115	105
$1B-4$	123	128	123
$1B-5$	136	117	112
$1B-6$	126	107	102
$1B-9$	90	84	86
$1B-13$	149	150	152
$1B-D-1$	145	123	114
$1B-D-2$	121	104	101
$1B-D-4$	164	162	160
$1B-D-5$	94	81	78
$2B-1$[a]	139	150	148
$2B-2$	142	148	145
$2B-3$	121	85	79
$2B-D-2$	147	140	143
$2B-D-4$	127	124	123
$2B-D-8$[a]	158	150	150
$2B-D-9$	147	143	145
$2B-D-10$	106	100	98
$2B-D-11$	149	149	138
$2B-D-12$	138	149	144
Average	138	149	144
Standard Deviation	20	26	27

[a]Strain gauge 2 was not used to calculate NA location